ISBN 978-82-326-1998-6 (printed version)
ISBN 978-82-326-1999-3 (electronic version)
ISSN 1503-8181

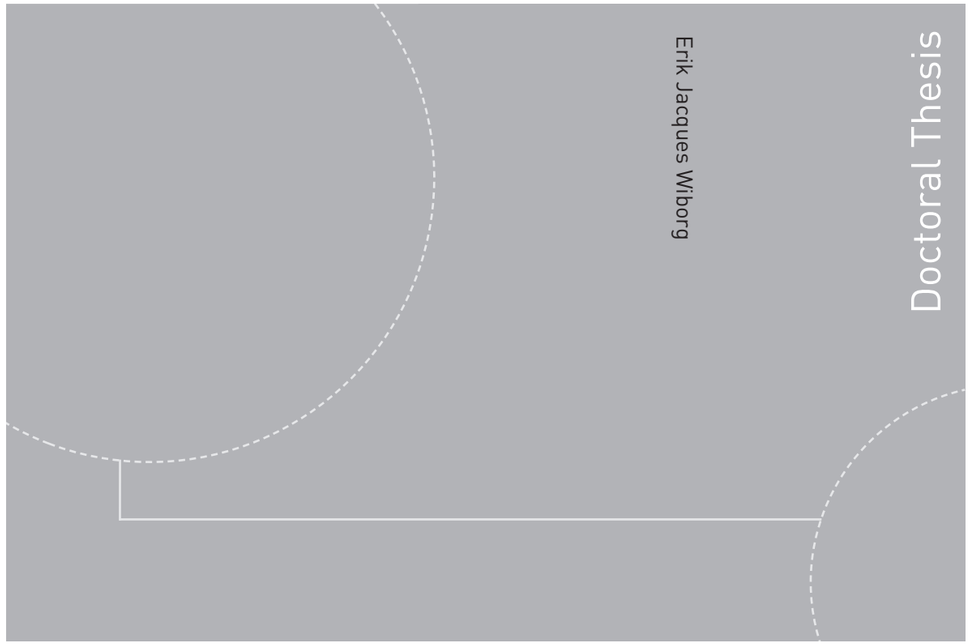

Doctoral theses at NTNU, 2016:330

Erik Jacques Wiborg

Continuous Efficiency Measurements on Hydro Power Plants

NTNU
Norwegian University of
Science and Technology
Faculty of Engineering
Science and Technology
Department of Energy and Process Engineering

NTNU
Norwegian University of
Science and Technology

Doctoral theses at NTNU, 2016:330

NTNU

NTNU
Norwegian University of
Science and Technology

Erik Jacques Wiborg

Continuous Efficiency Measurements on Hydro Power Plants

Thesis for the degree of Philosophiae Doctor

Trondheim, December 2016

Norwegian University of Science and Technology
Faculty of Engineering
Science and Technology
Department of Energy and Process Engineering

NTNU
Norwegian University of
Science and Technology

NTNU
Norwegian University of Science and Technology

Thesis for the degree of Philosophiae Doctor

Faculty of Engineering
Science and Technology
Department of Energy and Process Engineering

ISBN 978-82-326-1998-6 (printed version)
ISBN 978-82-326-1999-3 (electronic version)
ISSN 1503-8181

Doctoral theses at NTNU, 2016:330

Printed by Skipnes Kommunikasjon as

I Abstract

In 2012 the largest Norwegian power production company Statkraft initiated a research and development project initially named BlackBox. The company's main objective for the project was to develop an experimental condition monitoring system, later named *HydroCord*, tailored for Norwegian hydro power plants. Amongst the characteristics to be monitored, was the turbine efficiency.

The efficiency of the company's turbines is generally measured every decade for the major power plants in Norway. This gives poor basis for any type of prediction of the future turbine state. Continuous efficiency measurements would enable efficiency trending, and combined with a prediction model would provide an estimate of the future optimal refurbishment time.

Another vital use of the turbine state is within production planning, where it would enable a more regular and frequent update of the production model.

During this PhD work, Trollheim power plant has been the site for design, construction and testing of the HydroCord pilot system. The full system consists of a substantial number of miscellaneous measurements. The produced data is collected through five hubs spread out from the reservoir to the power plant outlet. The data is transferred between the hubs by fibre to a server, processing and storing the data. This project was led by the author of this thesis.

The focus of the PhD work was to establish a working method for continuous efficiency measurement, to be implemented in the HydroCord system. Three important issues had to be addressed. The design of an automated data validation method, its capability to reduce the high uncertainty caused by oscillations in the data, and the choice of the measurement method at site.

To prevent regulation from interfering with the efficiency measurement, which requires steady state measurements, a three-step automated quality control method was successfully designed and tested. The three steps consisted of a steadiness check, a normality check and a surge extraction process. The focus of the method was to reject any fluctuating measurements in order to ensure a good quality monitoring of the efficiency.

Simultaneously, the three-step method had to deal with potential mass oscillations in the waterways. This was done by numerically filtering the measured data, once the existence of such a surge was confirmed by the method. The reason for the

filtering was to reduce the uncertainty of the measured values.

A measurement method based on the acoustic transit time flow measurement method was selected for the HydroCord continuous efficiency measurement. Field efficiency measurements are generally entirely focused on low uncertainty of measurement. For automated field efficiency measurements, the focus had to be divided between a good accuracy, a reasonable cost and minimizing the chances of potential production interruption. Different efficiency measurement methods were tested and compared focusing on the flow measurement component of the efficiency measurement. The study and field tests revealed that a continuous efficiency measurement based on a clamp-on acoustic transit time flow measurement provided the results with the lowest uncertainty and a set-up in accordance with the requirements mentioned above.

By combining the steadiness control, the uncertainty reduction and a studied choice of measurement method, all elements required for the final design and installation of a continuous efficiency measurement system at Trollheim Power Plant are now in place.

II Preface

The PhD thesis "Continuous Efficiency Measurements on Hydro Power Plants" is the results of my work as an industrial PhD candidate for Statkraft Energy AS and the Norwegian University of Science and Technology, which I started in 2013. My research questions have evolved greatly during the process, formulated and moulded together with my main supervisor Torbjørn Nielsen from NTNU and my co-supervisor Morten Kjeldsen from FDB.

The project was financed partly by the company Statkraft Energi AS and partly by the Research Council of Norway. To both instances, I am grateful for this opportunity.

During my work I have been met with a tremendous amount of support and help from all of my surroundings. A special thanks to my co-workers, in-house mentor and superiors at Statkraft Energi AS, Kjell-Tore Fjærvold and Jan Petter Haugli in particular. Harald Hulaas from Norconsult has provide me with crucial information, comments and support, with his extensive expertise on field efficiency measurements. I am very grateful. A very special thanks to the brilliant engineers in Flow Design Bureau, the key architects of the HydroCord condition monitoring system. Håkon Francke, Jarle Ekanger and Morten Kjeldsen, many thanks for your help and support on all aspects of my PhD work. I could not have done this without you. Last, but not least, thanks to my family for understanding and helping me with every other aspect of my life during these three years.

III Table of Content

IV List of Figures

V Nomenclature

α ATT: angle between the pipe centreline and the acoustic path

$\bar{v}_a$ ATT: Average axial velocity in measurement section

$\bar{x}$ Mean value

η_g Generator efficiency

η_h Turbine runner hydraulic efficiency

κ ATT: Calibration coefficient

$\mathbf{A}$ FFT: array of amplitudes corresponding to each frequency bin

ω Surge extraction: Angular frequency

Φ FFT: array of phases corresponding to each frequency bin

ρ Water density

σ Standard Deviation

θ Water temperature(K)

ε ATT: = +1 or -1 if the signal is travelling downstream or upstream

φ Latitude (degrees)

A Surge extraction: Maximum amplitude of a detected wave

c ATT: Sonic speed if the fluid in question

D Hydraulic diameter

df Degrees of freedom

$F(\omega)$ FFT: Fourier transform of the function $f(t)$

$F^T(\omega)$ FFT: Fourier series of the sampled data $f(nT)$

f_D HLM: Darcy Friction Factor

$F_f(\omega)$ FFT: Fourier transform finite discrete form

f_m Measurement frequency

g Standard acceleration du to gravity

k ANOVA F-test: Number of groups

WKM: Calibration coefficient

HLM: Friction coefficient

L Length

l SPC: Control limit value

L_t ATT: Distance between transducers

$l_{\pm 2\sigma}$ SPC: Upper and lower 2-sigma control limit value

$l_{\pm 3\sigma}$ SPC: Upper and lower 3-sigma control limit value

MS ANOVA F-Test: Variability / Mean Square Value

n FFT: number of points in the acquired time-domain

n SPC: Dataset size / number of points in a measurement series

ANOVA F-Test: Number of samples in each group

p Pressure

P_m Mechanical power transmitted through coupling the runner and the shaft.

p_{abs} Absolute pressure(Pa)

Q_0 ATT: Calibration corrective term (bias)

S ANOVA F-Test: Sum of squared differences

s Standard deviation

s^2 Variance

t_m Surge extraction: Measurement time

v SPC: Violation count / number of points in violation of the stability criteria in question

z Altitude above sea level (m)

VI List of Abreviations

ANOVA	Analysis of Variance
ATT	Acoustic Transit Time
DFT	Discrete Fourier Transform
EPA	United States Environmental Protection Agency
FFT	Fast Fourier Transform
FPGA	Field-programmable gate array
GUM	Guide to the expression of Uncertainty in Measurements
HFEM	Hydraulic Field Efficiency Measurements
HHT	Hilbert-Huang Transform
HLM	(flow based on) Head-Loss Measurements
HPP	Hydro Power Plant
IGHEM	International Group for Hydraulic Efficiency Measurement
LCL	Lower Control Limit
masl	Meters Above Sea Level
NAS	Network-Attached Storage
PTP	Precision Time Protocol
SCADA	Supervisory Control And Data Acquisition
SPC	Statistical Process Control
SQC	Statistical Quality Control
TCP/IP	Transmission Control Protocol/Internet Protocol
UCL	Upper Control Limit
rms	Root Mean Square
WKM	Winter-Kennedy Measurement

1 Introduction

1.1 Motivation

Prior to the initiation of the PhD work, the largest Norwegian power production company, Statkraft, launched a project led by the author of this thesis. The project goal was the design, construction and testing of an experimental system for monitoring and optimization of hydro power plant maintenance and production.

The experimental system, named *HydroCord* was designed during the author's PhD work. A pilot system is close to completion at Trollheim Power Plant in Surnadal, Norway.

One of the main objectives of the system is a continuous monitoring of the turbine hydraulic efficiency. The focus of this PhD thesis was to conclude on all questions and issues relevant to the implementation. Three main issues, discussed in the next section, where brought forward and constitute the research questions of the thesis.

From the author's personal experience, after working ten years in Statkraft, the possible gain from such a system - and the efficiency monitoring in particular - has become apparent. The efficiency is one of the most essential characteristics for planning maintenance, refurbishments or replacement of a turbine. Timing of these activities is crucial, and can have a large impact on the net present value of a refurbishment project, which is in itself largely driven by the difference between the actual and potential turbine efficiency. Predictions based on historical development of the turbine efficiency are the keys to a good timing of the refurbishment. The better the historical data, the more accurate the analysis and trustworthy the results will be.

Maintenance aside, an important added value to the efficiency monitoring is the beneficial aspects for production planning. Norwegian power companies often use production planning models to help them optimize the output for their power plant portfolio at any given time. These models are based on, amongst other characteristics, the turbine efficiencies. Field efficiency measurements are time consuming and expensive to perform, they are therefore not frequently done (usually every tenth year or more, in the authors personal experience). This conclusion stems from the authors experience organizing three consecutive projects aimed at updating the efficiency curves of the company turbine portfolio. More than forty turbines were tested, proving in close to all cases that the values used for production planning were wrong, and most likely had been so for years.

Even with newly updated efficiency curves, the production can be based on wrong assumptions. The efficiency tested at site is only valid for the experienced head during testing (see limitations for approximations [1], section 8.1). This is because of the changes in the shape the efficiency curve has at different heads. To compute the efficiency values at heads significantly different from the test head, the full description of the efficiency - the hill diagram - must be used to correct the measured values (see [1], 6.1.2.2). For most turbines in the ageing company portfolio no such diagrams exist, and if they do, they are usually outdated or the results of numerical modelling. As of now, production planning is likely based on false presumptions of the efficiency.

To the authors knowledge, the HydroCord system will ultimately be the first system to provide live and continuously updated hill charts of a power plant. Although the goal is out of reach within the scope of this PhD, the author intends to continue working on the experimental system. Should this goal be reached, new interesting opportunities for research projects will present themselves. This is further discussed in the future work section 13.

1.2 Objectives of the studies

The three objectives will be the answers to the three major questions below. They will have to be answered in order to set up a continuous efficiency measurement of a hydro power turbine. This led to a natural disposition of this thesis, where the two first questions are related to the validation system dealt with in part 1, and the choice of method dealt with in part 2.

1 - How can the system automatically control and validate the data, making sure that it is suitable for efficiency computation, even during normal operation?

2 - How can that same system ensure a low level of uncertainty even during normal operation, where mass oscillations would distort the measurements?

3 - What method should be chosen for the flow measurement?

Field efficiency measurement methods and the theoretical background for computing it is regulated and described in the IEC 60041 standard [1] (hereafter denoted IEC41). Field efficiency measurements have been undertaken for decades, and is a well established type of measurement. Continuous monitoring is however not as common, and challenges arise from needs and demands of an unmanned system performing under normal operation conditions. The IEC41 does not propose any

kind of validation method for field efficiency measurement, only the use of the Grubbs test to detect outlier data (See IEC41, appendix B), designed to pinpoint singular spurious errors, affecting single measurement points. For a continuous efficiency measurement system, single outliers will not have a large impact on the mean, it is however imperative that the control system can detect and reject fluctuating measurement series or series with shifts of the mean during the measurement sequence.

It is the goal of this thesis' first part to present a possible method for data validation and dealing with oscillations, if present in the measured data. As will be explained further in the next section, none of the classic methods for data validation are usable for measurements on most of the larger Norwegian hydro power plants, mainly because of their long tunnels and waterways. Load changes due to regulation create slowly damping mass oscillations in the system. They will appear frequently and may be extremely long lasting (hours). Waiting for stable measurement situations i.e. no oscillation in the measurand, would hinder the continuous monitoring system in its main purpose.

The focus of the second part of this thesis is a presentation of the different efficiency measurement methods available and the choices made for Trollheim power plant (site of the HydroCord measurement system pilot) based on the results of a comparison test. One notable goal was to test and analyse the usability of a clamp-on acoustic transit time system for the purpose of continuous efficiency measurements.

The author led the HydroCord design and construction project, with Flow Design Bureau (FDB) as supplier. Leading the design of the functionality, operation form and main purposes of the system, the author also participated actively in HydroCord mechanical design and construction. The elaborate software for data collecting, handling, storing and processing was entirely created by Flow Design Bureau, with the exception of the validation software presented in part 1 of this thesis, solely created by the author.

1.3 Related Work

Continuous efficiency measurements is not a novel concept. Already in 1970 A. Whillier published *On-line determination of the performance of high-head pumps handling any liquid* [2] (a paper which would soon become a reference work for thermodynamic measurements on hydro power plants). The Canadian power company Hydro Quebec has also conducted some interesting work related to condition

monitoring in later years. One example is presented in their paper *Online flowrate monitoring experiences at Hydro-Québec* [4]. The method is however designed for low head power plants where mass oscillations present no problem. Equally interesting is their paper *Prototype Hill Chart testing of a saxo unit* [5], where a semi-permanent measurement system was used to gather the turbine efficiency at different heads and ultimately leading to a measured prototype Hill-Chart. The project is closely related to the one presented in this thesis, the main difference being that the measurement system was neither automatic or continuous.

Other than the work of Hydro Quebec, very few publications dedicated to on-line efficiency monitoring could be found dated from later years. The reasons for this lack of scientific push could be many. One likely reason is an assumption of a bad return on investments. Commercially available condition monitoring systems for hydro power plants often have the hydraulic efficiency included as a measurement point. To the authors knowledge, it is not however an actual measurement but rather an estimation based on static efficiency curves and the power output. It is therefore incapable of measuring efficiency degradation over time. A net present value analysis performed by the author revealed that the assumption of a bad return on investment is no longer valid. This mainly because of the technological advance of sensor technology, processing power, storage and communication systems.

Related work regarding the different flow measurements can be found throughout the thesis part 2 in the dedicated sections of each measurement method.

1.4 Summary of Results

The automatic quality control method developed through this PhD proved to be able to distinguish steady state measurements from transient or fluctuating measurement, while at the same time removing the effects of oscillations who are common during normal operation in hydro power plants. Figure 1 displays an example dataset subjected to the method.

A study of different methods for efficiency measurements lead to the conclusion that the Winter-Kennedy measurement (WKM) and the acoustic transit time measurement (ATT, clamp-on two paths) were to be candidates for the test site, Trollheim power plant. The ATT method proved to have significantly lower uncertainty of measurement judging from the results of the comparison test. Figure 2 displays the results of the uncertainty evaluation of the two different methods. A third method, based on head loss measurements (HLM), was also tested but the results were inconclusive for that method.

With the two issues stated in section 1.2 answered, continuous efficiency monitoring at Trollheim power plant will now be possible.

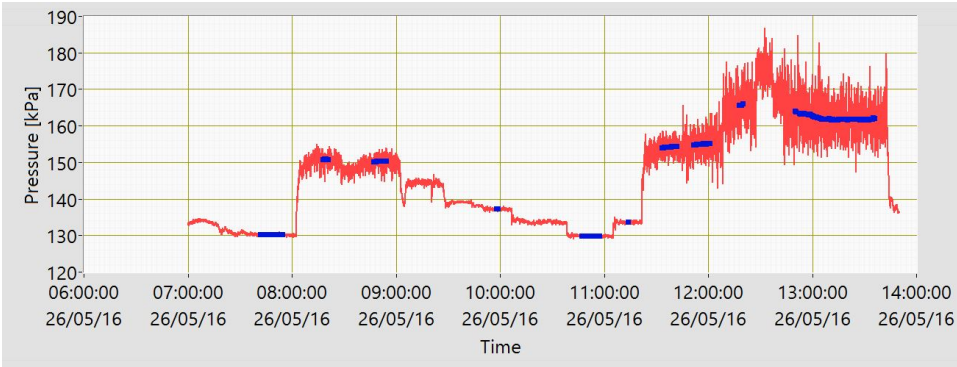

Figure 1: Validation Results On Measured Data
The red line represents a portion of the dataset used for the trial of the validation method. The values are averaged pressure measurements in the turbine draft tube (1 Hz measurement frequency). The blue points are accepted points for efficiency computation, i.e. the averaged values of a 500 points sequences deemed steady and where surge components have been removed.

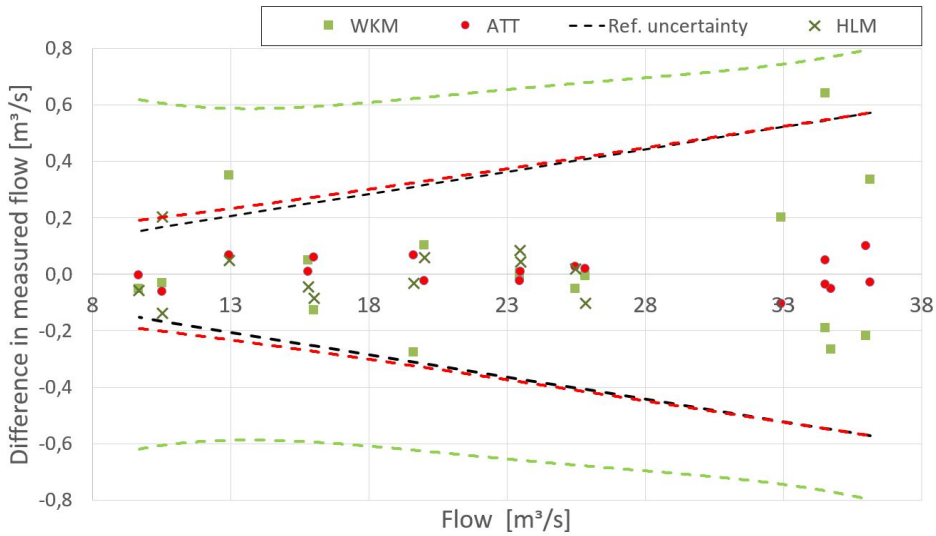

Figure 2: HydroCord Flow Measurements - Comparison Chart
The graph shows the difference between the three HydroCord flow measurements and the reference measurement (in m^3/s). Also displayed are the reference, ATT and WKM uncertainty bands centred around x-axis.

Part 1 - Automated Quality Control

2 Automated Quality Control - Introduction

Data validation is usually an essential part of any measurement. The United States Environmental Protection Agency (EPA) has worked a great deal on suggestions for methods and guidelines on this topic. Their *Data Quality Assessment: A Reviewers Guide* [6] describes a quality assessment routine where data validation plays a large role. Statistical testing of the data is the most common and useful way of validating data. The EPA's *Data Quality Assessment: Statistical Methods for Practitioners* [7] suggests a number of tests, mostly based on hypothesis testing.

In the case of continuous efficiency measurements on hydro power plants (HPP) validation of the data will be particularly important. The efficiency is computed based on measured values averaged over a long period of time. It is imperative that the measurements are done under steady conditions during the whole measurement sequence.

One of the main reasons for installing continuous efficiency monitoring is to provide the owners and operators data to trend the change (mainly degradation) of the efficiency over time. This will in turn help them to optimize maintenance and refurbishments. As the efficiency generally decreases extremely slowly, and varies both with the flow and the head, the measurement uncertainty must be reduced to a minimum. To decrease the uncertainty of any measurement, it is repeated a certain number of times. The mean value will have an uncertainty based on the number of measurement points and their variation. In short, the more stable the measurement points i.e. the lower the dataset variance is, and the longer the series, the more accurate the mean value will be. During field measurements five minutes measurement sequences or more per efficiency point is normal, this will be the case for the continuous efficiency monitoring as well.

During normal operation a multitude of events can cause fluctuations in the measurements but the most prominent is unit regulation, perpetually affecting the turbine governor. For all load changes, the elasticity in the water will cause short lived pressure surges (also known as "Water Hammer") in the system. Computing the efficiency during these transient states would undoubtedly lead to false result or, at the very least, with an unacceptable level of uncertainty.

Because of the long waterways composed of tunnels, surge shafts, creek intakes and other components, mass oscillations will also be born during the aforementioned load changes. Differences in level between the system components, like the

reservoir and the surge shaft for example, will have to stabilize after every change in the flow. This in turn will cause a mass oscillation to travel back and forth, disturbing measurement of the waterway characteristics. Friction in the tunnel walls will eventually cause the amplitude of the oscillation to fade away, however this process can take hours. For a continuous monitoring system to serve its purpose, an absolute criteria of Gaussian-like distribution of the data would be counter productive. The upside of the long lifetime of the oscillations is that within the time frame of one measurement sequence (minutes), they can usually be considered as steady (constant amplitude). This approximation will be used to avoid potential errors the oscillations may cause when assessing the mean value of the series.

The method described in this chapter serves the double purpose of controlling the stability of the measurement series i.e. no fluctuations or unsteady running mean value, as well as dealing with potential steady state oscillations present in the data.

In the statistical hypothesis testing jargon, rejecting good measurement or accepting bad measurements are often called type 1 (alpha) or type 2 (beta) errors respectively. The focus of continuous efficiency monitoring should be on minimizing type 2 error rates, ensuring that no unstable measurements are used for efficiency computation. As will be discussed later in the thesis, the abundance of measured data will make type 1 errors easier to tolerate.

3 Scientific Foundation and Research

3.1 The Method

The general flow of the method is shown in figure 3, and a brief overview of the steps is presented in this subsection. Each step is better described in their respective subsections.

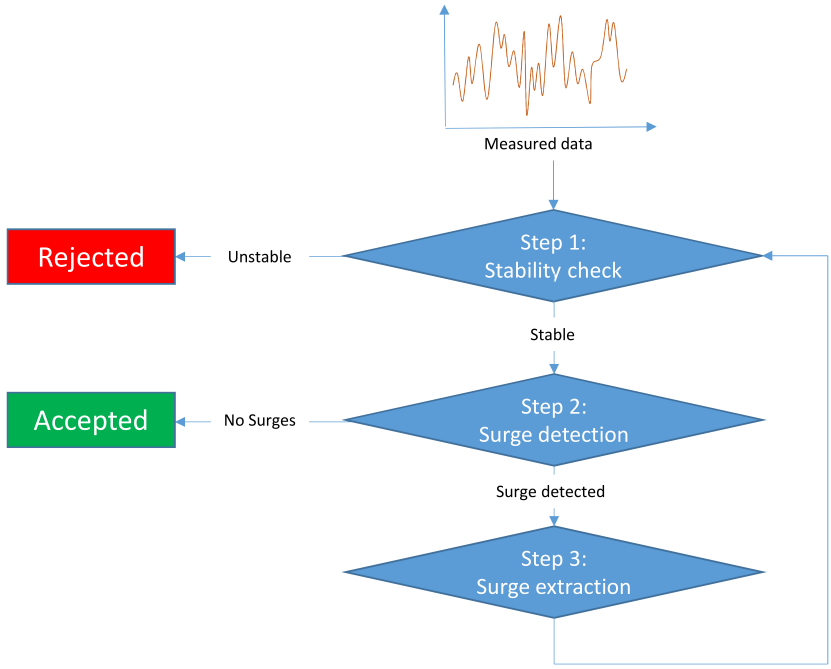

Figure 3: Automated Quality Control - Flow Chart
Stability check rejects measurements done during transient state, in accordance to its criteria. The Surge detection, in fact a normality test, accepts normally distributed data. Step 3 extracts the sinusoidal component with the highest amplitude detected in the data before resubmitting the filtered data to step 1 again. A dataset can be looped through these steps n times before rejection by default.

Step 1 - Stability verification through Statistical Quality Control (SQC)
The goal of the quality control is to accept only steady data, so to avoid efficiency

computation based on transient states of the measurand.
Mass oscillations in the signal is typically a state of non-stability. Most of the methods listed in the *Data Quality Assessment: Statistical Methods for Practitioners* aim to only accept Gaussian distributed data ([8] and [7]). Since a Gaussian like distribution of the measured data may be rare at best for the measurements at site, the stability criteria must be widened to accept the presence of steady sinusoidal components in the measured data.
The method used, Statistical Quality Control (SQC), is based on Statistical Process Control, adapted to the demanding conditions of monitoring hydro power plant waterways. The basis for the validation method is the use of control limits, determined by the measurand inherent mean and variation.
More details can be found i section 3.2.

Step 2 - Surge detection through ANOVA F-test
Once a dataset has been judged as steady by the SQC algorithms the dataset will be searched for surge components.
The analysis of variance (ANOVA) F-test is one of the normality tests presented in the EPA's *Data Quality Assessment: Statistical Methods for Practitioners* [7]. The method will partition the dataset and use the between and within variations of the data subsets, to judge whether to reject or not the null-hypothesis of similarity between the groups.
This enables the automated validation system to mark the datasets as containing a surge or not, as the SQC step has eliminated any other option for non-Gaussian distribution. Datasets that are normally distributed will be accepted for efficiency computation.
More details can be found i section 3.3.

Step 3 - Frequency domain search and surge extraction
As its name implies, step 3 will extract the surge components from the measured data, should step 2 mark the dataset as containing such sinusoidal components.
This will be done through an analysis of the Fast Fourier Transformed (FFT) dataset, identifying the major surge and extracting the component from the data.
The goal of this step is mainly to ensure a low level uncertainty in the measurements.
More details can be found i section 3.4.

3.2 Stability Verification - Statistical Quality Control

The Statistical Quality Control method was presented in an early stage of development at an IGHEM conference in 2014 [9]. At the time of writing the method

has been thoroughly tested and applied to actual measured data from the condition monitoring system.

Choice of Method

In cases of non-linear measurement profiles, validation through comparison tests is often used. Intel Corporation has patented an example of this type of method [10]. Another tool is the Non-linear Principal Component Analysis, as described by Matthias Scholz [11]. Common for these methods is the need of a dynamic model of the entire system, which in this case would be power plants and their usually quite complex waterways. It would exponentially increasing the amount of processing power required, as well as adding a substantial need for testing, calibrations and most likely costly additional measurements. The gain from such an intricate model would certainly not make up for the costs.

Looking back at the more simple and purely statistical tools, one of the suggested methods by EPA is the one-sample tolerance interval or limit method ([7], section 3.2.1.2). This particular method is also used in Statistical Process Control (SPC). It is well described by D. C. Montgomery in his *Statistical Quality Control - A modern Introduction* [12], and is the inspiration for the method used in this study.

This method was chosen because the validation criteria were not based on a normal distribution of the data, rather a non-deviation from the expected behaviour of the process.

Statistical Process Control

Since the method proposed in this thesis is inspired by Statistical Process Control (SPC), a brief summary of the method is provided in this section. It is based on the theory presented in Montgomerys *Statistical Quality Control* [12].

SPCs main goal is to perform a continuous stability control of a process aiming at homogeneous and uniform production.

Before submitting the process to the control system, a study has to be undertaken, often referred to as "phase 1". The goal of the study is to gather statistical information about the process to determine its normal performance, i.e. the mean and the variance of the process. The study is done under extraordinary supervision to make sure that no spurious errors corrupt this initiation phase.

The control limits are multiples of the processes standard deviation, with the process mean in the centre. Figure 4 is an example of a Shewhart diagram, visualising the SPC method.
In the example the four straight lines are the two and three sigma control limits; $l_{\pm 2\sigma} = \bar{x} \pm 2\sigma$ and $l_{\pm 3\sigma} = \bar{x} \pm 3\sigma$. With $\bar{x}$ the process mean and σ its standard deviation.

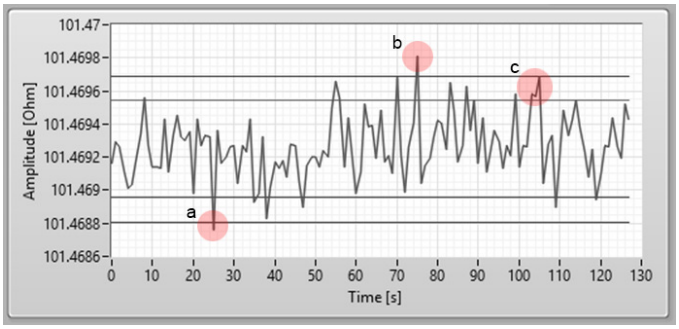

Figure 4: Shewhart Diagram - Example
Shewhart diagram example showing SPC control limits and three rule violations. Violations a and b are in breach of the three-sigma control rule, violation c in in breach of the two-sigma control rule

Depending on the process production method and the most important criteria for the production, different control rules may be applied. Eight such rules are well described by Montgomery [12], the equivalent of two of them were selected for further study.

The most simple and common one is the "three sigma rule" dictating that all measurement values should be contained within the three sigma limits. Figure 4 shows two such violations. Violation "a" is lower than the lower control limit (LCL) and violation "b" is higher than the upper control limit (UCL).

The second most common rule will be referred to as the "two sigma rule". A violation of this rule is described as when two out of three consecutive measurement points cross the same 2-sigma control limit. In figure 4 three consecutive measurements cross the same 2-sigma control limit at violation "c".

Both rules are designed to check the production for two issues, a shift in the mean

or an increased variance. This is congruent with a validation method for HydroCord efficiency measurements system, making this a good basis for the proposed method in this thesis.

As will be described later, only the "three sigma rule" was selected after completing the study and some further testing. The test results proved the second rule to be redundant.

SPC Adaptations

The SPC method, described by Montgomery [12] requires a study determining the process natural mean and variation, to determine the control limits. In the case of a continuous efficiency monitoring, one would have to assume that the situation remained stable though the study and the measurement following it. This will often not be the case as regulation of the turbine is frequent and unpredictable. Focus was therefore put in devising a method using no prior knowledge in the validation, rather assessing the characteristics of the measurand using the information available through the measurement series itself.

The chosen approach was to use parts of the actual measurement to set up the control limits. By using a small portion of the sampled points in the measurement series itself, enough information was available to set up reasonable control limits for the rest of the measurement series. The control limits would however be extremely sensitive to these points. A second set of control limits was therefore also computed, based on another part of the series, ensuring that the whole dataset went through the validation process at least once. Selecting the first and the last part of the series for the study maximised the sensitivity to shifts of the mean during the measurement. The control limit set with the highest amounts of rule violations was selected as the analysis results.

According to the literature ([12] and lecture notes). The size of the phase 1 subset of data should be at least 100 points for single measurements or 25 for averaged values. However, as both high- and low frequency measurements are to be subjected to the quality control, the size of the data sections used for phase 1 could not be based on a static number of sample points, rather a percentage of the dataset. Testing of the method revealed that 12.5% $(1/8)$ of the total sample size was satisfactory both during trials with synthetic data and actual data from the monitoring system.

The obvious flaw of the method was that the validation method would loose sensitivity if there were extraordinary large variations both at the start and the end of a measurement - with the same magnitude. A slight difference in the variation between them would undoubtedly cause numerous limit violations and cause rejection. The probability of such a situation occurring is however close to insignificant, and the mean value would still have to be relatively stable to be validated. After discussing this case with experts in the field of efficiency measurements it was decided that this flaw would be acceptable, the stability of the mean being the primary concern of the validation method.

The second issue that needed adaptation was a requirement for added flexibility to the method in order to prevent false rejections. The higher the number of sample points in the measurement series, the higher the risk of a rule violation. They will naturally occur if enough sample points are analysed, even with a perfectly normally distributed series.

A certain amount of rule violations would have to be accepted before rejection; a violation budget dependent on the size of the series.

A Monte-Carlo simulation was used for the study, described by figure 5.

Using randomly generated series with a Gaussian distribution ensured that the study was performed exclusively on data that were stable by nature. 1500 series of size n (start $n_{init} = 50$) were initially created and analysed with the validation method for every step i of the simulation. The process was repeated $i_{end} = 120$ times with a stepwise increasing sample count ($n_{i+1} = n_i + 20$). For each loop, the 1500 points sized array of violation counts was sorted for each step, to provide a weighted range of violation counts $[v_{i,min}; v_{i,max}]$.

Each range was then used to suggest a violation count limit $v_{lim}(i)$ related to the specific size n_i. Because of the random distribution of the synthetic datasets, some particularly erratic sets would return violation counts far beyond what could be considered as normal. Basing a violation budget on the highest returned violation count from the 1500 datasets would not be a good solution. A 95% confidence limit is standard in the industry, $v_{lim}(i)$ was chosen so that $[v_{i,min}; v_{lim}(i)]$ would satisfy this, i.e. $[v_{lim}(i); v_{i,max}]$ represented the weighted upper 5% of the range.

Finally, plotting sample violation budgets $v_{lim}(i)$ against the sample count n_i made it apparent that there existed a linear function between them.

This study was repeated five times, for each rule and for both rules combined.

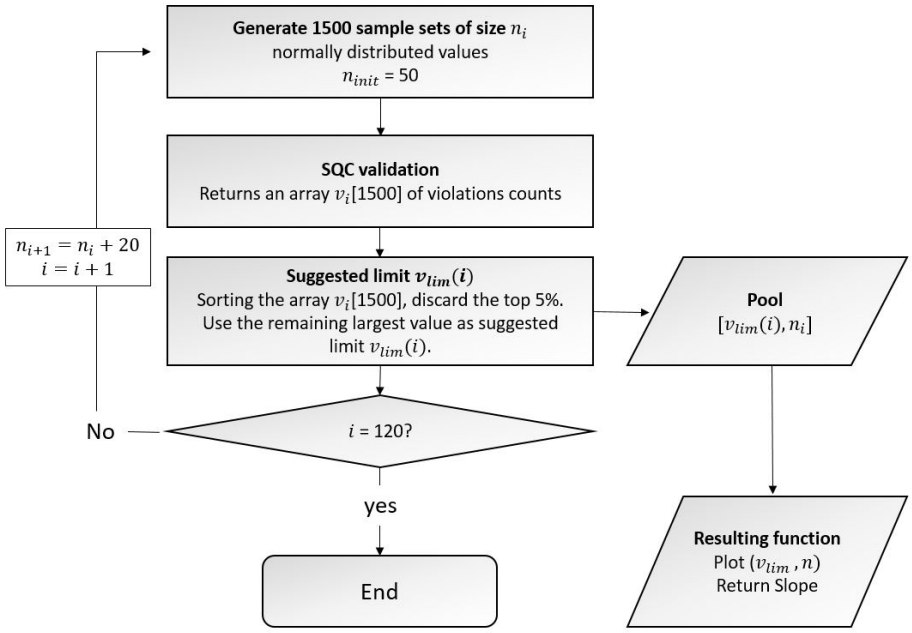

Figure 5: Violation Budget Study Flowchart
Synthetic normally distributed data was created in loops and fed to the SQC control method to provide a distribution of the violations that would naturally occur. This resulted in a linear equation providing a suggested violation budget depending on the sample size.

The resulting violation budget for the 3-sigma rule, the two-sigma rule and the rules combined where, 3.1%, 4.2% and 7.2% of the sample size, respectively.

After testing the method on data from the HydroCord system, only the more strict 3-sigma rule was selected for further use in the validation method. Using both rules proved to be a redundant action, as no significant changes in results came from using both compared to only using the three sigma rule.

3.3 Analysis of Variance F-Test

Choice of Method

Searching for the presence of oscillations, once the stability confirmed, could have been done in different ways. An obvious option would be a analysis of the fre-

quency spectrum of the signal. Another options was one of the normality tests unsuitable for the first step of this method described in the *Data Quality Assessment: Statistical Methods for Practitioners* [7]. If an analysis of the series revealed a non-Gaussian distribution, it would confirm the presence of an oscillation in the data.

A search through the frequency spectre would have taken up a lot of processing power compared to a purely statistical process. The Analysis of Variance (ANOVA) was selected for the surge detection step of the validation method. It is a well known and frequently used statistical test, described amongst others by Montgomery [12]. It would be easy to implement and require a minimum of computational power. The test has clear and quantifiable limit values, making it well suited for an automated system.

ANOVA F-test - Theoretical Background

The following description of the method is based on Montgomery's book (sections 4.5 and 8.7.2) and lecture notes from the course UNIK 4520 *Quality validated measurement techniques and statistical analysis methods* (UiO - University of Oslo).

The F-test is a Hypothesis test, used in situations with several groups of repeated measurements. The null-hypothesis (H_0) is that the means of each group differ only because of random variation, i.e. the data is normally distributed. The test result in an F-test statistic defined by equation 1.

$$F = \frac{Variability\ between\ groups}{Variability\ within\ groups} = \frac{MS_B}{MS_W} \tag{1}$$

To reject the null-hypothesis, i.e. proclaim the existence of a statistically significant oscillation in the data, the computed F-statistic must be larger than the critical F-statistic value, F_{crit}. The F-statistic follows the F-distribution, and the critical F-statistic value is found using the two degrees of freedom $df_1 = k - 1$ and $df_2 = k(n - 1)$, where k is the number of groups, and n the number of samples in each group. The chosen confidence interval are usually 90%, 95% or 99 %.

The variability, or Mean Square Value between and within groups, respectively MS_B and MS_W are defined by equations 2 and 3 bellow.

$$MS_B = \frac{S_B}{df_1} = \frac{n\sum_{i=1}^{k}(\bar{x}_i - \bar{x})^2}{k-1} \tag{2}$$

With S_B the between-group sum of squared differences, $\bar{x}_i$ the mean of group i, and $\bar{x}$ the overall mean of the sample values in the study.

$$MS_W = \frac{S_W}{df_2} = \frac{\sum_{ij}(x_{ij} - \bar{x}_i)^2}{k(n-1)} \tag{3}$$

With S_W the within-group sum of squared differences and $\bar{x}_{ij}$ the j value (within group index) in group i.

Use in the Validation Method

If the stability criterion of the SQC are met and the ANOVA reveals that no mass oscillation is present in the data, the data is by definition normally distributed and therefore validated for efficiency computation. One should note that high frequency mass oscillation may not be detected depending on the measurement frequency and the amplitude of the Gaussian Noise in the signal. In this case the frequency is so high that the ANOVA F-test interprets the oscillation as or fails to distinguish it from the Gaussian noise. The oscillations will have no significant impact on the end result i.e. the mean. Consider the equation for a simple sine wave, ignoring the phase shift, $A\sin(\omega t)$ [13], with A the amplitude and ω the angular frequency. Integration over the measurement time $[0; t_m]$ gives the following:

$$\int_0^{t_m} A\sin(\omega t)\, dt = \frac{A}{\omega}\left[1 - cos(\omega t_m)\right] \tag{4}$$

By dividing the integral with the measurement time t_m, one gets the effect of the surging noise component on the mean value. We see that the higher the frequency ω, the lower the possible impact of the mass oscillation.

3.4 Surge Filtering

The data is subjected to the third step of the method in the case where lower frequency mass oscillation are detected by the ANOVA. The oscillatory component should be considered as process noise in the signal. We have seen that the effect of the mass oscillation on the mean value can vary within $[-\frac{A}{\omega t_m}\ ;\ \frac{A}{\omega t_m}]$ (see equation 4), a potentially large error. To avoid this problem two methods could be applied. Either ensuring that only whole periods were used for computing the efficiency i.e. $1\text{-}cos(\omega t_m) = 0$, or removing/filtering the mass oscillation component of the

process noise all together. The choice fell on the latter. Cutting of the data in whole periods would be impossible in the common situation where several mass oscillation out of phase - with different frequencies - travel through the waterways. On the other hand, extracting the sinusoidal components one by one can easily be done, for example by looping the surge extraction process (which is the method used here).

Choice of Method

Surge filtering can be done in two ways; mechanically or numerically. The filter patented by Burgess Battery Co [14] is one out of many examples of mechanical filters. They can be viable and useful, but are by nature not very flexible. A numerical approach was preferable because of the potential use of the unfiltered dynamic measurements in other applications.

The detection and removal of the low frequency mass oscillation is done through the frequency spectrum of the Fourier transformed data (FFT) [15].
The automated surge filtering system, created in LabView, detects the frequency, amplitude and phase of the wave with the highest amplitude and creates a data array (same size as the measurement series) that perfectly fits said wave. The values are then subtracted from the measurement data.

Other methods for wave filtering were tested. The Hilbert-Huang transforms (HHT see e.g. [16]) showed good results. However, in the settings of an automated validation system, this method would have required more processing than the chosen FFT-based method. Keeping in mind that also the HHT transformed data would require phase-alignment of each component.

The Fast Fourier Transform and Surge Analysis

The Fast Fourier Transform (FFT) is well known and widely used. The author will assume that the reader is familiar with the basic concepts and will only present some general points of the theory behind this well known algorithm. The theory is explained in a multitude of forms and means, e.g. F.J. Harris's *On the Use of Windows for Harmonic Analysis with Discrete Fourier Transform*[17], which will be used as reference in the following chapter as well.

The Fast Fourier transform algorithm converts a dataset into the frequency domain, in this case from the time domain. The method takes its roots and name from M. Fouriers work on heat propagation [18].

The Fourier transform in the frequency domain $F(\omega)$ of a signal in the time domain $f(t)$, is defined by equation 5. In a discrete form, the signal (uniformly sampled with sampling frequency $1/T$), $f(nT)$ will have it's Fourier series expansion $F^T(\omega)$ defined by equation 6, n the index in the time domain.

$$F(\omega) = \int_{-\infty}^{+\infty} f(t)e^{-j\omega t}dt \tag{5}$$

$$F^T(\omega) = \sum_{n=-\infty}^{+\infty} f(nT)e^{-j\omega nT} \tag{6}$$

With
$|F(\omega)| = 0, \quad |\omega| \geq 0.5[2\pi/T]$
$F^T(\omega) = F(\omega), \quad |\omega| \leq 0.5[2\pi/T]$

To make use of the transform, a finite approximation of the discrete form is often used, defined by equation 7.

$$F_f(\omega) = \sum_{n=-N/2}^{+N/2} f(nT)e^{-j\omega nT} \tag{7}$$

Where NT is the sample time. N even.

By representing the measured signals in the frequency spectrum, peaks will reveal the oscillations present in the measured signal series **X**, and provide the means to identify them. Peak frequencies are found directly from the single-sided power spectrum real part (although windowing - discussed in the next subsection - will be required to assess the amplitude of the oscillating noise component correctly). Once the peak frequencies found, phase and amplitude information can be retrieved from the FFT spectrum in it's complex form, by scaling and converting to polar form [19].

$$\mathbf{\Phi} = \frac{180}{\pi}\, arctan\left(\frac{FFT(\mathbf{X})_{imag}}{FFT(\mathbf{X})_{real}}\right) \tag{8}$$

Where $\mathbf{\Phi}$ is the phase spectrum in degrees, i.e. the array of phases corresponding

to each frequency bin, and $FFT(\mathbf{X})_{imag}$ and $FFT(\mathbf{X})_{real}$ the imaginary and real components of the $FFT(\mathbf{X})$ power spectrum, respectively.

$$\mathbf{A} = \sqrt{2}\,\frac{\sqrt{FFT(\mathbf{X})_{imag}^2 + FFT(\mathbf{X})_{real}^2}}{N^2}, \quad for\ i = 1\ to\ \frac{N}{2} - 1 \tag{9}$$

$$\mathbf{A} = \frac{\sqrt{FFT(\mathbf{X})_{imag}^2 + FFT(\mathbf{X})_{real}^2}}{N^2}, \quad for\ i = 0 \tag{10}$$

With $\mathbf{A}$ the single sided amplitude spectrum in bar rms, N the number of points in the acquired time-domain and i the frequency bin number (array index) of the $FFT(\mathbf{X})$.

Windowing

Because it is unlikely that the measurement period coincides with a whole oscillation period or multiples of it, the data had to be "windowed" before analysis. The technique is well described, amongst others, by National Instrument [20] - the provider of the programming software used (LabView). The Hann window - chosen because of its good applications in handling trigonometric functions - is used to weight the centre values of the sinusoid rather than the extremities. The extremities are the root of the problem as the FFT would create a non continuity when periodic extensions of the sequence are made. The non continuity will be reduced, or eliminated with the Hann window, reducing the so-called FFT leakage and in turn the loss in amplitude.

FFT-Based Surge Extraction

Datasets subjected to the third step of the validation method the data are steady, but contain oscillation components. Through the FFT analysis described in this section, the oscillations are analysed. Their frequency, amplitude and phase are used to create a perfect sinusoidal dataset recreating the detected oscillation with the highest amplitude. By subtracting the created values from the original signal the oscillation component is removed from the dataset.

3.5 Quality Control Looping

After going through the three steps of the validation process, the data is re-submitted to the validation process. The surge extraction may or may not have removed all oscillatory components. In the case of transient state, where the oscillation is slowly damping, heavy Gaussian noise could hider the SQC stability control from detecting the unsteadiness (see case 5b in appendix A). However, the surge extraction process would naturally not be able to completely remove the oscillation from the signal. If the SQC once again fails to detect the fluctuation the ANOVA step would once more detect a non-Gaussian distribution and resubmit it to the surge extraction process and loop the process. After reaching the maximum number of authorized loops the data would eventually be rejected by default.

Another incitement for the re-submission is the fact that oscillatory components naturally desensitize the effect of the SQC stability control. Once a major wave component has been removed, the SQC control limits will be narrowed, and a more accurate steadiness verification will be possible.

To minimize data manipulation and processing power a limit of two loops through the validation method was set.

4 Automated Quality Control - Trials and Results

4.1 Trials on Simulated Data

To test the method before acquiring data from the HydroCord system, a software was designed to create synthetic series of data. They were composed of a randomized linear slope, Gaussian noise with randomized variation, and up to four wave components with all randomized characteristics.

The variety of the created series was naturally not in accordance with the typical behaviour of the waterway in a power plant, but represented a good way to test limitations and possible issues with the validation method. Some of the major discussion points and results are listed bellow.

1 - The study proved the importance of looping all three steps of the process seen in figure 3, and not only have the method loop the surge extraction process (third step) a certain number of times. Even with perfectly normally distributed data, the algorithms would still search for the highest peak in the white noise spectrum, and would extract a surge believed to be present. Trying to extract a non-existing

surge resulted in the addition of one instead. Although low in amplitude this made the whole process highly counter-productive. A system had to be put in place to confirm the actual existence of a surge before trying to extract it, a system like the two first steps of the validation method presented here.

2 - The surge extraction process only succeeded if the amplitude of the discovered waves were assessed correctly. As mentioned in section 3.4, windowing was used to minimize frequency leakage and the following underestimation of the amplitude [17]. By definition the method would be successful in it's task if a signal with an oscillation was accepted by the ANOVA test on the second loop i.e. it would be considered as normally distributed, after a surge extraction. This proved to be the case.

3 - During the trials some high amplitude surges managed to mask fluctuations or even shifts in the mean (by largely influency the data variance, and therefore the control limits of the SQC step). Only during the second loop of the process were these errors uncovered leading to rightful rejection of the data, underlining the importance of the surge extraction process.

4 - Testing on randomized data also proved that high frequency oscillations, mistaken for Gaussian noise by the ANOVA F-test did not have any impact of significance of the mean as long as it met the stability criterion of the SQC. Tests were done on the same dataset with and without the oscillation component, with a two-sample t-test.

5 - For some of the more unnatural combinations of waves and noise (signals that would not be expected in a Hydro Power waterway) the surge filtering system would fail. All these cases were however rejected by the validation method after the extraction was attempted.

One of the main concerns and goals of these trials was to test the method for type 2 errors, i.e. to test if the method could accept measurement series with unsteady running mean values or fluctuations. The conclusion was positive, revealing only some tendencies for type 1 errors, i.e. rejecting measurements who could be considered stable by other control methods (mainly visual inspection and histogram-based normality tests). This was deemed acceptable in view of the large amount of data the measurement system will gather, and the expected slow change in efficiency a turbine experiences.

4.2 Trials on Measured Data

The Measured Data

The measurement system is presented in details in later sections, this section will present the data subjected to the trials.

The dataset used for the trials, and as examples throughout this first part were pressure measurements from the power plant draft tube outlet. They were selected because of the early access to the data, and represented a god example of the data expected at site. The data contained transient passages due to tertiary regulation, some situations of unsteadiness caused by grid fluctuations, and some passages of turbine stand-still. A section is presented in figure 6 (red line).

For additional study results appendix A presents of the validation method applied to other measurements.

The data acquired from the HydroCord is recorded in two ways. One set contains the high frequency measurement values (in the case of the draft tube outlet pressure 200 Hz). The other set contains averaged data, so to present 1 Hz measurement values. The 1 Hz measurements offer a more clear visual picture of fluctuations and variation, and are the ones planned to be used at Trollheim power plant. They were therefore selected for the examples presented in the main body of the thesis.

In view of the data and the now acquired expectations of the data to be analysed, the two variables of the validation method (the ANOVA group size and the loop count limit) were chosen for the use of draft tube pressure measurements. The results are presented later in this section.

Trials and Results

Trials on the measurement data collected by the HydroCord system were conclusive, the validation method worked as planned.

As can be seen from figure 6 and the cases presented in appendix A, during transient states the SQC system rejected all measurement series. This was also the case during fluctuating pressure situation, often presumed to be a result of grid frequency variations. In steady situations, low frequency mass oscillations were detectable (frequencies between 0,006 and 0,007 Hz) such as the one in the example used in this section (see figure 7a). A higher frequency disturbance (0,25 Hz) was also noticeable in most datasets. The SQC validation method worked well in these situations, as no unsteady measurements were accepted by the method (no type 2

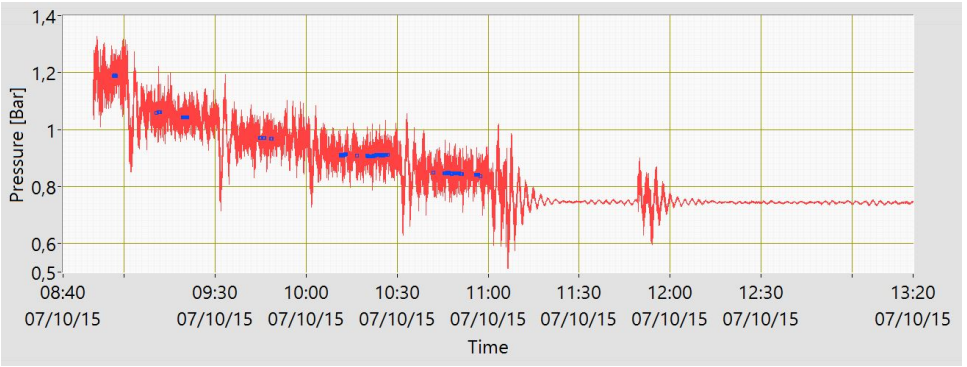

Figure 6: Validation Results on Measured Data
The red line represents a portion of the dataset used for the trial of the validation method. The values are averaged pressure measurements in the turbine draft tube outlet. The blue points are accepted points for efficiency computation, i.e. the averaged values of a 500 points sequences deemed steady and where surge components have been removed. Measurement frequency 1 Hz.

errors). On the other hand, as with the synthetic data trials, some seemingly valid measurement series were rejected because of temporary unusual erratic high frequency random noise. These unsteady situations would not have had a significant impact on the mean, and could have been considered for efficiency computation. It could therefore be viewed as a faulty rejection (type 1 error), a flaw deemed acceptable as discussed earlier in section 4.1.

Testing of the ANOVA F-test confirmed the ability to detect the mass oscillations of the power plant, as long as the amplitude was significant, compared to the more Gaussian-like Noise and erratic behaviour caused by the influence of the grid on the regulator. In the opposite case the mass oscillations would not have a significant impact on the mean (see equation 4, with a low A value).

The ANOVA analysis of the example series in figure 7a before extraction, a dataset accepted by the SQC method, reveals the presence of a mass oscillations, with an F-value of 9.2 larger than the critical value of 2.6.

With the presence of a standing mass oscillation confirmed, the data was filtered. The resulting ANOVA F-value of the signal after surge extraction, displayed in graph 7b was 2.4.

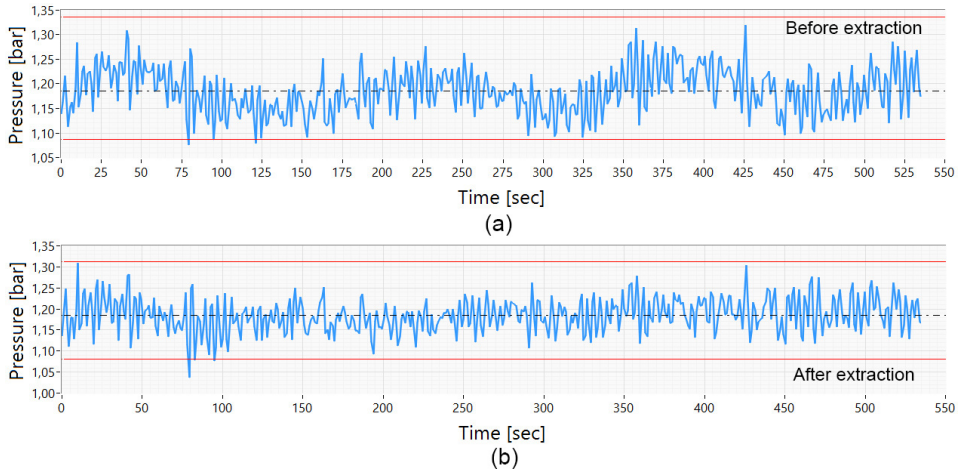

Figure 7: Surge Extraction - Example
Graph (b) shows the signal after extraction of a detected low frequency mass oscillations (0,006 Hz), visible in the original series, graph (a). The SQC control limits, in red, indicate that both series are considered steady, according to the SQC criteria of stability.

A discussion on the benefits that the wave extraction has on the measurement uncertainty can be found in section 5.2.

ANOVA Group Size

The ANOVA F-test results will vary depending on the size of the groups selected for the analysis. A group of 25 points was used with satisfactory results for 1 Hz frequencies for the pressure measurements in the draft tube. This value was selected after trials on the measured data, where normality was controlled visually by the means of a histogram-based approach. Figure 8 shows an example, the values used are the series before and after extraction shown in figure 7.

From figures 7 and 8, one can clearly see that these were the expected results. Figure 8a, the histogram containing the surge visible in figure 7a, shows a more squared distribution than the red lined Gaussian distribution. This is as expected from a convolution between the normally distributed noise and the oscillations which will typically have a close to rectangular distribution.

Further testing will have to be conducted for higher measurement frequencies and other measurement types. Depending on the measurand and sensor stability the

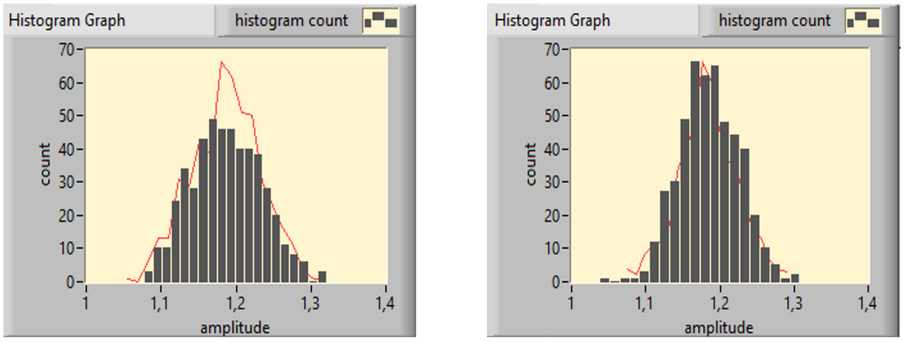

Figure 8: ANOVA Group Size Study - Draft Tube Pressure Measurement
Histograms of samples rejected (a) or accepted (b) by the surge detection step of the validation method. The red line is randomized normally distributed data created to provide a visual aid to the expected general shape of the histogram. We see that the outcome of the F-test is as expected, 25 point samples is a good group size.

group size will be selected in accordance with a study equivalent to the one performed for the draft tube pressure measurements.

Process Loop Count

With the acquired HydroCord data, a study was performed to assess a good limit for the number of loops the data should go through the validation process. After controlling that the data displayed typical behaviour (and was not unusually steady or erratic) a limit of two loops was selected. In most cases only one dominant pressure surge was visible in the dataset.

4.3 Dataset size

As mentioned earlier a five minutes measurement sequence is common for field efficiency measurements. The automated condition monitoring system was tested with 400 and 500 points 1 Hz frequencies series, i.e. 6,7 and 8,3 minutes long sequences. Although both test sizes gave good results, longer sequence would naturally require more long term stability and rejected more measurement points as well as require more processing power.
It was chosen to use 500 points sequences for 1Hz measurements and 400 points

for high frequency measurements to save processing power.

5 The Automated Quality Control - Discussion

5.1 Metrological View on Continuous Efficiency Measurements

Measurements providing the necessary data for efficiency computation are numerous and diverse. Many of the measurands are of different nature, and the measurements are often situated in different geographical locations and environments. The goal of each single measurement is the mean value of the measurand in question. Any fluctuation in any of the measurement suspected to be by a systematic or spurious error will lead to a failed measurement of the efficiency. Considering these facts the author has chosen to view the efficiency measurements not as one single continuous measurement, but rather as sets of consecutive measurements. Each with its own uncertainty and premises for filtering. Efficiency measurements are not in fact repeated, but rather reproduced for each load.

5.2 Measurement Uncertainty

This section is based on uncertainty computation in accordance to the *Guide to the expression of uncertainty in measurement* (GUM) [21].

As explained in section 2, the wave component of the process noise is a source of increased variance and therefore larger uncertainty of measurement.

The real mean X ,i.e the actual state of the measurand, can be described as the mean of the measurement values $\bar{x}$, added an error of Gaussian distribution (representing both measurement and process random noise) ϵ_g, and a possible error due to sine wave impacts on the mean ϵ_w.

$$X = \bar{x} + \epsilon_g + \epsilon_w \tag{11}$$

The probability distribution of the sine wave component impact ϵ_w is challenging to determine when the phases is considered as an unknown. To simplify the comparison of the signals before and after extraction, the data from the FFT analysis will be used, and the uncertainty of the wave component will be considered as having a rectangular distribution.

In accordance with the GUM method of uncertainty computation, for type-A evaluation of uncertainty, the contribution to the total uncertainty, $u(y)$ is given by the

equation below.

$$u(y) = c_x u(x) = s(\bar{x}) = \frac{s(x)}{\sqrt{n}} \tag{12}$$

With c_x the sensitivity coefficient ($c_x = 1$, in this case), $u(x)$ the standard uncertainty of the measurement, $s(x)$ and $s(\bar{x})$ the standard deviation of the series and the series mean, respectively.

However, a requirement for evaluating measurement uncertainties as type A is that the repeated measurements must be independent ([21], section 4.2.6). The signals with sine wave components are unfitted for a type-A evaluation. Taking this into account, the standard uncertainty $u(x)$ would not be the series mean standard deviation $s(\bar{x})$, rather the standard deviation of the dataset $s(x)$. For a rectangular distribution the standard deviation is $s(x) = a/\sqrt{3}$, with $2a$ the width of the rectangular distribution [22].

The uncertainty component of the sine wave will have a significantly larger contributions to the uncertainty than the random uncertainty, by a factor of 10. The random uncertainty component will be insignificant and therefore ignored in the evaluation of the expanded uncertainty U of the data prior to surge extraction. U is given by $U = ku_c$, with k the coverage factor, $k = \sqrt{3}$ for rectangular distribution and %95 confidence interval and $u_c(y)$ the combined uncertainty defined as $u_c(y) = \sqrt{\sum u_i(y)^2}$, the root sum square (RSS).

The reported measurement results for the mean value of the example series before and after surge extraction in figure 7 are $p_b = 1,18596 \pm 0,033\ bar$ and $p_a = 1,18554 \pm 6,5 * 10^{-6}\ bar$, respectively. This is a significant reduction of the uncertainty.

Should one have consider the uncertainty contribution of the wave component for a type A evaluation, the result would have been $p_b^* = 1,18596 \pm 6,63 * 10^{-5} bar$ (in this case random uncertainty would also have to be considered). The results uncertainty bands would not overlap ($[p_b^* \pm U_b^*] \bigcap [p_a \pm U_a] = 0$), proof that a type A evaluation is invalid on the wave uncertainty component.

5.3 A Generic Method

This method, although created for the purpose of efficiency measurements should be useful for other application. The general settings should be, as in this application, a need for a steady situations, and the effects of oscillations should be unwanted. Surges and fluctuations are common in pipe flows such as in oil, gas or water distribution. The use of this method should prove to be useful as these often

are connected to a paid provisional service. Both the customer and the provider should benefit from a correct measurements of the flow.

5.4 Use for Field Efficiency Measurements

During hydraulic field efficiency measurements on hydro power plants (HFEM) an experienced measurement crew will generally perform an assessment of the gathered data through a visual graphical inspection. Their experience and knowledge of the expected data distribution and stability is usually sufficient to detect spurious errors. The problem is that the judgement is subjective to the measurement expert's experience and knowledge. No deterministic rules can support the chief of tests judgement on whether to keep or reject a measurement.

For a HFEM doubtful and uncertain measurement data can be grouped into three categories.
- Unstable mean value, often caused by premature measurement start.
- Occurrence of surges during the measurement. This may be caused by outer influences, like the start up of a secondary unit in the power plant.
- Measurement errors, such as temporary sensor failure, e.g. signal saturation, obstructions of the sensory path or effects of outer changes in the measurement set-up (the fancy way of describing someone tripping over a cable).

These sources of errors will impact the data to a varying degree. An obstruction of the sensor path during a fraction of time may result in one outlier point, with no real impact on the end result. Others errors may be so obvious that the impact is detected through the visual inspection of the data. In between these two cases lies a multitude of possible faulty measurements that may or may not cause a rejection of the data, all depending on the subjective judgement of the chief of test during the visual inspection.

From personal experience, measurements have usually allocated very limited time for execution. In addition, long working hours in noisy environments and working under pressure can wear out the measurement crew, opening for human error. An instant data validation method for the measured data could be useful in these circumstances. This kind of automated data validation system could have its merits also for field efficiency measurements.

5.5 Signal Filtering

During the tests on randomized data, false high frequency patterns, generated from random noise, were misinterpreted by the ANOVA test and caused faulty results.

To counter this, a short term variance filter (a smoothing filter) was applied to the data. A natural choice for this type of filter was the Savitzky-Golay filter, described in Abraham Savitzky and Marcel J.E. Golays *Smoothing and Differentiation of Data by Simplified Least Squares Procedures* [23]. The filter does not have a significant impact on the mean. It smooths out the values, reducing the Gaussian noise and high frequency oscillations while the low frequency oscillations remain unaffected.

False high frequency patterns were however not an issue when testing the method on the HydroCord data. The filtering will not be used for the full implementation of the validation method, hereby avoiding unnecessary tampering with the data.

Part 2 - Continuous Efficiency Measurements

6 General Remarks

As mentioned in the introduction section, two questions need answer before a continuous efficiency measurement can be set in place. Part 1 of the thesis gave an answer to how the system could automatically validate and improve measurements. This part will provide the answer to what method should be employed for the task. The questions, although intuitively interlaced, were studied separately. It was done so because time did not allow the full implementation of the validation method to the HydroCord system prior to the tests presented in this section. It was possible because of the generic nature of the validation method (suited for any and all measurement types).

Field efficiency measurements are usually done in accordance with the IEC 60041 standard *Field acceptance tests to determine the hydraulic performance of hydraulic turbines, storage pumps and pump-turbines* [1] (IEC41). This document lists a number of options for efficiency measurements, discussed in the next section.

As any normal field efficiency measurement, care was taken to prevent disruptions during the test described in section 10. The turbine governor was locked in position during the measurement sequences, and time was given for potential pressure oscillations to die out before initiating the sequences.

From the choices of measurement methods selected (see section 7), it is clear that this second part of the thesis aims at discussing and comparing efficiency measurement methods based on different flow measurements. The other characteristics needed for efficiency computation will not differ depending on the chosen method, leading to the fact that the best flow measurement will give the best efficiency measurement. Because of this, flow measurement results will be presented and discussed, not efficiency measurement results as such. The computational steps from flow measurement results to efficiency are only briefly presented in subsection 8.1 and in the efficiency measurement report in appendix G (in Norwegian). The IEC41 provides more details which will not be presented, as it is not necessary to conclude on the question this part aims to answer.

7 Choice of Methods

Field efficiency measurements usually aim at minimizing the uncertainty of measurement. For commercial operations such as guarantee measurements, the uncertainty is critical and has a potential large financial impact. These commercial activities support the acquisition of expensive measurement sensors and costly meas-

urement set-ups. While developing the continuous efficiency measurement system other factors had to be considered. The focus was split between minimizing the uncertainty, the cost both in terms of investment and maintenance and the chance of production interruption caused by the system.

The most common methods for efficiency measurement in Norway are the thermodynamic method and the pressure-time method. For a high-head Francis turbine such as the Trollheim unit, the thermodynamic method (see IEC41, section 14) would have been a natural choice for efficiency measurements. It was considered unfit for several reasons. The measurement requires a submerged measurement frame in the draft tube. The author had concerns towards the long term durability of the frame and the costs of such a permanent installation (i.e. the frame usually occupies the draft tube gate slot for the duration of a measurement, a second shaft with lifting arrangements would most likely have been required).

The pressure-time method (IEC41, section 10.4) requires forced shut-downs to evaluate the flow. This requirement would naturally not be compatible with the goal of continuous monitoring. Also, no suitable measurement sections were available at Trollheim power plant.

Other measurement option would have been the current meter or Pitot tubes method described in the IEC, section 10.2 and 10.3. But here again a measurement frame and an expensive permanent set-up would have been needed.

For these and other reasons the choices fell on less elaborate index type methods of measurements. These measurements require calibration, but would be considerably less costly and easier to maintain. The most common method of index measurements in Norway is the Winter-Kennedy measurement (WKM). It was selected for trials with the HydroCord system at Trollheim Power plant. The choice will be better explained in the following sections.

The acoustic transit time flow measurement (ATT) is covered by the IEC41, appendix J. Numerous comparison tests with primary measurement methods (e.g [24] or [25]), have proven the measurement to be reliable. An intrusive measurement as suggested in the IEC41 would have been too costly. The comparison test *Comparison of discharge measurements -Thermodynamic to US Clamp, stationary US and Needle Opening Curve* presented by Tobias Rau, Marco Eissner at the 2012 IGHEM conference [25] provided an interesting option. The paper revealed a large relative deviation between the clamp-on ATT measurements and the thermodynamic measurements. However, the measurement section and the fact that

only one path was used were highlighted as possible explanations to the deviation. At Trollheim power plant an adequate measurement section was available. A two path clamp-on ATT flow measurement system was installed at Trollheim for trials.

Amongst the HydroCord measurements not directly related to the efficiency measurements was head-loss measurements over the emergency closing valve. Pressure loss is relative to the flow (see section 8.4) and should theoretically provide the means to estimate it. The state of the valve, naturally degrading over time would be an influencing factor, but within a limited time frame it would provide an interesting auxiliary measurement. This measurement, if relatively reliable, could be used for short-term measurement validation and comparison analysis of dynamic behaviour. The idea would be to develop an auto-calibration software running yearly and update the friction coefficient of the valve.

8 Efficiency and Flow Measurements - Scientific Foundation

This section will provide the basics of the scientific foundation used in the comparison test.

8.1 Efficiency Measurements

The hydraulic efficiency of a turbine, η_h can be computed using equation 13 (IEC41, or [26])

$$\eta_h = \frac{Mechanical\ Power}{Available\ Energy} = \frac{P_m/\eta_g}{\rho g H Q} \tag{13}$$

With P the produced power by the generator, η_g the generator efficiency, ρ the water density, g the standard acceleration due to gravity, H the turbine head and Q the flow of the water through the turbine.

Apart from the thermodynamic efficiency method, all methods aim at measuring the different characteristics listed in equation 13.

For the HydroCord system, the generator power output is monitored by an already existing system and is fed from the station Supervisory Control And Data Acquisition (SCADA) system to the HydroCord. The generator efficiency is considered static, provided by the generator supplier.

The water density ρ is computed with the use of Herbst and Rögener formula bellow [27], depending on the water temperature θ (K) and the absolute pressure

p_{abs} in (Pa).

$$\rho = 10^2 \left[\sum_{i=0}^{3} \sum_{j=0}^{3} R_{ij} \cdot \alpha^j \cdot \beta^{(i-1)} \right]^{-1} \tag{14}$$

Where:

$$\alpha = \frac{1}{\theta^*}(\theta - \theta_1)$$

$$\beta = \frac{1}{p^*}(p_{abs} + 200 \cdot 10^5)$$

With $p^* = 10^5$, $\theta^* = 1\ (K)$ and

$$\theta_1 = \begin{cases} 273.15\ for\ \theta \in [273.15; 293.15] \\ 293.15\ for\ \theta \in [293.15; 323.15] \end{cases}$$

A table providing the R_{ij} values can be found in the IEC41, section E8.

The standard gravity is given by equation (IEC41,appendix E).

$$g = 9,7803(1 + 0,0053sin^2\varphi) - 3.10^{-6}z \tag{15}$$

With φ the latitude (degrees) and z the altitude above sea level (masl).

The turbine head H is computed based on the pressure measurements upstream and downstream the runner.

The flow measurement Q is usually the measurement with the highest contribution to the combined measurement uncertainty and therefore described in details in the IEC41. The following subsections will give further details to the different flow measurements set-up within the HydroCord system.

8.2 Winter-Kennedy Flow Measurement

The Winter-Kennedy index method is described in the IEC41, section 15.2.1. The measurement set-up is simple, only a differential pressure measurement is needed between an inner and an outer tap on a section of the spiral casing.

The IEC41 states that the flow $Q(m^3/s)$ can be estimated by the equation 16.

$$Q = kh^n \tag{16}$$

Where k is a calibration coefficient, h the measured differential pressure and $n = 0.5$ (theoretically).

During the comparison test (see the full paper in appendix D) different models were tested and a polynomial model such as the one described by equation 17 was deemed superior, i.e. showed smaller residual values when comparing the regression models, and therefore selected.

$$Q = b_1 h^2 + b_2 h + b_3 \tag{17}$$

Where b_{1-3} are the calibration coefficients.

8.3 Acoustic Transit Time flow Measurement

The acoustic transit flow method is described in the IEC41, appendix J. The measurement is based on the principle that the travel time between acoustic emitters will be altered in accordance to the velocity of the fluid the signal crosses.

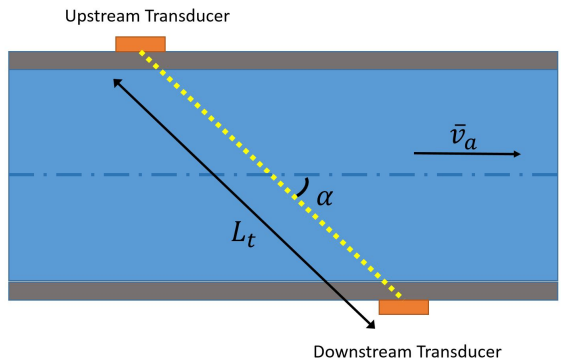

Figure 9: Clamp-On Acoustic Transit Time Principle Diagram
Audio emitters/transducers send a signal back and forth to each other through the pipe walls. The average velocity $\bar{v}_a$ of the flow in the pipe is measured by the affected signal travel time between transducers.

The transit time is given by equation 18.

$$t = \frac{L}{c + \varepsilon \bar{v}_a cos(\alpha)} \tag{18}$$

Where: L_t is the distance between transducers, c the sonic speed in the fluid, α the angle between the pipe centreline and the acoustic path, $\bar{v}_a$ averaged axial velocity in the measurement section and ε = +1 or -1 for signals travelling downstream or upstream.

The equipment was supplied with a data acquisition and processing module. Once computed, the flow measurement results Q_{raw} were collected by the HydroCord system. The embedded calibration software was used prior to the test by input of the required static values, i.e. measurement section size and shape, distance between probes, and so on. The data collected was therefore a flow estimation with high systematic uncertainty, as the input values were partially based on measurements and partially on estimated data. An example is the pipe thickness which was retrieved from the production drawings of the pipe, not measured.

To reduce the systematic uncertainty a second calibration was performed to compute the flow Q_{ATT} with reduced uncertainty. The calibration model is described by equation 19.

$$Q_{ATT} = \kappa Q_{raw} + Q_0 \tag{19}$$

With κ the calibration coefficient and Q_0 the bias.

8.4 Head-Loss Based Flow Measurement

The HydroCord system monitors a number of characteristics. Amongst these are several head-loss measurements. The emergency closing valve, a butterfly type valve, head-loss measurement was selected for the third flow measurement. The head-loss ΔH is proportional to the squared velocity of the water V^2, and can be characterized by the Darcy-Weisbach equation, in terms of Q as in equation 20 [28].

$$\frac{\Delta H}{L} = f_D \cdot \frac{8}{\pi^2 g} \cdot \frac{Q^2}{D^5} \tag{20}$$

Where L is the length, f_D the Darcy Friction Factor and D the Hydraulic diameter of the pipe.

A bias Q_0, likely caused by an offset of the measurement system was detectable and added to the model. The regression model was improved further (ANOVA test results) by also adding a first order term. This is because of fact that the friction factor f_D is a function of the Reynold number Re, varying with the flow. The equation for head-loss based flow measurements is defined as below.

$$\Delta H = k_1 Q^2 + k_2 Q + Q_0 \tag{21}$$

9 Measurement Set-Up

9.1 Trollheim Power Plant and HydroCord

Trollheim power plant is a single unit 130 MW Francis type power plant situated in Surnadal, Norway. Because of minimum flow requirements, the power plant is often run at part load. To improve production and maintenance the plant was selected for the HydroCord pilot project, called "BlackBox".

The system is presented in paper II (appendix C). This section will give a brief overview.

Figure 10 displays on a generic hydro power plant figure, the location of five data acquisition hubs. All hubs communicate via Transmission Control Protocol/Internet Protocol (TCP/IP) through a fibre system partly upgraded through the project. All hubs collect data from multiple sensors placed in the vicinity through a compact-RIO with an Field-programmable gate array (FPGA). The figure displays the different measurements performed at each location. At the time of writing most of the measurements listed are in place and submitting data to the HydroCord system.

Location 1, the intake, had the hub installed close to the innlet gate shaft. Most of the instrumentation had to be placed in the waterway, with cables clamped up the shaft. These where installed during a waterway maintenance project and are about the only sensors unavailable for control and maintenance during normal operation.
Location 2 is the emergency closing valve chamber where, amongst other measurements, the acoustic transit time flow measurement was placed.
Location 3 is in the control room, where the hub in fact is the HydroCord system server. The server is programmed to perform post measurement data analysis and computes secondary measurement values and derived values directly usable by the power plant owner stakeholders. This location is also the only hub acquiring data from exterior channels, i.e. the server communicates to the plant SCADA system through an IEC 101 protocol at this location. It also records bearing vibrations from a newly acquired turbine protection system. Connected to the hub is a data storage unit (NAS), where all data both processes and raw are stored.
Location 4, the turbine floor, is naturally the hub collecting the most data, referring here to figure 10.
Location 5, the outlet was one of the locations where the project had to upgrade the communication system to fibre.

An interesting challenge the team faced while designing the measurement system

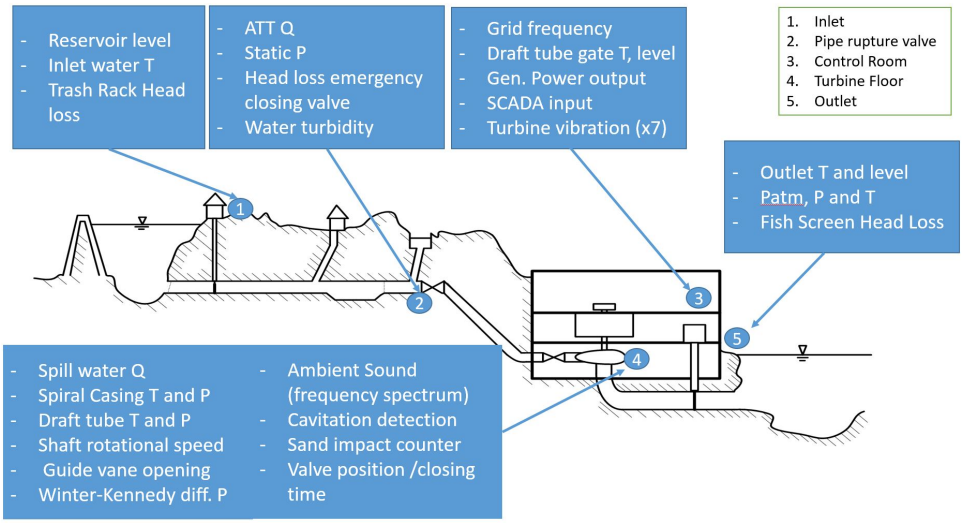

Figure 10: Trollheim - HydroCord Data Acquisition Hubs
Location of the HydroCord data acquisition hubs collecting the raw data from the measurement set-ups spread through the waterway system. The letters Q, T and P designate in order a flow, temperature or pressure measurement. Note that the power plant figure is generic.

was time synchronisation. The measurement hubs are geographically far apart and some of the computed secondary results would be false without a proper synchronisation. A Precision Time Protocol (PTP), defined in the IEEE 1588-2002 standard was used with good results. A GPS (placed in hub 5) was coupled to the HydroCord system to ensure correct timestamping for comparison and computation with measurements outside the HydroCord system.

9.2 Hydrocord - Flow Measurements

The ATT transducers were mounted upstream the emergency closing valve. The section was chosen because no bends, constrictions or disturbing elements exist upstream, within and beyond the recommended ten conduit diameters (IEC41, appendix J). Downstream on the other hand, the emergency closing valve was estimated to be approximately two diameters away from the measurement section, closer than the IEC41 recommendations. This still represented the best measurement section available, and the disturbance being merely the valve disc it was believed that the measurement would be acceptable.

The access to the tunnel leading to the chamber was difficult. Snow-scooters could be used when the snow was ample, and regular vehicles could be used during summer but all conditions in between where problematic and the project experience many delays because of this. The valve was replaced after the first attempt to mount the ATT system, causing further delays.

The Winter Kennedy measurement pressure taps were located in accordance with the IEC41 section 15.2, in the bottom half of the spiral casing (because of accessibility). The pressure taps where made during the project where a third party was hired to control the welding as the spiral casing is a high pressure component. To prevent debris from clogging the pressure taps an automated flushing system was designed and installed. Two valves connected to the pressure taps open at a set frequency (twice a day at the time of writing). During the flushing sequence the measurement will be disturbed. The automated quality control software will ensure that the data is not used for efficiency computation or for any controlling purposes of the other flow measurements.

A differential pressure measurement was installed over the emergency closing valve for head loss measurements. Both the upstream and downstream section has installed four pressure taps connected to a collector. The pressure taps were evenly distributed around the section with a maximum distance to the top and bottom of the pipe to avoid air or debris in the taps.

10 Continuous Flow Measurements - Results

10.1 Calibration

The flow measurement computed based on thermodynamic efficiency measurement, stated as a primary method in the IEC41, was used as a reference measurement to calibrate the index-type flow measurements of the HydroCord system. The efficiency measurement project was lead by the author, but performed by Flow Design Bureau (FDB), with H. Francke as the chief-of-tests. The measurement set-up, methods and theory can be found in the attached measurement report by FDB in appendix G. Note that the owner of the technology used to design the Trollheim runner has allowed the publication of the efficiency report, see appendix F.

Most measurements necessary for the thermodynamic efficiency measurements were set up temporarily and were apart from the HydroCord measurement systems own measurements, i.e. rented sensors and a separate data acquisition system

was used. This enabled a broad test of the different measurements of the Hydro-Cord in addition to the flow measurements discussed in this section.

The calibration work was done by the author, the reports can be found in appendix E. The following subsections are summaries of the calibration reports.

Winter-Kennedy Flow Measurement

As can be seen from figure 11, the linear model described in section 8.2 is well suited. The deviations of the measured points is acceptable, and the repeated measurements indicate an acceptable repeatability. The variation of the data seem to increase with the flow.

The uncertainty of the flow measurement is shown in figure 12. Although clearly showing a trend, the uncertainty could not be described by a simple polynomial form like the ATT and HLM uncertainties.

Acoustic Transit Time Flow Measurement

As can be seen from figure 13, the linear model described in section 8.3) is also well suited. The deviations of the measured points are small, and the repeated measurements underlines the good repeatability of measurement.

The uncertainty of the flow measurement is shown in figure 14. The uncertainty shows a trend (polynomial of the second degree) added to the figure.

Head-Loss Based Flow Measurement

Because of a technical error during the measurement set-up, the head-loss measurement reached saturation for flows above 28 m^3/s. There were therefore significantly fewer measurement points to base the calibration on.

As can be seen from figure 15, the linear model described in section 8.4) is well suited for the recorded measurements. The deviations of the measured points from the modelled values is acceptable, and the repeated measurements indicate an acceptable repeatability. However with measurement only up till 28 m^3/s one should expect a larger model uncertainty than the ATT or WKM measurements.

The uncertainty of the flow measurement is shown in figure 16. The uncertainty shows a trend (polynomial of the second degree) added to the figure.

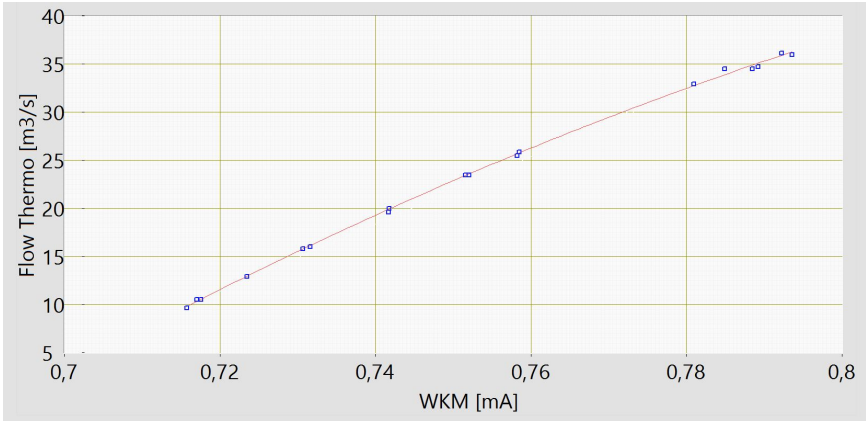

Figure 11: HydroCord Calibration - Winter-Kennedy Flow Measurement
The graph shows the measured WKM values in relation to the reference flow. The curve shows the selected model for calibration.

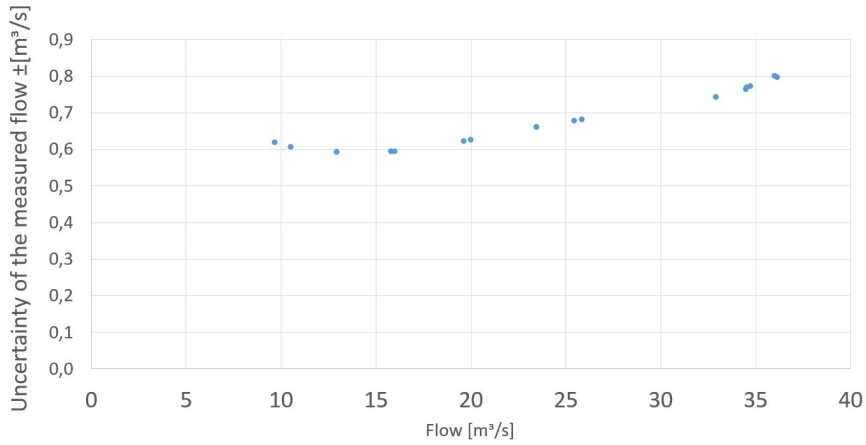

Figure 12: HydroCord Calibration - Winter-Kennedy Flow Measurement Uncertainty
The graph shows the WKM measurement uncertainty in relation to the reference flow.

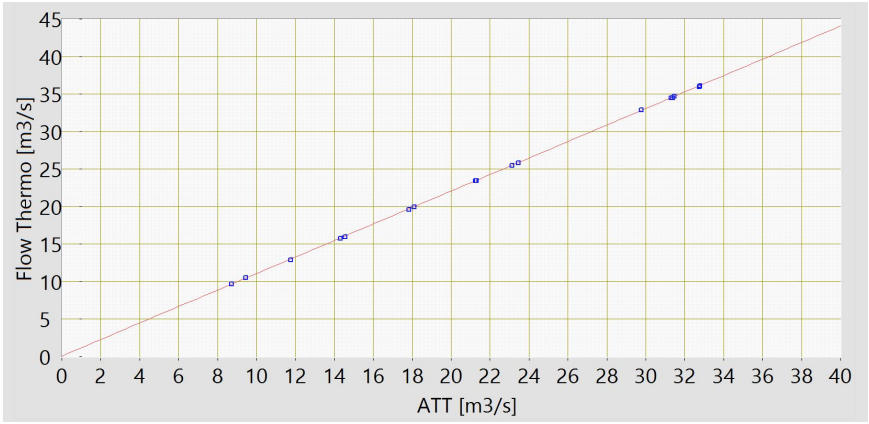

Figure 13: HydroCord Calibration - Acoustic Transit Time Flow Measurement
The graph shows the measured ATT values in relation to the reference flow. The curve shows the selected model for calibration.

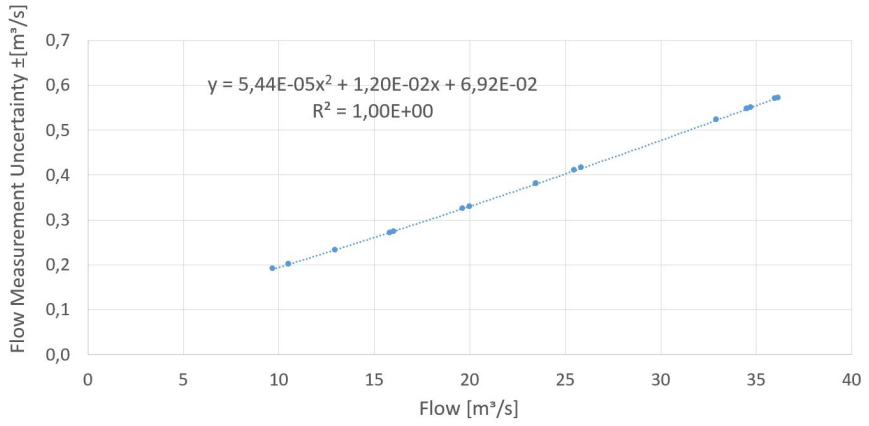

Figure 14: HydroCord Calibration - Acoustic Transit Time Flow Measurement Uncertainty
The graph shows the ATT measurement uncertainty in relation to the reference flow. A polynomial trend line was added with it's equation displayed in the figure.

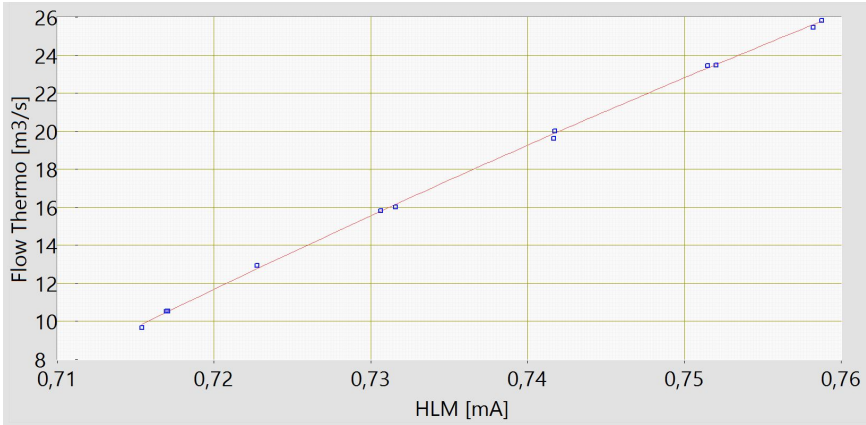

Figure 15: HydroCord Calibration - Acoustic Transit Time Flow Measurement
The graph shows the measured ATT values in relation to the reference flow. The curve shows the selected model for calibration.

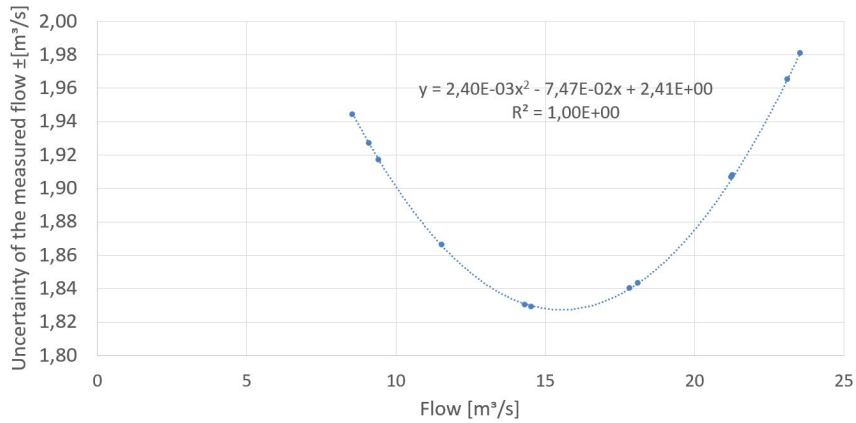

Figure 16: HydroCord Calibration - Head-loss Based Flow Measurement Uncertainty
The graph shows the HLM uncertainty in relation to the reference flow. A polynomial trend line was added with it's equation displayed in the figure.

10.2 Comparison

Figure 17 presents the calibrated flow measurements by the three methods. To better visualise the signals figure 18 shows a cut out of the series. From a visual inspection it is clear that there is a good correlation between the measurements, confirmed by the correlation analysis presented in paper II appendix C.

Some deviations between the measurements are observable, e.g. the HLM values are significantly lower at the highest flow presented. This - like all deviations observable in the graph - is however not consistent we can therefore conclude that it is not due to a systematic error.

From the graph in figure 18 we see that the ATT shows less variation than the two other methods.

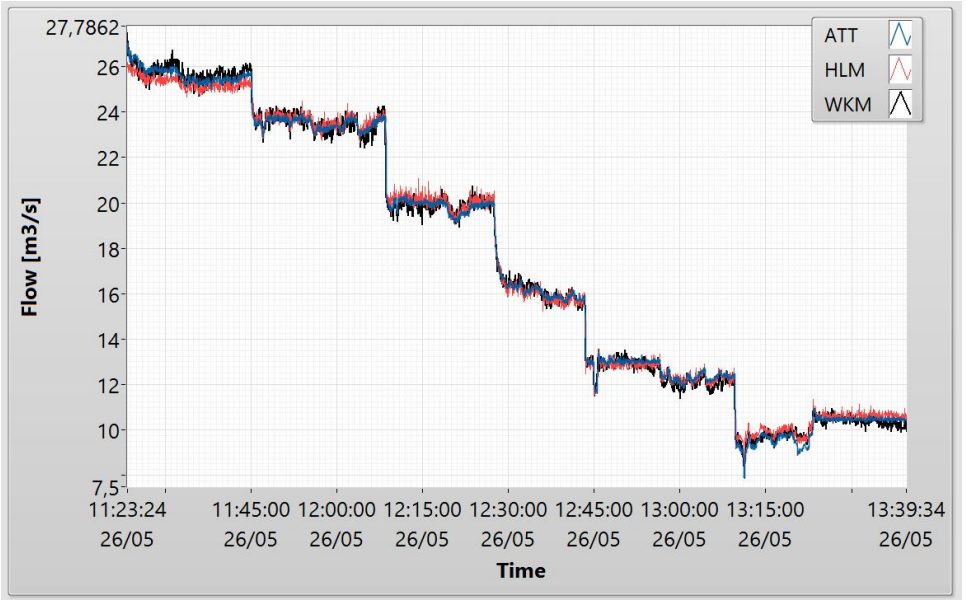

Figure 17: HydroCord Flow Measurements
The graph shows the measured ATT (blue), WKM (black) and HLM (red) flow measurements recorded during the test after calibration.

The paper *Continuous Efficiency Measurements on Hydro-Power Turbines - A Comparison Between Acoustic Clamp-on Flow Measurement and the Winter-Kennedy*

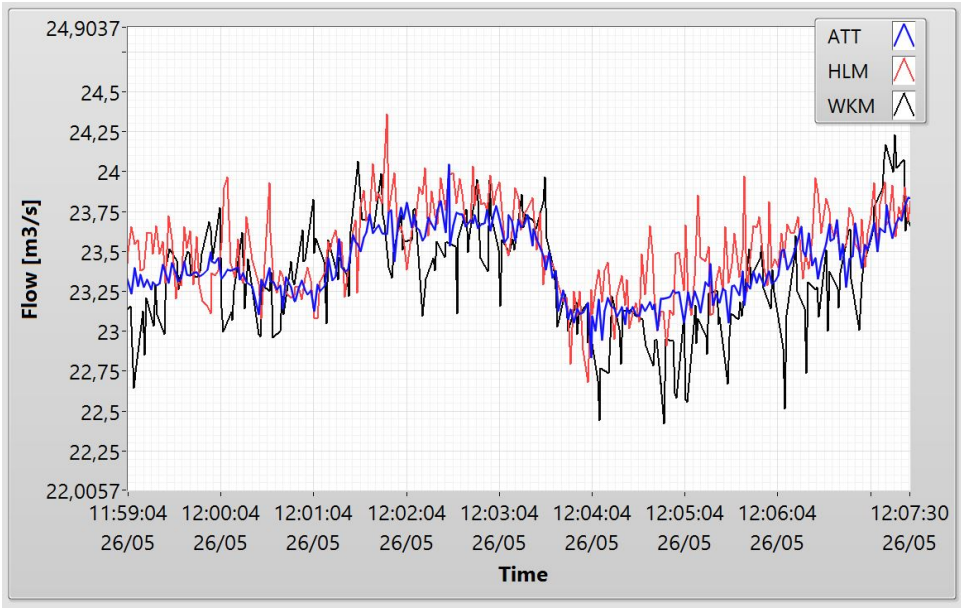

Figure 18: HydroCord Flow Measurements Sample
The graph shows the measured ATT (blue), WKM (black) and HLM (red) flow measurements recorded during the test after calibration.

Index Method, appendix D [29] presents the comparison test results. Below are the main results.

Figure 19 displays all measurements performed during the calibration test. The uncertainty bands of the ATT and WKM measurements clearly show that the ATT measurement is superior i.e. has lower uncertainty, than the WKM. This is confirmed by the visual display of larger variance of the WKM measurements in particular for high loads.

The HLM uncertainty band was omitted from figure 19 for visual purposes. It is off-chart and clearly inferior to the two other measurement. The fact that the regression model was based on significantly fewer measurement points may be part of the reason.

Apart from the uncertainty the ATT and WKM method have very different requirements when it comes to the measurement set-up. The WKM only requires two

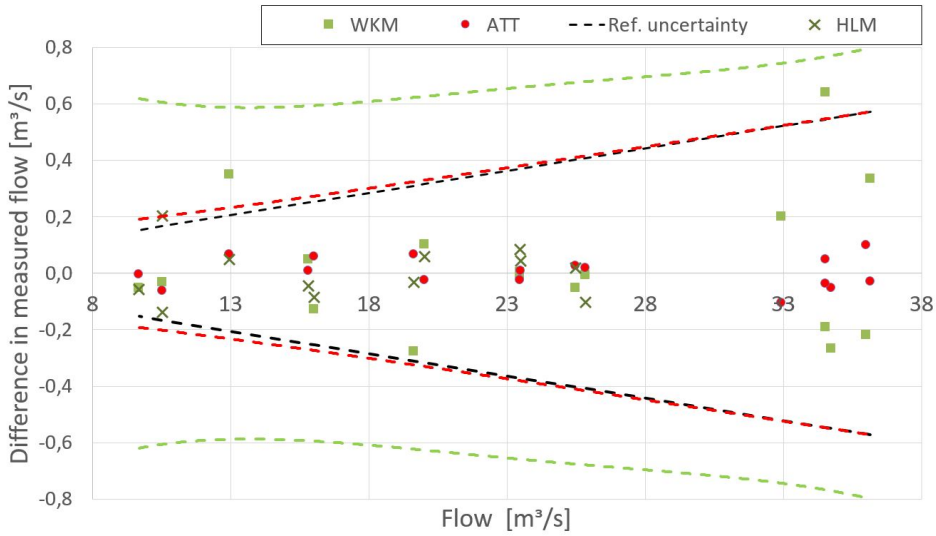

Figure 19: HydroCord Flow Measurements - Comparison
The graph shows the difference between the three HydroCord flow measurements and the reference measurement (in m^3/s). Also displayed are the reference, ATT and WKM uncertainty bands centred around x-axis.

pressure taps on the spiral casing, and therefore access to a segment of the spiral casing, and a differential pressure measurement. It remains the less costly method, both in terms of investment and maintenance. To ensure a good ATT measurement an adequate measurement section must be available (IEC41, appendix J or section 8.3). This was the case for Trollheim, but experience show that this may not always be the case [25].

11 Flow Measurements - Discussion

The thermodynamic efficiency measurement is a direct measurement of the losses through the turbine. It has proven its worth through numerous comparison tests (e.g. [24], [30], [25] and many more). The only flaw of the method when it comes to the calibration of the flow measurements at Trollheim is the fact that it is a direct measurement of the efficiency and therefore does not include a direct flow measurement. As such the flow uncertainty may have been larger than it would have been using another method. This is further discussed in paper III (appendix D).

The calibration and comparison test presented here show that the uncertainty of measurement for the ATT method is the smallest, and that this should be considered as the main flow measurement for the HydroCord system. It is, as mentioned early a confirmation of a good measurement section even with the emergency closing valve situated closer to the section than recommended by the IEC41.

Part 3 - Final Conclusion and Further Work

12 Final Conclusion

The automated quality control method presented in part 1 of this thesis has proved that it meets the requirements needed for a continuous efficiency monitoring system. It is now ready for implementation in the HydroCord system. Studies performed on the data where successfully conducted to determine initial parameters and settings for the three steps of the method.

The three-step method ensures that only stable measurements are processed for efficiency computation. The study performed on both synthetic and actual HydroCord data, proved that the method rejects all measurements during transient states and periods of fluctuating measurements, such as may be caused by grid instability.

Steady state pressure oscillations, often evident in the data and the cause of high uncertainty in the measured mean value, where successfully extracted numerically by the method, ensuring the uncertainty was kept to a minimum. The tests confirmed the oscillations not to be a source for rejection by the three-step validation method.

The test results proved that the clamp-on two path acoustic transit time was the best method for flow measurement. General requirements for the method for continuous efficiency measurements, i.e. the cost-benefit and ease of maintenance requirements, discouraged the use of any primary method. The selection between the available index methods was done after a comparison test of three different measurement methods, all implemented to the HydroCord system at Trollheim power plant. The Winter-Kennedy method and head-loss based method will serve as controlling measurements for the ATT flow measurement.

The design of a fully functional and trustworthy continuous hydraulic efficiency monitoring system for Trollheim Power Plant is completed and ready for implementation. The combined efforts both in terms of pre-processing validation and signal handling along with the good results from the flow measurement tests, will ensure a reliable automatic efficiency monitoring, even during day-to-day operation.

13 Further Work

13.1 Validation

During field measurements, sensor errors like signal saturation or blocked sensory path are usually easily detected by visual review of the data or through the Grubbs test. To ensure that these types of errors are detected in the case of continuous measurements, an additional control rule could be added to the system. Should, for example three consecutive sample points return the exact same value - given that the sensor resolution is high enough - one should be notified of the possibility that an error of this kind has occurred.

Using the method for field efficiency measurements, as mentioned in section 5.4 would require some additional work with the software. Mostly this would be to avoid automatic rejections of good measurements (type 1 errors) which are time consuming and must be minimized. A visual displays of the detailed analysis results aiding a human interaction process as a final judgement of the measurements would have to be added to the validation software.

13.2 Efficiency Measurement Methods

As mentioned in paper III (appendix D), the head-loss based flow measurement shows promise, and a new calibration test should be performed after ensuring that the signal does not saturate.

Time and financial constraints hindered another planned test for efficiency monitoring, a simplified index type version of the thermodynamic efficiency measurement method. The simplification would have consisted in a downstream temperature measurement without the use of a measurement frame. The hypothesis is that a single point temperature in the outlet could lead to an assumption of the average temperature in the draft tube.

As mentioned earlier, no pressure taps existed in the pennstock for the use of the pressure-time (Gibson) method of efficiency measurement. Had this been the case, a step-wise flow measurement based on a method presented at the tenth IGHEM conference in Brasil in 2014 [31] could be endeavoured. This should be considered in future installations.

13.3 New Potential for Future Research

Some of the large quantities of data recorded by the HydroCord system will be released publicly to support research and development projects to the industry in

general. A piece of software sorting and translating the binary data to a more user friendly format should also be made and released.

One of the most interesting future results from the installation of the HydroCord system at Trollheim will be the continuously updated Hill-chart of the runner. In some years the data collected should be analysed and hopefully help understand more about the efficiency degradation over the years.

Bibliography

[1] IEC, "Iec-60041, field acceptance tests to determine the hydraulic performance of hydraulic turbines, storage pumps and pump-turbines," 1991.

[2] A. Whillier, "On-line determination of the performance of high-head pumps handling any liquid," *The South African Mechanical Engineer*, vol. 20, no. 1, 1970. [Online]. Available: http://www.ighem.org/Papers_GPMT/53.pdf

[3] H. Larsson, "Method and apparatus for monitoring hydro turbine plants," Aug. 4 1987, uS Patent 4,683,718.

[4] J. Nicolle, G. Proulx, and L. Martell, "Online flowrate monitoring experiences at hydro-québec." IGHEM, 2012. [Online]. Available: http://www.ighem.org/Papers_IGHEM/364.pdf

[5] E. Coté and E. Cloutier, "Prototype hill chart testing of a saxo unit." IGHEM, 2010. [Online]. Available: http://www.ighem.org/Papers_IGHEM/299.pdf

[6] "Data quality assessment: A reviewer's guide," U.S. Environmental Protection Agency, Tech. Rep. EPA QA/G-9R, 2006.

[7] "Epaqa/g-9s - data quality assessment: Statistical methods for practitioners," Unites States Environemental Protection Agency, Tech. Rep., 2006. [Online]. Available: http://www.epa.gov/quality/qs-docs/g9r-final.pdf

[8] P. I. Good and J. W. Hardin, *Common errors in statistics (and how to avoid them)*. John Wiley & Sons, 2012.

[9] E. Wiborg, H. Hulaas, H. Francke, and T. Nielsen, "Applied statistical quality control on field measurement data," International Group for Hydraulic Efficiency Measurement, Tech. Rep., 2014. [Online]. Available: http://www.ighem.org/Papers_IGHEM/392.pdf

[10] R. Strong, "Method and apparatus for forms data validation and processing control," Dec. 26 2000, uS Patent 6,167,523. [Online]. Available: https://www.google.com/patents/US6167523

[11] M. Scholz, "Validation of nonlinear pca," *Neural processing letters*, vol. 36, no. 1, pp. 21–30, 2012.

[12] D. C. Montgomery, *Statistical Quality Control, A Modern Introduction, 7 - International Student Version ed.* Wiley, 2013.

[13] J. Walker, R. Resnick, and D. Halliday, *Fundamentals of physics*. Wiley, 2008.

[14] R. Leadbetter, "Surge filter for pulsating gases," 1940, uS Patent 2,189,425. [Online]. Available: https://www.google.com/patents/US2189425

[15] C. Alexander, C. K. Alexander, and M. Sadiku, *Fundamentals of electric circuits*. Urban Media Comics, 2006.

[16] N. E. Huang, Z. Shen, S. R. Long, M. C. Wu, H. H. Shih, Q. Zheng, N.-C. Yen, C. C. Tung, and H. H. Liu, "The empirical mode decomposition and the hilbert spectrum for nonlinear and non-stationary time series analysis," in *Proceedings of the Royal Society of London A: Mathematical, Physical and Engineering Sciences*, vol. 454, no. 1971. The Royal Society, 1998.

[17] F. J. Harris, "On the use of windows for harmonic analysis with the discrete fourier transform," *Proceedings of the IEEE*, vol. 66, no. 1, pp. 51–83, 1978.

[18] J. Fourier, "Mémoire sur la propagation de la chaleur dans les corps solides," *Nouveau Bulletin des Sciences de la Société Philomathique de Paris*, vol. 6, 1808.

[19] National Instrument, "The fundamentals of fft-based signal analysis and measurement in labview and labwindows/cvi," 2009. [Online]. Available: http://www.ni.com/white-paper/4278/en/

[20] ——, "Understanding ffts and windowing," 2015. [Online]. Available: http://www.ni.com/white-paper/4844/en/

[21] JCGM, "Evaluation of measurement data - guide to the expression of uncertainty in measurement," 1995. [Online]. Available: http://www.bipm.org/en/publications/guides/gum.html

[22] NIST Physical Measurement Laboratory, "Evaluating uncertainty components: Type b," NIST. [Online]. Available: http://physics.nist.gov/cuu/Uncertainty/typeb.html

[23] A. Savitzky and M. J. Golay, "Smoothing and differentiation of data by simplified least squares procedures." *Analytical chemistry*, vol. 36, no. 8, pp. 1627–1639, 1964.

[24] H. Hulaas and F. Rasmussen, "A comparison of thermodynamic and acoustic measurements at kobbelv power plant," SINTEF, Tech. Rep., 1988. [Online]. Available: http://www.ighem.org/Papers_GPMT/158.pdf

[25] M. E. Tobias Rau, "Comparison of discharge measurements -thermodynamic to us clamp, stationary us and needle opening curve," IGHEM, Tech. Rep., 2012. [Online]. Available: http://www.ighem.org/Papers_IGHEM/363.pdf

[26] P. Dörfler, M. Sick, and A. Coutu, *Flow-Induced Pulsation and Vibration in Hydroelectric Machinery: Engineers Guidebook for Planning, Design and Troubleshooting*. Springer Science & Business Media, 2012.

[27] G. Herbst and H. Rögener, *Eine neue kanonische Zustandsgleichung des Wassers und ihre Anwendung auf das" Thermodynamische Messverfahren" bei hydraulischen Kraft-und Arbeitsmaschinen:(mit Arbeitsblättern für e. vereinfachtes Auswertungsverfahren)*. VDI-Verlag, 1977.

[28] G. O. Brown, "The history of the darcy-weisbach equation for pipe flow resistance," *Environmental and Water Resources History*, vol. 38, no. 7, pp. 34–43, 2002.

[29] E. Wiborg, H. Francke, and T. Nielsen, "Continuous efficiency measurements on hydro-power turbines a comparison between acoustic clamp-on flow measurement and the winter-kennedy index method," *Journal of Fluids Engineering*, [To be pulished].

[30] E. N. Harald Hulaas, L. Parr, "Comparison between the pressure-time and the thermodynamic method on a 52m net head plant," IGHEM, Tech. Rep., 2014. [Online]. Available: http://www.ighem.org/Papers_IGHEM/377.pdf

[31] R. Eckerstoerfer, L. Gotsh, and J. Lanzersdorfer, "Feasibility study of the cascading mass flow rate evaluation as a new variant of gibson's method." IGHEM, 2014. [Online]. Available: http://www.ighem.org/Papers_IGHEM/381.pdf

Appendix

A Automated Validation Case Study

1 Case study

The following will present the results of a case study of the automated validation method developed for the HydroCord system. This should be considered as a supplement to the example data presented in the PhD thesis *Continuous Efficiency Measurements on Hydro Power Plants*, by Erik J. Wiborg.
Below are the full measurement series used in the case study. The graphs are the equivalent to the ones that can be found in the thesis, but for acoustic transit time flow measurements and the pressure measurements upstream the turbine (penstock outlet pressure). Marked on the graphs are measurement series who's analysis results are presented in the following sections. To cover a larger spectre of cases the high frequency penstock pressure measurements (200 Hz) where selected instead of the 1 Hz values.

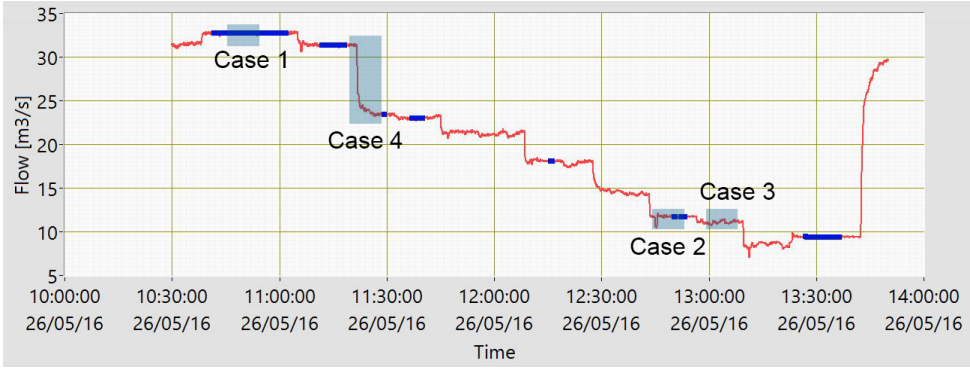

Figure 1: HydroCord ATT flow Measurements Values - 1 Hz

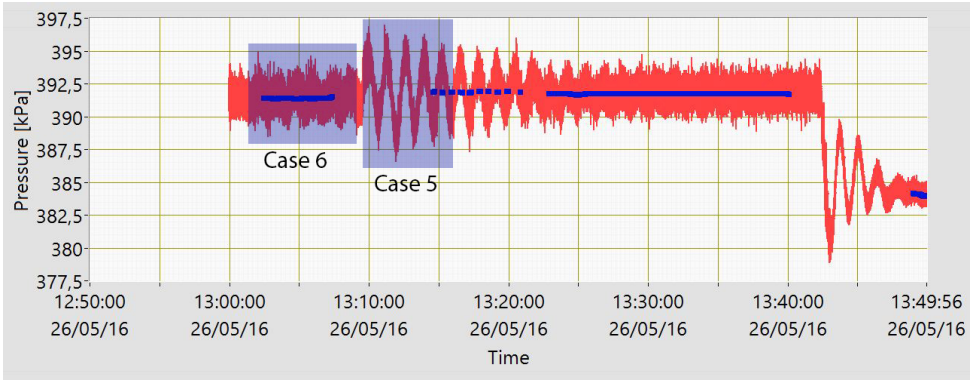

Figure 2: HydroCord penstock outlet pressure - 200 Hz

Case 1 - Normal distribution

Displaying the results of example case 1 - normally distributed data. The dataset was run through the automated validation method and approved for efficiency computation without undergoing surge extraction. Figure 1 displays the measured data and visualises the control limits (red lines). Below the graph is a table with the analysis main results, and a histogram of the data distribution for control purposes.

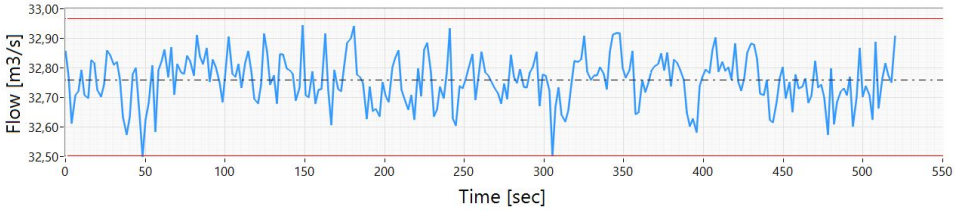

Case	1
Measurement	ATT Flow measurement
Violation count	1
Allowed Violations	8
SQC result	Accepted
ANOVA F-ratio	0.78
ANOVA Critical F-ratio	4.00
ANOVA results	Normal distribution
Surge extraction	0
Verdict	Accepted

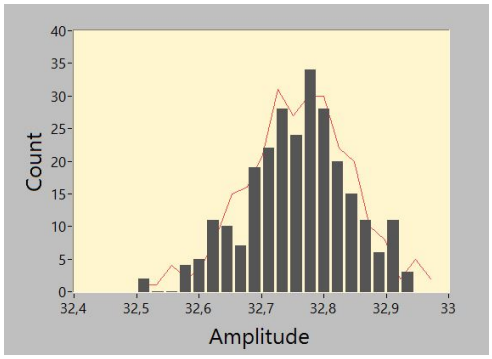

Case 2 - Causal Error

Displaying the results of example case 2 - Causal Error. The dataset was rejected by the SQC step because of a too high rule violation count. The data fluctuation is an example of a short lived causal error manifested in a deviation of the values.

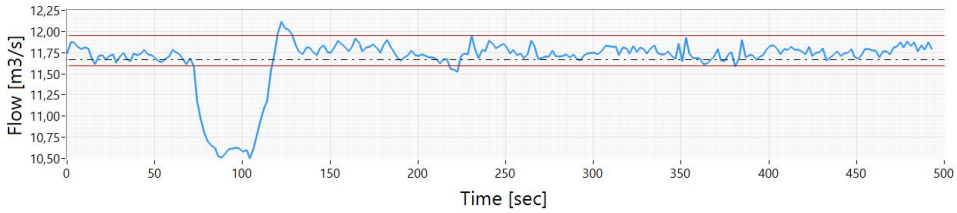

Case	2
Measurement	ATT Flow measurement
Violation count	33
Allowed Violations	8
SQC result	Rejected
ANOVA F-ratio	-
ANOVA Critical F-ratio	-
ANOVA results	-
Surge extraction	0
Verdict	Rejected

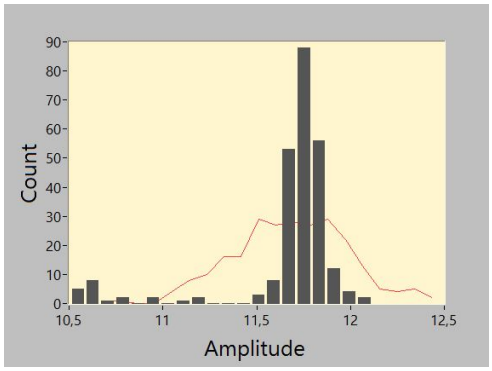

Case 3 - Fluctuating values

Displaying the results of example case 3 - Fluctuating values. The dataset was rejected by the SQC step because of a too high rule violation count. The data fluctuation was likely caused by temporary grid instability. Note that the observed oscillation does not have a set frequency or amplitude, excluding a waterway surge as the main cause for the fluctuations.

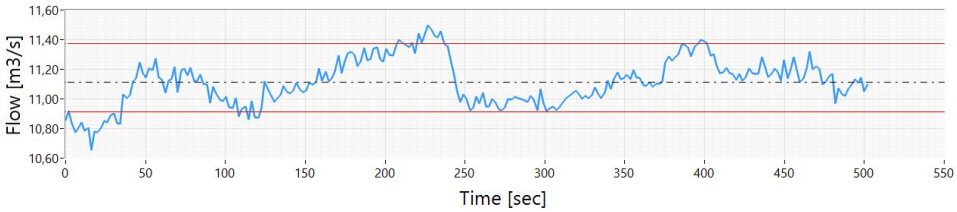

Case	3
Measurement	ATT Flow measurement
Violation count	35
Allowed Violations	8
SQC result	Rejected
ANOVA F-ratio	-
ANOVA Critical F-ratio	-
ANOVA results	-
Surge extraction	0
Verdict	Rejected

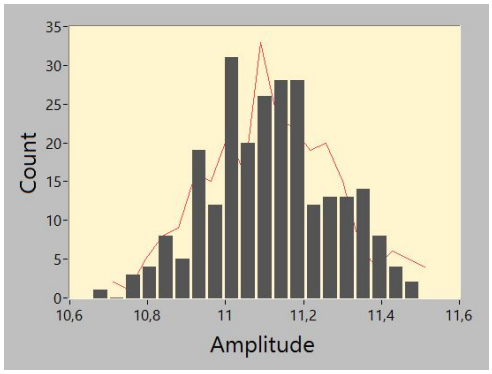

Case 4 - Unit regulation

Displaying the results of example case 4 - Unit Regulation. The dataset was rejected by the SQC step because of a too high rule violation count. The measurement is clearly performed during regulation and is rejected.

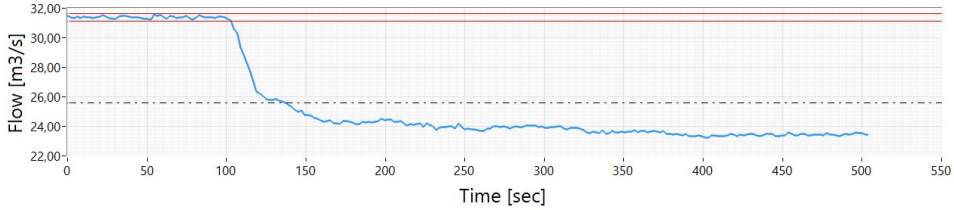

Case	4
Measurement	ATT Flow measurement
Violation count	199
Allowed Violations	8
SQC result	Rejected
ANOVA F-ratio	-
ANOVA Critical F-ratio	-
ANOVA results	-
Surge extraction	0
Verdict	Rejected

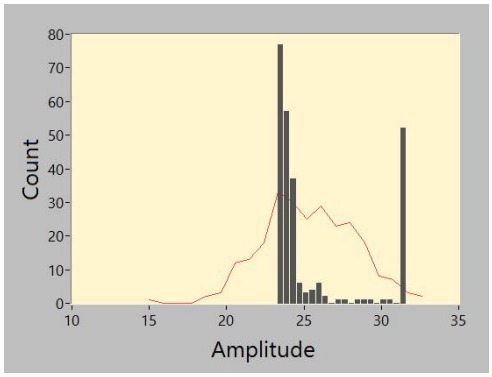

Case 5a - Transient State Amplitude Rejection

Case 5 presents typical data collected from transient states, as in this case after a load change. The surges are of such an amplitude that the SQC method recorded too many violation.

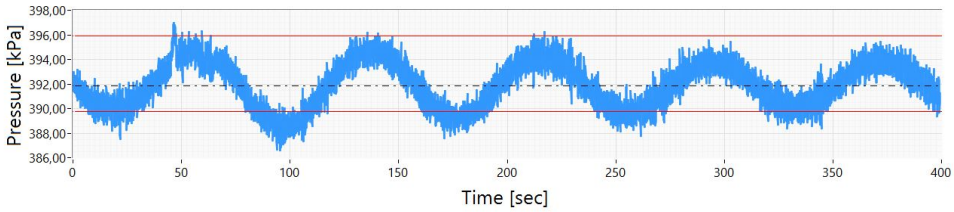

Figure 3: Original data

Case	5a
Measurement	Pennstock outlet pressure
Violation count	11678
Allowed Violations	2396
SQC result	Rejected
ANOVA F-ratio	-
ANOVA Critical F-ratio	-
ANOVA results	-
Surge extraction	0
Verdict	Reject

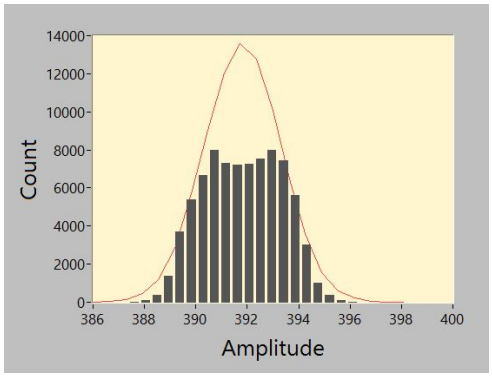

Case 5b - Transient State Unsteady Surge Rejection

The difference from case 5a is that the SQC study period managed to capture enough of the surge to produce control limits encasing most of the surging dataset. However, the surges are unsteady and will therefore not be correctly removed by the surge extraction process. Typically - like in the case presented here - the surge removal process will actually add oscillations after the first loop. This case illustrated the need for a default rejection after a certain number of loops, in cases where the SQC does not reject the data after a failed surge extraction.

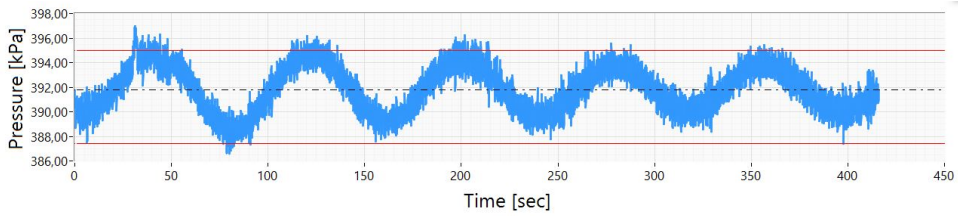

Figure 4: Original data

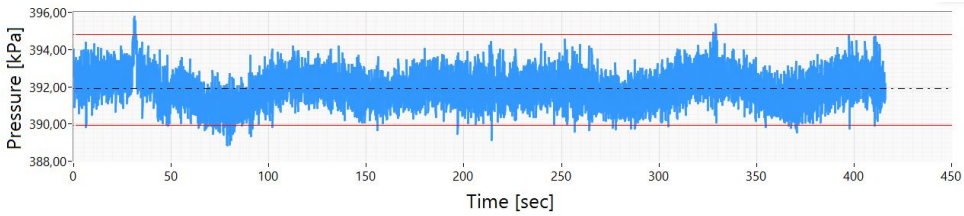

Figure 5: Surge extracted data

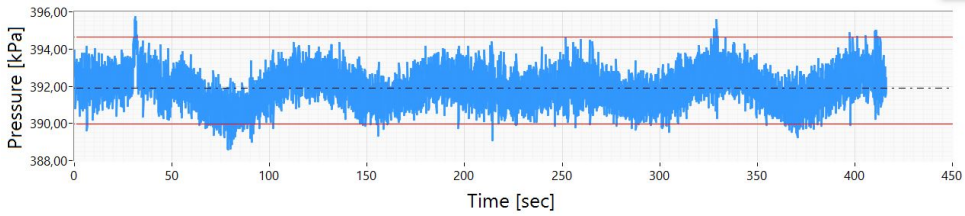

Figure 6: Twice surge extracted data

Case	5b	5b	5b
Measurement	Pen. outlet P	Pen. outlet P	Pen. outlet P
Violation count	1831	429	904
Allowed Violations	2496	2496	2496
SQC result	Accepted	Accepted	Accepted
ANOVA F-ratio	11.5	8.05	8.25
ANOVA Critical F-ratio	2.49	2.49	2.49
ANOVA results	Not Normal	Not Normal	Not Normal
Surge extraction	0	1	2
Verdict	Surge extraction	Surge extraction	Reject

Case 6 - Successful surge extraction

Displaying the results of example case 6 - Successful surge extraction. Contrary to case 5, the oscillation are relatively steady state and the surge extraction process was successful. From the first 100 seconds of measurements we see that the extraction is not perfect, the ANOVA step of the method indicate does however indicate a normal distribution. This implies that the mean value will not be significantly altered by the remains of the surge visible in the dataset first part.

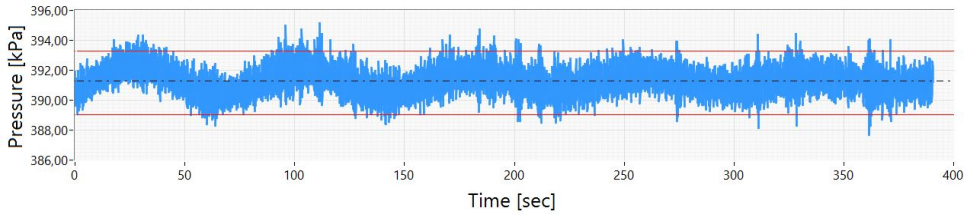

Figure 7: Original series

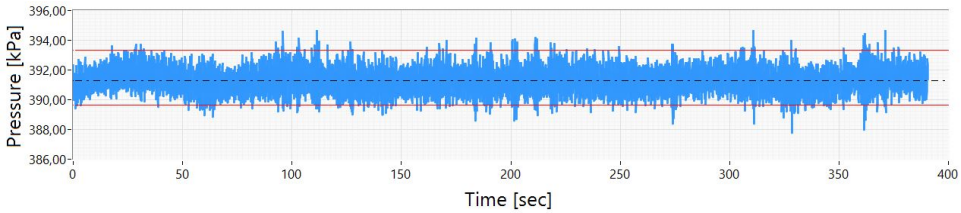

Figure 8: After surge extraction

Case	6	6
Measurement	Pennstock outlet pressure	Pennstock outlet pressure
Violation count	1018	1164
Allowed Violations	2343	2343
SQC result	Approved	Approved
ANOVA F-ratio	7,30	1,15
ANOVA Critical F-ratio	2,57	2,57
ANOVA results	Not Normal	Normal Distribution
Surge extraction	0	1
Verdict	Surge extraction	Accepted

B Paper I - Applied Statistical Quality Control On Field Measurement Data

Published and presented at the IGHEM 2014 conference in Itajuba.
Co authors: Harald Hulaas,Torbjørn Nielsen,and Håkon Francke
available online: http://www.ighem.org/

Applied statistical quality control on field measurement data

Wiborg, Erik
Statkraft / NTNU
erik.jacques.wiborg@statkraft.com

Hulaas, Harald
Norconsult
harald.hulaas@norconsult.com

Francke, Håkon
Flow Design Bureau
hf@fdb.no

Nielsen, Torbjrn Kristian
NTNU
torbjorn.nielsen@ntnu.no

August 5, 2014

Abstract

Field efficiency measurements on hydro power plants usually do not have a validation check during the ongoing field work. If the end results of the field test is analysed during the test itself, field engineers have a chance to check for obvious mistakes. Results clearly deviating from the expected trend (subjective to the field engineer) may be questioned and a repetition of the measurement is then performed. This does not usually apply for errors that are relatively small (but not necessarily insignificant). Operation of a secondary turbine during a performance test may alter the flow in the waterway, potentially leading to an error in the measurements. Disturbances like water surges, temporarily blocked sensors, temporary resonance; there are multiple reasons for a measurement to be slightly off during testing. Statistical Quality Control (SQC) of the data, running continuously within the acquisition system is a possible solution to this problem. Logged data can with this tool be checked for validity before advancing the measurement schedule. This would allow the field engineers an instant check, and the possibility to immediately re-measure any doubtful measurement. Such a system in being designed during the phd work of EJW and tested on data provided by Norconsult and by FDB on three different Statkraft power plant. Results are interesting, underlining the usefulness and the potential of the method. There are however still some unresolved issues, they will be presented in the hope of getting feedback towards possible solutions.

1 Background

Field measurements on hydro power plants are costly, not only because of the measurement itself, but also because of down time on the runner in question. This is why power plant owners wish the measurement to be as short as possible. At the same time, the measurement results may have large financial impacts and need to be done properly. During the measurements, many different types of data logging are performed, and one can simply not control manually every measurement manually. An automated check would be helpful for this task.

The paper is a continuation of the paper "Statistical Quality Control and Field Measurements in Hydro Power Plants" [1] still unpublished. Most of the theory presented here can also be found in this first paper.

2 The method - general approach

To validate data during field measurements a strong statistical tool is employed. The method itself is inspired by process control, and the use of Shewhart diagrams [2].

In process control, a good way of monitoring the stability of a production line is to perform sample measurements displaying the results in a Shewhart diagrams, and check if the data follows some simple rules of normality. This enables the owner to control that the production maintains stable, accounting for natural variations in the production, which should by default be normally distributed around a target mean. A set of rules ensuring the normality are proposed [2]. A rule violation implies that the measurements show deviation from the expected distribution, and additional control should be performed.

One of the simplest and most commonly used rule is the "three-sigma control limit" [2]. Based on the 25[1] first measurement points one can compute a mean and standard deviation, the basic values needed to set up our control limits. This is what one could call "phase 1". During the continuation of the measurement ("phase 2"), If a measured value crosses the control limits, it is in violation, see Figure 1.

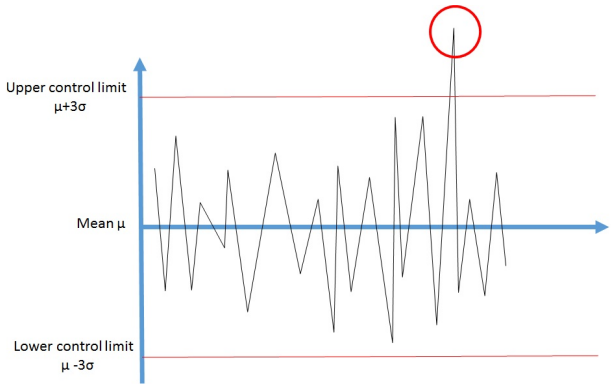

Figure 1: Shewhart Diagram Example - Three-sigma rule violation

In this study the three-sigma rule has been chosen, along with an other of the most commonly used rules: Two out of three consecutive measurements cross the same two-sigma control limit. This rule will be denoted as the double-two-sigma rule henceforth.

This method is the theoretical basis for a validation software (created in LabView) that can be implemented to the data acquisition system used during field testing.
The main goal being, of course, to check that the measurand (pressure, vibration, flow, level, temperature, and so forth) is stable during the data acquisition phase. The assumption of stability being, for process control, a normal distribution around a mean. Dealing with water power one expects there to be residual pressure waves in the system that may disturb the measurements. Some waves may take too long to dissipate and the software will have to accept the presence of a wave, which could lead to a discrepancy in terms of distribution. This topic is addressed later in the paper.

3 The method, adapted to hydro power field measurements

It is important to underline that some rule violations are bound to occur, even in stable conditions. By definition there ia a 0.3 % chance for a measurement point to violate the three-sigma rule [3], for example. We wish to avoid unnecessary hold-ups during field testing, our software therefore needs to accept a certain amount of rule violations. For the purpose of assessing a correct amount of authorized rule violations, a

[1]This number is suggested by Montgomery [2]. Based on the assumption of normal distribution, one should have enough statistical information with these measurements to lay down "rules of normality" that are well balanced for this use.

study was done earlier, and presented in the first paper dealing with this issue [1].
The main task of the study was to find the relationship between the number of sample points and the expected amount of natural violation. Using repeated randomly generated values with a normal distribution (therefore, by definition without any causal disturbances) a linear relationship was found for both of the rules and their combination.

Another issue that became apparent while developing the validation software. The sensitivity to the first 25 measurement points ("phase 1", see chapter 2) was troublesome. This will be explained in details further along this paper, but mainly one would have problems with measurands that stabilized themselves during testing, leading to false (too wide) control limits. The need for a second check became apparent. A back-to-back approach was therefore undertaken.
Two checks are therefore performed by the software. Once in the normal way described i section 2, and then another one, this time with phase 1 based on the 25 last values. The check with the highest amounts of violations is the one selected for the analysis. This way, if the measurand stabilized itself during the acquisition phase, the second measurement would detect higher variation in the beginning of the acquisition period and visa-versa.

Finally, it became quickly obvious that some of the measurements, branded as invalid by the tool, where in fact usable. The software can not be entrusted to automatically discard data. As a results, a report will now be displayed for invalid measurements, leaving the final judgement in the hand of the chief of test. Figure 2 is an example of such an report. Examples of such usable data will be described in the next chapter.

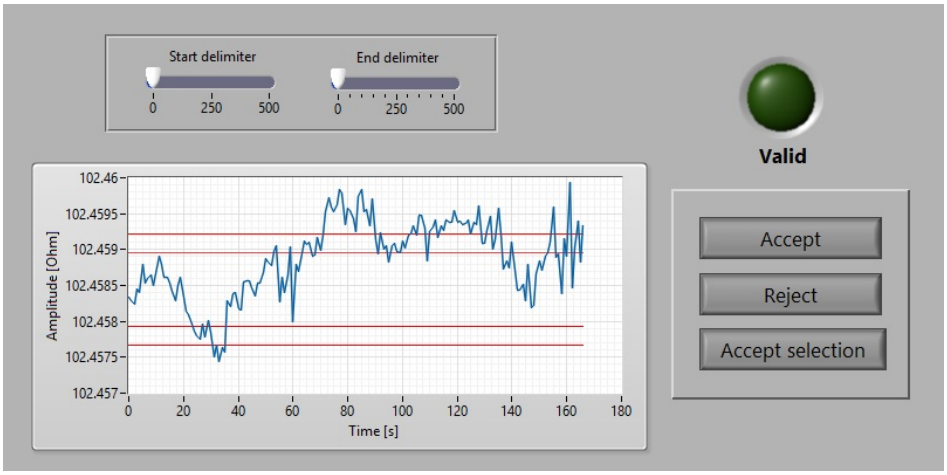

Figure 2: Validity report

4 Testing on real data

Upon testing on real data the use of the software proved its worth. Most of the data from the three site tests where accepted by the software, with right. Some measurements where however picked up as invalid by the system. Bellow are some selected results, examples of different cases of issues.
This is more or less a repetition of the different situation uncovered in the first analysis [1].

4.1 Hasty start

Depending on the power plant, the time needed to reach a stable situation after load change may vary. The necessary waiting time will of course vary accordingly. A hasty start may be the cause of faulty measurements, figure 3 is an example of just that.

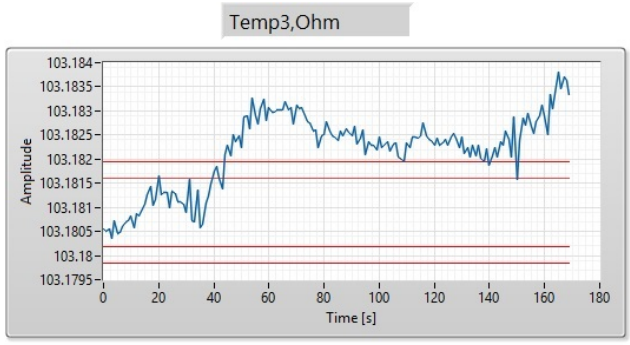

Figure 3: PP1 101rv - Temperature measurement (Ohm)

Hasty starts are not uncommon, but it may be counter productive to automatically discard the whole measurement just because of a small amount of offset measurement points.

This is a typical case where one could use the "accept selection" choice of the softare report (see figure 2).

4.2 Causal variation

This was the original case that the software was supposed to detect. Picking up variations due to causal effects (in contrast to random errors, caused by static).

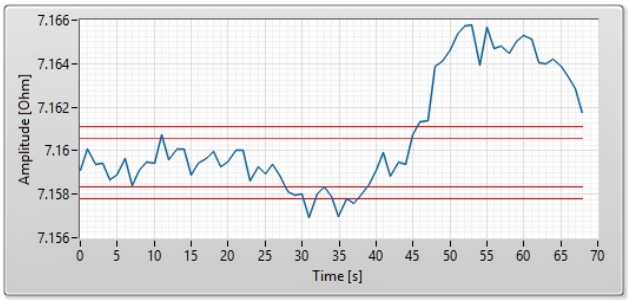

Figure 4: PP2 107 Temperature Diff (Ohm) - Causal variation

4.3 False alarm

Here are examples of why there is a need for human judgement (see 3). Statistics are never 100% accurate, and some rejections may not be justified.

In the first example (figure 5) the number of violations is indeed above the suggested limits, but the mean seems stable and centred. The cause of the invalidity of this measurement is simply an above average erratic static noise. It would be wrong to discard this measurement.

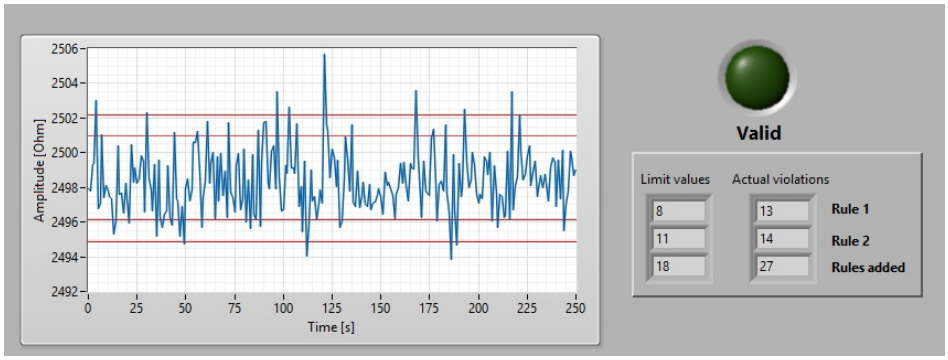

Figure 5: PP3 05 Pressure (kPa) - Possible false alarm

In the second example (figure 6) there are still surges that need to dampen, this is actually a case of hasty start mentioned above. However the wave amplitude and phase would suggest that the mean does not deviate much from the true mean. By using the validity report (see figure 2) one could verify the mean for the whole set, and compare it with the mean of a selection after the wave has dampened. Leaving the option of excluding the first wave with the largest amplitude.
This is a good example of why the back-to-back approach was needed. The control limits are the ones computed by the second check, with phase 1 based on the last 25 measurement points.

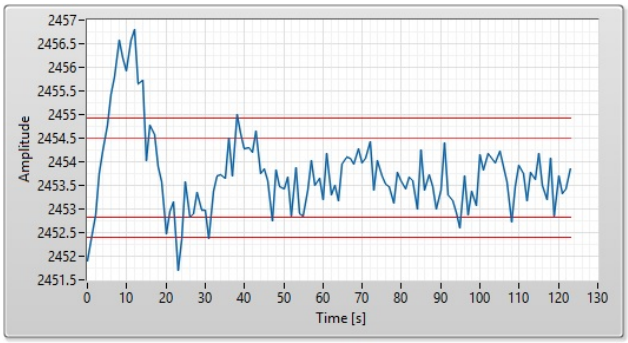

Figure 6: PP3 07Pressure (kPa) - Surges - Valid

5 Issues and future improvements

5.1 Phase 1

During phase 1, where the control limits and mean are computed, we must assume perfect stability and Gaussian distribution of the measurement values. This is of course rarely the case, surges give sinusoidal disturbances to pressure, flow and temperature. Especially for high frequency measurements, we are likely to encounter problems related to autocorrelation error if standing waves are present.
Highly correlated measurements will provide a poor initialization of the mean and control limits.

To study the effects of autocorrelation, an autocorrelation analysis was performed on some sample measurement series. This was done with the statistical tool R [4]. Bellow are example of the results provided by R.

For measurements with no apparent standing wave, like the one shown in figure 5 no autocorrelation was detectable allready after the second point, see figure 7. In this case the 25 points rule is deemed applicable.

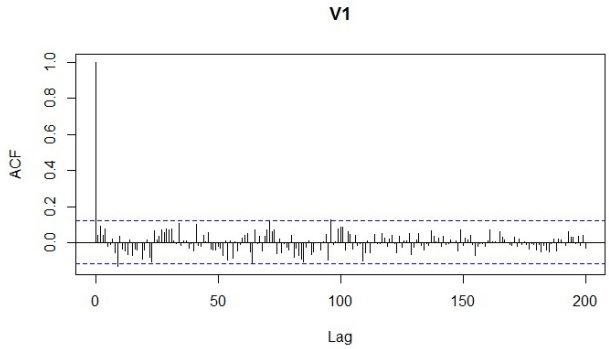

Figure 7: PP3 05 Pressure (kPa) - Possible false alarm - Autocorrelation

The measurement in figure 8 is the "PP1 101rv" measurement, displayed in figure 3.

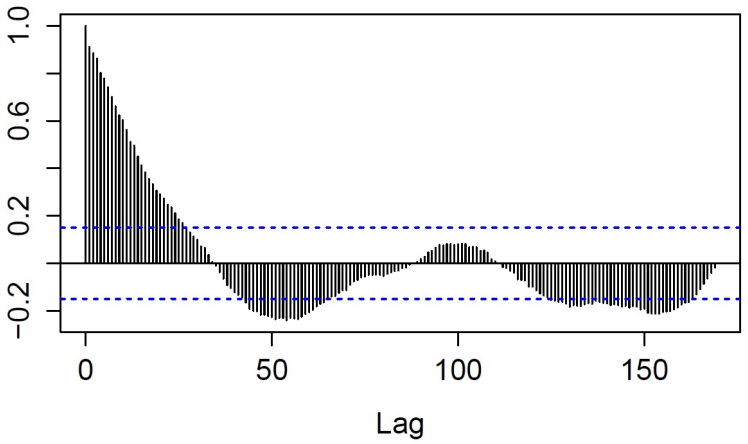

Figure 8: PP1 101rv - Autocorrelation plot

And as we can see from figure 8 we still have autocorrelation issues after 25 measurements. In this case we should have used at lest 30 measurements for phase 1.
Such an autocorrelation check should be implemented to the software, ensuring that we have a sound initialization of the control limits.

Note that for standing sinusoidal waves the autocorrelation may not stabilize itself. But once we have reached a satisfactory level (neglectable autocorrelation) we should have recorded at least half a period of the largest standing wave, which should be enough for a satisfactory phase 1 initiation.

This being said, the 25 measurement points offer a more strict limitation. One could argue that it would be better to check the invalidity report more frequently than necessary, only to accept falsely rejected measurements, rather than the alternative.

5.2 Instability consequences

As one may have noticed from the different figures presented in the paper, the amplitude of variation is usually very small. The validation method is purely statistical, and does not take into account the consequences for the end result.

As mentioned before, human judgement should always be included. A possible improvement to the software could be to have it quantify the effects of a (small) change of the measurand value on the end results. This way the chief of test can decide to accept unstable measurements if they are of little consequence to the end results.

5.3 Statistics criteria

As it has been mentioned a number of times, the software presented is purely a statistical tool. Statistical predictions need a certain amount of data to be valid, this is no exception.

The law of Small Numbers [5] is applicable here: Too few measurement points may not give a proper representation of the true state of the measurand, and extreme ratios are more likely to occur for smaller populations [5]. This implies that the tool will be more correct in its assessment of a valid/invalid measurement if it contains a large amount of measurement points. Experience from the studies performed with the tool would suggest a minimum requirement of about 100 points.

5.4 The rules of validity

Two rules have been used for the validity check up untill now (the "three-sigma" and the "double two-sigma" rules, see 2). These are the most commonly used rules for process control, and seem appropriate for field measurement use.
There is however one other rule that may be interesting to implement: one should check for a faulty sensor/transducer, should three or more consecutive measurements be repeated exactly (to the last decimals given by the instrument). One other situation that may give these results is if the measurand saturates the measurement sensor, in which case we also have an error i measurement.

This rule should be easy to implement and should provide extra safety during measurements, as long as the instrument is of high precision and static noise is unavoidable as long as it is functioning properly.

6 Conclusion

The statistical control tool could be beneficial for a quick check of measurement stability during field measurements. It will however probably never be good enough to be entrusted to automatically discard faulty measurements, as it may result in unnecessary delays. The only exception would be on-line measurements where time is abundant.
It is noteworthy that all the accepted measurements where in fact truly stable. The control function of the tool may be harsh and may reject acceptable measurements, but it is certain: accepted measurements are indeed stable and valid.

Some improvements to the software are still necessary, the repetition rule mentioned in chapter 5.4 should be implemented but probably also optional since it would not function properly for low resolution measurements. Also a quick example computation of the end result consequences of unstable measurements would help in choosing whether to discard a measurement or not.

This study has proven the importance of human judgement, there is no doubt that an efficient and easy-to-use human interface is vital for a proper use of the tool.

The tool has yet to prove its worth on a live field measurement. How helpful it actually will be remains to be seen.

7 References

References

[1] E. J. Wiborg, T. Nielsen, H. Hulaas, and H. Francke, "Statistical quality control and field measurements in hydro power plants," *Journal of Dynamic Systems, Measurement, and Control [UNPUBLISHED]*.

[2] D. C. Montgomery, "Introduction to statistical quality control," 1991.

[3] R. E. Walpole, R. H. Myers, S. L. Myers, and K. Ye, *Probability and statistics for engineers and scientists*. Macmillan New York, 1993, vol. 5.

[4] "Autocorrelation function r." [Online]. Available: http://stat.ethz.ch/R-manual/R-patched/library/stats/html/plot.acf.html

[5] K. Daniel, "Thinking fast and slow," *Allen Lane, New York, USA*, 2011.

C Paper II - HydroCord Condition Monitoring System

Published and presented at the IGHEM 2016 conference in Linz.
Co authors: Torbjørn Nielsen,and Håkon Francke
available online: http://www.ighem.org/

HydroCord Condition Monitoring System

Erik J. Wiborg (erik.jacques.wiborg@statkraft.com)
Dr. Håkon H. Francke (hakon.francke@fdb.no)
Prof. Torbjørn Nielsen (torbjorn.nielsen@ntnu.no)

June 10, 2016

Trollheim Power Plant in Norway is being equipped with an experimental condition monitoring system called HydroCord. The measurement system is complex and designed to monitor a large number of characteristics, notably and maybe most importantly, the turbine runner hydraulic efficiency. Through the use of an automated stability control, the efficiency will be continuously computed when the stability criteria in the waterway are met. Because of the size and complexity of the HydroCord system, this paper is restricted to only present the systems main ideas and concepts, it's goals and benefits, along with some results from an early correlation analysis of the newly acquired data.

1 Background

Condition monitoring is a well established tool for optimizing maintenance on industrial equipment, increasing efficiency and profitability [1]. Countless standards and guides exist on the matter. As of May 2003, there where 98 published ISO standards related only to TC108, the technical committee guiding standards for machinery vibration monitoring and analysis.

Hydropower is no exception, with numerous research papers published world wide (e.g. [2], [3] and many more). The Norwegian research institution SINTEF started a project in 2014 who's goal was to collect state of the art in hydro power condition monitoring technology and methods [4].

All the systems are aimed at establishing a good monitoring system for the mechanical equipment. Some, like the HAICMON hydro system (HAINZL, see www.hainzl.at) integrate damage detection systems (in this case a cavitation detection system). Most are however, as the name implies, systems aimed at providing data to optimize maintenance and survey only the condition of singular vital components in the production system. The HydroCord system stands out as it is designed not only to assist the maintenance process, but also the production planning through a holistic view of the power plant.

This paper aims to present the system, its benefits and presenting some early results and discussions.

2 The HydroCord monitoring system

2.1 The project - aim and scope

Trollheim power plant is a single unit 130MW Francis type power plant situated in Surnadal, Norway. The Norwegian power production company Statkraft initiated in 2010 a research and developmental (R&D) project aiming at the design, production, installation and testing of a condition monitoring system (later named HydroCord), lead by the author of this paper.

The system was designed to support both Statkraft's production and maintenance units. This would be done in several ways, listed bellow are three of the main goals of the system.
- Supplying vital information as input for Statkraft's models production planing and hydrological prediction
- Supply useful information to plan refurbishments of major components
- Warn the operators and the maintenance crew of damaging behaviour to the runner during operation.

Flow Design Bureau (FDB), greatly involved in the initiation and realisation of the main ideas and hypothesises behind the system, where selected as suppliers for the system.

A study was undertaken to list the main characteristics needed to optimize production and maintenance, a study leading to a list of desired continuous measurement. First and foremost a good monitoring of the flow (and thereby the runner hydraulic efficiency) proved to be in high demand. Most of the measurements, now part of the HydroCord system in Trollheim power plant, are listed bellow.

- Hydraulic efficiency of the runner
- Water flow through the power plant
- Headloss measurements in the tunnels and penstock
- Dynamic pressure measurements in the system waterway
- Cavitation intensity measurements
- Sand transporting indexing
- Turbine pressure pulsations
- Grid frequency
- Turbine floor sound frequency
- Water temperature through the system and downstream
- Water turbidity measurement

As is probably quite apparent, some of the measurements listed will not be vital for the operation and maintenance optimization, but where added to gather experimental data for future R&D projects. Many of the listed measurements are in fact values computed from sets of single point measurements. The list of these single point measurements is provided in the next section.

2.2 The system

2.2.1 General description

Much like the spinal cord, the HydroCord was designed to relay signals from the sensors, placed through the whole body of the hydro power plant system, through a high speed fibre network to a "main brain" for processing.

Data acquisition hubs are placed in five positions through the power plant system as

shown in figure 1. At the time of writing, most of the sensors are in place and supplying data to the system. Note that the figure is only an illustration of a generic power plant and should not be considered as a scaled visualisation of the Trollheim Power plant. All data is relayed to the control room hub containing a processor for data analysis and computation. The raw and processed secondary data is stored locally in a network-attached storage system (NAS). The distribution of the data beyond the local system is discussed in section 6.
Added to the control room hub is also a human machine interaction system (HMI). The HMI, still under development at the time of writing. It should provide navigation options through the collected data, displaying key figures and graphs with historic data for visual inspection of trends.

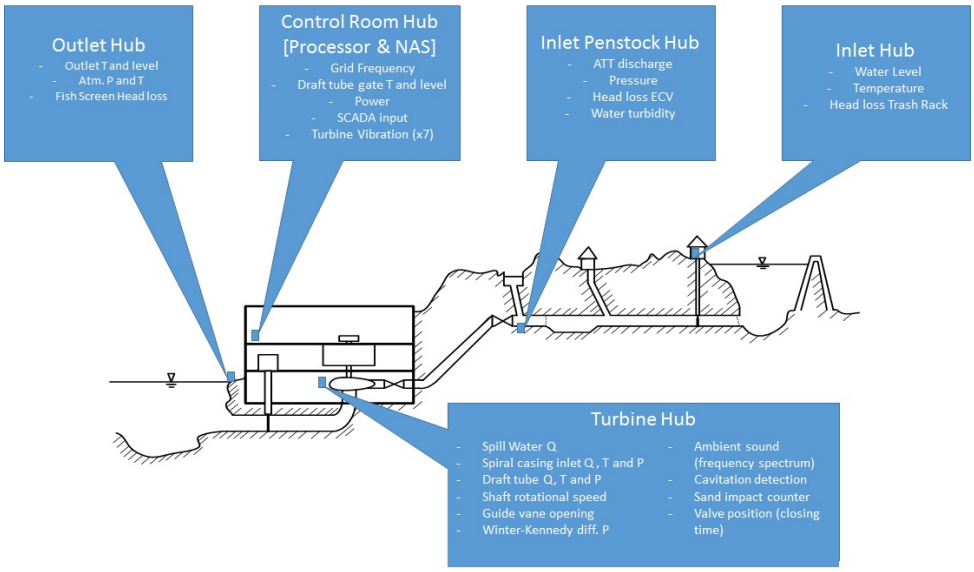

Figure 1: **HydroCord system overview**
Five data acquisition hubs are place in different geographic locations, all communicating through a fibre based network. The control room hub is also ecquiped with a processor for analysis and computation and a network-attached storage system.

The HydroCord software is entirely programmed in LabView and was designed to be scalable. Future installations on other power plants will most likely vary in terms of which characteristics need monitoring, and to easily provide a tailored solution for new installations an appropriate software architecture had to be devised. The general idea behind the programming was to design a generic base (including standardised code for data storage, communication, averaging, and so on), and connected to the base code, a set

of smaller optional software modules (applications) performing more specific processing routines (ranging from computation of the hydraulic efficiency to an alarm application for high surge chamber level). This design provided a time saving ease of scalability, while at the same time made the code uniformed and easy to work with. These benefits where proven on several occasions during the Trollheim project lifetime.

2.3 Flow measurements

The discharge, vital for computing the efficiency, and a highly valued characteristic by the hydrological department, is measured in several ways listed bellow. By comparing the results, the condition monitoring system will be able to detect errors in measurements or indicate if a discrepancy exist between them, notifying the owners of the system that a measurement error exist or that some of the equipment requires recalibration.

The Winter-Kennedy measurement is a relative measurement that once calibrated should provide a solid measure of the flow through the turbine. It is described in the IEC41, section 15.2. The main benefits of the method is its ease of implementation and low cost (with only a differential pressure measurement needed). At the same time, it is placed close to the runner and therefore displays a good indication of the flow and hydraulic conditions of the turbine, compared to some of the measurements listed bellow.

The Acoustic Transit Time (ATT) measurement is placed upstream the emergency closing valve (approximately two diameters upstream). The placement is not ideal, but in view of the available placements it was the only option. This measurement was the most interesting because of its presumed high uncertainty, and because of the less than ideal placement. The benefits, should this measurement prove to be reliable, would be great. For Trollheim, as it is the only direct measurement of the discharge it would represent a good way of controlling the other methods validity over time. For future installations, since the equipment is relatively cheap, and easy to place, it would make an excellent option to the Winter-Kennedy method should the spiral casing be out of reach (embedded in concrete) for future installations. Also for a mobile version of the HydroCord system, this would be the preferred method, as it would not need calibration (as long as the internal diameter of the measurement section is known). For more information on how the method work refer to e.g. the IEC41, appendix J.

Finally, as a third option for discharge estimation, head loss measurements will be used. Once calibrated (head loss coefficient k known) the flow can be estimated by the simplified head loss equation 1 (a simplification of the Darcy Weisbach equation, see e.g. [5]).

$$\Delta H = kQ^2 \tag{1}$$

This is of course assuming the head loss coefficient is constant, which is not the case over time. A self calibrating routine will have to be set up to re-assess the k-values at a certain frequency (estimated twice a year). Because of this, the flow estimation will

only be used to verify coherence in data over shorter periods of time, and will not be used for long-term evaluations.

A correlation analysis was performed to compare the three types of measurements. It is presented in section 3.

2.4 Continuous efficiency measurement

The main issue with a continuous efficiency measurement is the fact that it must be performed during normal operation. To provide a usable efficiency estimation, the uncertainty must be reduced to a minimum. This is usually done by sampling the required data over a long period. During normal operation the turbine is subjected to regulation (primary, tertiary, and for some power plants also secondary). Every load shift provokes the birth of a pressure oscillation through the system that would potentially cause false measurements.

To ensure that the efficiency is computed based on steady measurement conditions an automated validation system had to be set up. The validation would have to reject measurements during transient states, but accept and deal with the long lasting oscillations present in the datasets after a larger shift of the flow (typically after tertiary regulation). The method devised during the main authors PhD will be presented in his thesis, but some of the basic concepts where presented in an earlier conference [6].

In brief the validation system loops through three steps. The first rejects measurement series containing fluctuations or with unstable running means. If accepted, the second step checks if the data in normally distributed. If it is, the data is accepted for further computation of the efficiency. If not, the data is subjected to an FFT-based surge extraction process removing the sinusoidal component of the the data with the highest amplitude. Once the oscilatory component removed, it is resubjected to the three steps of the validation process.

The validation system has been tested thoroughly and is ready for implementation to the Trollheim HydroCord system.

Both the Winter-Kennedy differential pressure, the ATT flow measurement, and all other pressure measurements relevant for the computation of the efficiency of the runner will be subjected to the validation method. This means that the continuous efficiency measurement will not have a static frequency, but will provide data only during steady condition, ensuring good quality measurements at all time.

Once the quality of the measured data ensured, the data will be plotted continuously in the turbine Hill-Chart. It is expected that after a years worth of measurements, the Hill-Chart will be fully updated. It will then be saved, such as it is, and be used for

visualisation in other application (see section 4.2). The newest Hill-Chart will at any time be the one displayed and used by the system. The outdated charts will be stored for R&D purposes (see section 6).

3 Testing the system

To fully test and calibrate the HydroCord system a thermodynamic field efficiency measurement is planned to be performed on site. It will provide the means to verify the measured results and to evaluate static and semi-static characteristics needed for the Winter-Kennedy efficiency measurement and head-loss measurements.

At the time of writing the calibration test has yet to be performed, and as such only the results of a correlation analysis of the three flow measurement methods presented in section 2.3 can be presented. It is important to note that we therefore only can test the signal variations and not their actual value. Discrepancies are to be expected between the different datasets, but the correlation analysis will show that that the samples have a linear relationship with each other.

The correlation coefficient between two datasets is defined as in equation 2.

$$corr[X,Y] = \frac{cov[X,Y]}{\sqrt{var[X]var[Y]}} \tag{2}$$

With the covariance estimated as in equation 3.

$$cov[X,Y] = \frac{1}{n}\sum_{i=1}^{n}(x_i - \bar{x})(y_i - \bar{y}) \tag{3}$$

Where n is the dataset size, and x_i and y_i the index i value of datasets X and Y.

The correlation coefficient, ranging from -1 to 1 quantifies how much two samples change together, i.e. if two datasets have a covariance of 1 they are perfectly synced and experience the same variances. If two datasets have a covariance of -1 they are 180 degree out of phase and vary equally in the opposite direction from one another.

The graphs presented in figure 2 are normalized values (displayed in percentage of the datasets highest recorded value during the measurement period) to help visualize the correlation between them. The values are the recorded flow from the ATT (red), the square root of the differential pressure from the Winter-Kennedy measurement (green) and the square root of the head loss measurement (red - differential pressure over the emergency closing valve).

The correlation matrix is displayed in table 3. There is an excellent correlation between the head-loss measurement and the ATT method. This is not surprising as they

are geographically very close. The correlation coefficient between the Winter-Kennedy method and the two others is 0.8, which would indicate that other factors influence the measurement.

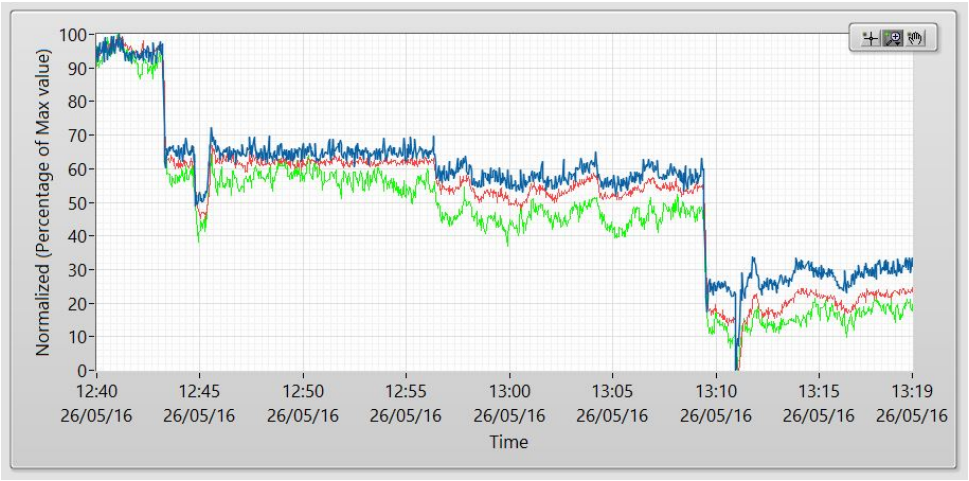

Figure 2: **Normalized raw values for correlation analysis**
Data subjected to a correlation analysis used in the determination of the flow, using three separate methods. Red: ATT, Blue: Head-Loss, Green: Winter-Kennedy

	Winter Kennedy	ATT	Head-loss
Winter Kennedy	1	0.79	0.79
ATT	0.79	1	0.99
Head-loss	0.79	0.99	1

Table 1: **Correlation analysis results**
The correlation analysis results corresponding to the values displayed in figure 2

Adding the guide vane opening to the correlation analysis, the coefficient of these values with the square rooted Winter-Kennedy measurements was 0.99, while the correlation with the two measurement near the emergency closing valve was 0.80. Again, these results are not surprising because of the geographic situation, and correspond well with the results of the first analysis.

Another interesting analysis was the influence of the grid frequency on the flow, i.e. the effect primary regulation has on the flow in the power plant. Figure 3 displays the data

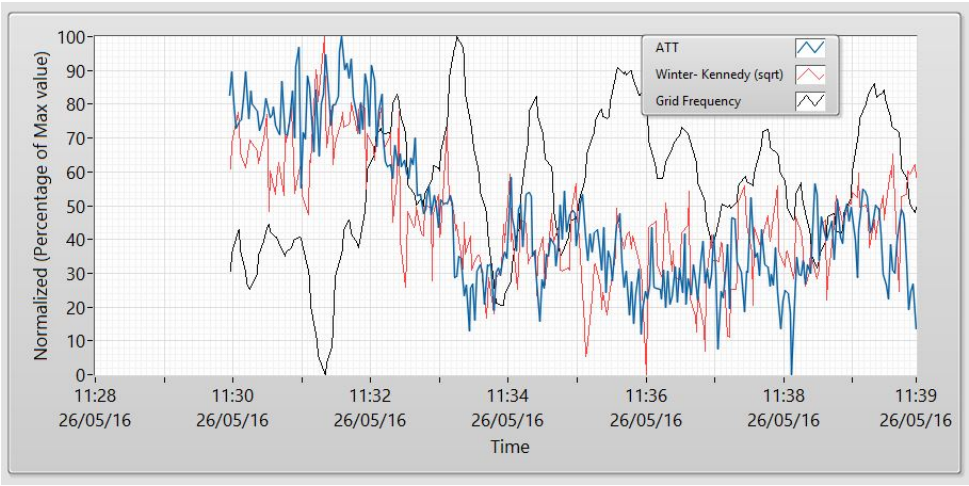

Figure 3: **Normalized raw values for correlation analysis - Grid influence**
Similar data as those presented in figure 2, but aiming at evaluating the influence of the grid on the flow. Black: Grid frequency, Blue: ATT, Red: Winter-Kennedy

selected. The correlation coefficients of the frequency with the squared Winter-Kennedy differential pressure and the ATT discharge measurement where, in order, -0.32 and -0.27. Both coefficients indicate a significant influence. This indicates that primary regulation (or frequency variations in the grid) do influence the guide vane, and in turn the flow in the power plant waterways. This is a confirmation that a validation system is required for continuous efficiency measurements. Large fluctuations in the grid will most likely cause fluctuations in the flow, disturbing the efficiency measurements.

It could seem that the ATT measurements are less influenced by primary regulation than the Winter-Kennedy measurements. Repeating the correlation test with other datasets revealed the same pattern, with a varying degree of correlation to the grid frequency, but always higher with the Winter-Kennedy than with the ATT.

4 Benefits of the HydroCord system

4.1 Benefits for maintenance

Condition monitoring system are, as mentioned in the introduction section 2.1 usually installed to support the maintenance of the equipment in question. This is of course the case for the HydroCord as well. However the focus has not been on components usually monitored like the shaft, bearings, generator or transformer. Commercially available systems already exist for that. The focus has been on providing specific hydro power

related data, such as cavitation intensity, head-loss coefficients and of course the runner efficiency. Monitoring the runner efficiency is not novel in its self, but the low uncertainty through the use of the validation process, and the vast amount of parallel measurements performed, makes the system quite unique.

Stakraft is in the process of upgrading its maintenance scheme. Up until now the maintenance has usually been either frequency based or based on low frequency condition assessments (e.g. efficiency measurement are done every tenth year or more). Prediction based maintenance is a more efficient and economically sound scheme, however the prediction models will need to be fed data describing the condition of the system. Most of all, the HydroCord system aims at providing information to optimize refurbishment timing for some of the larger components of the system (i.e. the runner, the penstock or the tunnels). Weeks of down time for a power plant are very costly, and ensuring that the project is initiated at the right time will have large financial benefits. As an example, the gain from delaying the refurbishment of one of Statkrafts largest runners with one year could be in the order of two million Euro. High uncertainty to the condition and the evolution of it gives poor basis for the refurbishment planing.

As previously mentioned, new installations of the HydroCord system are to be tailored to the power plant in question. This means that through input from the local staff, all measurement of interest to the maintenance team will be added. As an example, the next implementation of the system is in one of Statkrafts power plants where the part load draft tube vortex heavily damaged the draft tube walls. To notify the dispatch centre of damaging conditions, vibration measurements of the draft tube will be added. Some power plants may have a history of problems with a certain bearing, if that was the case a temperature measurement of the oil, and a differential pressure measurement on the filter would be added.

4.2 Benefits for production planning

Statkraft production planing staff relies on models to help optimize the production of the machine portfolio. The model is based on a number of characteristics, one of them is the efficiency of the turbines. After field efficiency measurements are performed the models are updated. But as mentioned in section 2.4, they are performed every tenth year or more. The models base their calculations on outdated values most of the time. Also, when performing a field efficiency measurement the resulting efficiency curve is only valid for a certain head range. A yearly updated Hill-Chart provided by the HydroCord system would ensure valid efficiency curves for the models to base their calculations on.

To prevent damaging the runner technical restrictions are applied to the production. Overload and part-load, for francis turbines in particular, have a heavy life time reducing effect (see e.g. [7]). The two major damaging mechanisms are cavitation, usually

occuring at high loads, and heavy draft tube pressure pulsations, usually at part load. Setting technical restrictions has up until now mostly been done through rules of thumb and subjective human interpretation of sound and vibration in the power plant. Another factor to take into account is that because of head variations, the mechanisms may very well appear at a certain power production level in some cases, and be non-existing when the head is significantly different (and visa-versa).

Providing a yearly updated Hill-Chart would in itself be extremely useful to update production models. If the chart also mapped actual damaging Head/flow areas, new technical restrictions based on actual cavitation (for the detection system, see [8]) and pressure pulsation measurements would ensure valid technical restriction and enabling the full use of the runners flexibility.

4.3 Benefits for research and development

To the authors knowledge, no hydro power plant is monitored to the extent that Trollheim power plant is today. The amounts of data collected will be vast, not necessarily compared to other industries, but for Hydro Power these data files should represent a great potential for future and ongoing use in R&D projects.

Naturally the data collected will be used by Statkrafts own analysis group, but to help the global community, some of the data will be publicly released. All data generated during a weeks production, along with datasets from special events (grid failure, emergency shut-downs, and so on) will be available from Statkrafts home page. The release date is expected to be end 2016 - beginning 2017. A collaboration project with the Norwegian University of Science and Technology (NTNU) and the Norwegian Hydro Power Centre NVKS will be started by the end of 2016 to help coordinate R&D projects related to condition monitoring or heavily based on the collected data from the HydroCord system.

5 Discussion

The results displayed in this paper are still inconclusive to the well functioning of the HydroCord system when it comes to efficiency measurements, however the correlation study shows promise, and may have revealed some interesting facts about the different methods strong and weak points for studies on Hydro Power plants.

As we have seen good correlation exist between the Winter-Kennedy approach and the guide vane opening. An equally good correlation exist between the head-loss based estimation of the flow and the ATT measurements. The correlation between these two sets of measurements is acceptable, but it seems that the Winter-Kennedy and guide vane opening are influenced by other factors, as it displays more erratic behaviour than the ATT measurements (see 2). The difference in water velocity and regulator hysteresis

may explain some of the differences.

Considering these results, an important question still remains unanswered. Should the ATT values or the Winter-Kennedy flow measurements be used in the efficiency computation? This is of course a subject for discussion, as the Winter-Kennedy measurement shows a more accurate picture of the flow through the turbine (because of its geographical position). On the other hand, the more steady measurement conditions of the ATT could ensure lower uncertainty to the end result (less influence visible from primary regulation for example, see section 3). The uncertainty evaluation of the measured results will be critical in the assessment of which method should be used.

6 Future Work

6.1 Field efficiency measurement

A thermodynamic field efficiency measurement (FEM) will be undertaken on Trollheim power plant. The results of the test will serve multiple purposes, i.e. calibrate the Winter-Kennedy measurement. Calibrate the flow estimation based on head-loss, and control/calibrate the flow measurement through the ATT measurement.

The measurement uncertainty will be a major contributor to the uncertainty of the continuous measurement methods for flow, it is imperative that the FEM is done under good conditions.

The results of the FEM and the comparison test are expected to be published as soon as possible.

6.2 Data distribution

Condition monitoring has well documented merits. The HydroCord system will collect data and process it into useful and meaningful values to be used in maintenance, production and research. However, the efforts put into the development of the system are in vain as long as the data can not be communicated in a good way to the stakeholders. Creating translators of the data, to fit the various uses for Statkraft will be key to the success of the project. Although not particularly sensitive, the data must reach the users, and as it is collected at site, security measures must be taken to provide a safe communication out of the local network.

6.3 HMI

The focus of the HMI will have to be user friendliness, as a way to ensure that system actually get used to its full potential. This includes work to make the system intuitive, and pleasing to work with. It includes an ease of access, and tools to provide relevant information in an easy to understand manner. Finally it includes applications to mould the data in a matter that is usefull for all relevant application frequently used by the stakeholders.

The HMI should provide the local maintenance staff with information helpful when performing tasks at cite through a hand-held device.

6.4 R&D projects

Statkraft has already initiated the construction of another experimental system at Trollheim power plant. Its main goal is damping of pressure pulsations at part load (see [9] and [7]). The extensive instrumentation at Trollheim makes the power plant ideal for impact asessements, and to control the effects of the experimental system on the power plant components and waterways.

A future project that the authors hopes will be realised, is a study of the development of the turbine characteristics over time. This could be done by using the collecting yearly updated Hill-Charts, along with the rest of the data gather by the HydroCord.

References

[1] B. Rao, *Handbook of condition monitoring.* Elsevier, 1996.

[2] Z. Lihua, Z. Shuyun, L. Zhong, and Z. Rujun, "Labview-based turbine condition monitoring and fault diagnosis system," *Water Power*, vol. 3, p. 029, 2010.

[3] Y. Power, G. Neil, E. S. Fouad, and S. Crisafulli, "Advanced condition monitoring of a hydroelectric power generation facility." [Online]. Available: http://www.rockymug.org/Meridian%20PAM%20Paper%20-%20Asset%20Health%20Monitoring.pdf

[4] SINTEF, "Handbooks on condition monitoring of hydropower plants," 2014. [Online]. Available: https://www.sintef.no/en/projects/handboker-for-tilstandskontroll-av-vannkraftverk/

[5] A. R. Rao and B. Kumar, "Friction factor for turbulent pipe flow," *Journal of Indian Water Works Association*, pp. 29–36, 2006.

[6] E. Wiborg, H. Hulaas, H. Francke, and T. Nielsen, "Applied statistical quality control on field measurement data," International Group for Hydraulic Efficiency Measurement, Tech. Rep., 2014. [Online]. Available: http://www.ighem.org/Papers_IGHEM/392.pdf

[7] H. Francke", "Increasing hydro turbine operation range and efficiencies using water injection in draft tubes," Ph.D. dissertation, NTNU, 2010.

[8] J. Ekanger", "Investigation of the relationship between water quality variations and cavitation occurence in power plants," Ph.D. dissertation, NTNU, 2016.

[9] E. J. Wiborg and M. Kjeldsen, "Francis at part-load with water injection," 2012.

D Paper III - Continuous Efficiency Measurements on Hydro-Power Turbines A Comparison Between Acoustic Clamp-on Flow Measurement and the Winter-Kennedy Index Method

Submitted for publishing to ASME Journal of Fluids Engineering.
Co authors: Torbjørn Nielsen,and Håkon Francke
Submitted in 2016.

Continuous Efficiency Measurements on Hydro-Power Turbines A Comparison Between Acoustic Clamp-on Flow Measurement and the Winter-Kennedy Index Method

Erik J. Wiborg
Ph.D. Candidate
Dept. of Energy and Process Engineering
NTNU
Alfred Getz vei 4, 7491 Trondheim, Norway
Email: erik.jacques.wiborg@statkraft.com

Dr. Håkon H. Francke
Turbine Specialist
Flow Design Bureau AS
Holtet 45, 1368 Stabekk
Norway
Email: hakon.francke@fdb.com

Prof. Torbjørn K. Nielsen
Professor, Head of the Water Power Laboratory
Dept. of Energy and Process Engineering
NTNU
Alfred Getz vei 4, 7491 Trondheim, Norway
Email: torbjorn.nielsen@ntnu.no

An experimental condition monitoring system, called HydroCord, currently under design at Trollheim power plant is planned to continuously monitor the runner efficiency. Two methods in particular where tested for the flow measurmenent and compared (thermodynamic efficiency measurement was used as reference). Based on the comparison presented in this paper the clamp-on acoustic transit time method (two paths) shows lower uncertainty and spread of measurement results than the Winter-Kennedy measurement.

Also a method based on head-loss measurements was tested, but because of technical problems the results, although seemingly interesting, are deemed inconclusive.

1 Introduction

Trollheim Power Plant in Surnadal, Norway, is currently being equipped with an experimental monitoring system named "HydroCord". The system is to include a continuous hydraulic efficiency monitoring of the turbine runner. This work is related to the main author's PhD, and more details about the system and the goals of the project will be available through his upcoming thesis [1]. This paper aims, as the title indicates, to present the results of a comparison test of two different methods for monitoring the efficiency.

Runner field efficiency measurements on cite are common and have been performed for decades. Established methods and procedures are standardised by the IEC 60041, *Field acceptance tests to determine the hydraulic performance of hydraulic turbines, storage pumps and pump-turbines* ([2] hereby referred to as IEC41).

Not all methods presented in the IEC41 are apt for continuous measurements on site. Field efficiency measurement methods aim at minimizing the uncertainty of measurements. For a continuous measurement system other considerations must be taken as well. Notable amongst these considerations are the cost of the measurement equipment, a required ease of maintenance, and it's independence from the core system (maintenance and the measurement set-up itself should not interfere with daily production of the power plant). These new considerations are mainly driven by a very different cost-benefit perspective between on-line monitoring of an equipment with very long life expectancy (see e.g. [3] , E6-4) and field measurement equipment used for commercial purposes such as guarantee testing.

Two methods presented themselves as natural candidates for the efficiency monitoring on Trollheim power plant. The first method was the Winter-Kennedy index measurement (WKM), the second an Acoustic Transit Time method (ATT). Both systems where installed and compared with a thermodynamic measurement of the efficiency during a calibration. It should be said that both the WKM and the ATT are method for measuring the flow of the water running through the turbine, not the efficiency as such. However the flow measurement is the key for any runner efficiency measurement (see [2]). This paper will therefore solely focus on flow

measurements (not the efficiency), as it is merely computed based on this measurement and others (who would not differ depending on the flow measurement method). In addition the flow was also estimated based on a head-loss measurement over a valve.

The International Group for Hydraulic Efficiency Measurement (IGHEM) is an international group specialized in the domain of efficiency measurements. The collection of papers presented to the group (available on www.ighem.org) should be considered the state-of-the art of efficiency measurements. Comparing the clamp-on ATT and WKM for continuous measurement purposes is, to the authors knowledge, novel.

2 Trollheim Power Plant and the HydroCord System

Trollheim power plant is a single unit 130 MW Francis type Hydro power plant situated in Surnadal, Norway. The power plant was selected for the design, installation and testing of the prototype HydroCord system.

The system is an experimental condition monitoring system. It differs from the standard commercially available systems in that it's main goal is not only to monitor the different components state, but also provide a hydrodynamic monitoring of the power plant waterways as a whole. More can be read in the paper that will be presented at the IGHEM conference in august 2016 [4]. The project is lead by this paper's main author, with Flow Design Bureau as the main supplier and architect (key architect is the second author of this paper).

The main authors PhD's focus, and the background for the research presented here is the HydroCord's continuous efficiency monitoring of the runner. There is a natural mismatch between the steady-state requirements of the measurands during an efficiency measurement and the constantly disrupted situation of the turbine and waterway during normal operation, i.e. the required measured characteristics for an efficiency computation will constantly be influenced by grid regulation. A control system had to be devised. More can be read in the main authors thesis [1].

Three measurement systems provide an estimate of the flow either directly or indirectly. These are the Winter-Kennedy method (WKM), the Acoustic Transit Time clamp-on system (ATT) and a head-loss based measurement system over the emergency shut down valve (HLM). To calibrate and assess the uncertainty of the flow measurements a calibration test was performed using the flow computed during a Thermodynamic field efficiency test - a primary method according to the IEC41 - as reference.

3 The Measurement Methods

3.1 The Winter-Kennedy method

The Winter-Kennedy method (WKM) is a well known index-type method to estimate the flow through the turbine. The measurement set-up and theoretical background is described in the IEC41, section 15.2.1.

The IEC41 states that the discharge "*is usually well represented by* $Q = kh^n$" where h is the reading og the differential manometer and n theoretically equals 0,5. The model is however inferior to a normal second degree polynomial with a first degree term. The model used for the calibration will be $Q = b_1h^2 + b_2h + b_3$, with b_{1-3} the polynomial regression coefficients.

The WKM results and merits have been displayed through a number of papers, particularly as a good method for repeating the efficiency measurements at a later time, with a different head. A good example is the paper *Special Instrumentation and Hydraulic Turbine Flow Measurement Using a Pressure-Time Method* [5] where the intent of doing such a repeated measurement is explicitly written in the abstract.

The simplicity of the WKM is the methods major benefit. Essentially, only one differential pressure sensor is needed to compute the flow, which makes the method the least expensive in terms of both procurement and maintenance. This is assuming that the two pressure taps already exist in the turbine spiral casing.

With this in mind, along with the fact that the method has been prized for being an apt repetitive measurement, the WKM was a natural candidate for the HydroCord systems flow estimation.

The differential pressure sensor installed at Trollheim power plant is a Honeywell ST 700 pressure transmitter, see [6], set-up in accordance with the IEC41. An automated flushing system was added, ensuring that no clogging of the pressure taps occurred during operation. This was deemed as a necessity for continuous operation of the WKM. A control system integrated to the HydroCord will ensure that the data collected during flushing will not be used for computation of derived values.

3.2 The Clamp-On Accoustic Transit time method

The Acoustic Transit Time method (ATT) is also included in the IEC41 (appendix J) as a secondary method. Although the equipment is more costly than the single differential pressure sensor of the WKM, the ease of maintenance of the clamp-on system rivals it. Note that also the cost could be roughly comparable, should there be no premade pressure taps on the spiral casing and if only a two-path clamp-on ATT set-up was selected. This made the ATT an interesting second candidate for the flow estimation for the HydroCord system.

The ATT system has more requirements as to the location of the measurement set-up. The WKM's only requirement is the accessibility of an adequate portion of the spiral casing. The ATT system on the other hand requires a uniform flow through the measurement section, a requirement not always achievable on hydro power plants. The IEC41 lists recommendations and rules for the placement of the measuring section. An adequate section was available at Trollheim power plant upstream the emergency closing valve.

The importance of an adequate section has been underlined on several occasions, notably after analysis of the com-

parison test of T.Rau and M. Eissner presented in their paper [7]. Unlike the test presented in their paper, this test proves the clamp-on system to be correlated over the whole load range.

The ATT system installed at Trollheim power plant is an Ultraflux Uf811 flow-meter with four clamp-on audio-sensors (Two paths). Technical sheet can be found at Ultraflux home page [8].

3.3 The Head-Loss based estimate

As a part of the HydroCord system, the head-loss over the emergency closing valve is being monitored. The Head-loss is a loss of energy due to friction in the component, proportional to the squared volumetric flow rate for turbulent flows (see Darcy-Weisbach equation, e.g. [9]). Assuming the friction factor is constant (a correct assumption within the time frame of a measurement session, but not over a longer period of time) the head loss should provide the basis for an index type measurement of the flow.

It is assumed to have high uncertainty, but could be useful as a control measurement of the flow for simpler versions of the HydroCord system not dotted with both the ATT and the WKM flow measurement systems. Redundancy of measurement should generally prove itself useful for troubleshooting and monitoring self-diagnostics.

The measurement system would have a more demanding calibration requirement than the ATT and WKM systems, as the friction factor of the valve is expected to increase over time.

3.4 The Thermodynamic efficiency measurement, the reference

To calibrate the different flow measurements of the HydroCord system, a primary measurement was required to use as reference. A thermodynamic measurement, performed by the two first authors of this paper (second author Dr. H. Francke as chief-of-tests) and Dr. Jarle Ekanger (Flow Design Bureau) supplied the flow measurements needed.

The test was done in accordance with the IEC41 under good conditions. The resulting flow had an uncertainty of approximately 1,58 % of the total flow (with insignificant variations depending of the load).

The thermodynamic method is a direct measurement of the runner efficiency, not a method based on the computation of it based on an accurate flow measurement. This means that the flow is a derived value from the measurement, and as such may have a higher uncertainty than flow-measurement based methods. This is regrettable, but it was the only method available given the circumstances. Pressure-Time (sometimes referred to as Gibson) requires pressure taps in the pennstock to which there is no access to at Trollheim power plant. Another option would have been a method based on current-meter (point velocity measurements over a known section of the waterway), but our team did not have access to current-meters (nor any experience with the method). Other options would likely lead to similar or higher uncertainty than the one provided by the thermodynamic method.

3.5 Other options, not included

As a fourth estimate of the flow, the guide vane position combined with the square rooted head (see [10], equation 6 and 7) should provide the means to assess the flow. The correlation analysis reported in the paper presenting the HydroCord system [4] supports the hypothesis, at least for the simple linear regression (only based on the guide vane opening). The guide vane position correlation coefficient with the square rooted Winter-Kennedy measurements was 0.99. The authors chose not to include the results of the simple regression model in this paper, as it represents an incomplete measurement method without the head variable. More data at different heads will be needed to determine appropriate coefficients.

4 Results of the uncertainty evaluation

4.1 General

All measurement where calibrated using a regression model. Uncertainty contributors identified where the uncertainty of the regression models, the random uncertainties of the measured values by the sensors and the uncertainty of the reference (thermodynamic measurement uncertainty). The goal of the analysis is to determine the calibrated flow measurements uncertainty.

The uncertainty of the reference where computed in accordance with the IEC41 guidelines and can be found in the measurement report. The uncertainty of the model was found using MatLab's "polyconf" function. Theory behind regression model uncertainty can be found, for example, in Tunghai University lecture notes [11].

The uncertainty computation for the calibration project presented here was done in accordance with the *Guide to the Expression of Uncertainty in Measurement* (GUM, [12]).

During the calibration work a technical error was detected after the first four measurement points already had been taken. These measurement points where discarded. Pressure to complete the measurements within the set time frame explains why no points where taken between 28 and 33 m^3/s.

4.2 Uncertainty - Winter-Kenendy Measurement

For a better visualisation of the uncertainty, figure 1 displays the residual plot with the corresponding measurement uncertainty. The values are shown in table 1. The residuals, R_{WK} are the difference between the reference flow Q_r and the calibrated flow $Q_{c,WK}$. the uncertainty bars displayed are the expanded combined uncertainties of the measurements U for the corresponding measurement point. We see from the figure that there is a good correspondence between the measured values with an acceptable uncertainty. Apart from the expected increase in variance with the flow, no obvious trend in the variation of the residuals is visible. This confirms that the regression model is adequate.

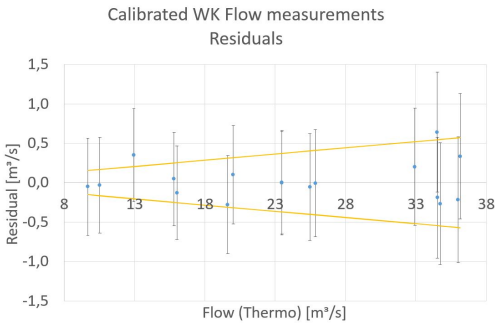

Fig. 1. Winter-Kennedy flow measurement calibration - Residual plot with uncertainty bars. The yellow lines represent the uncertainty in the reference values.

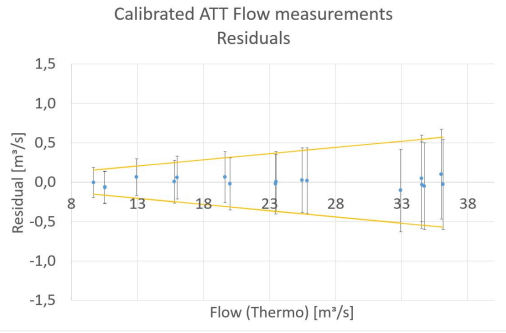

Fig. 2. Acoustic transit time flow measurement Calibration - Residual plot with uncertainty bars. The yellow lines represent the uncertainty in the reference values.

Q_{thermo}	Residual	Model	Thermo	Total
y	$y-\hat{y}$	u_m	u_c	U
36,15	0,334	0,29	0,29	0,80
36	-0,218	0,29	0,28	0,80
34,73	-0,267	0,28	0,27	0,77
34,53	-0,190	0,28	0,27	0,77
34,52	0,641	0,28	0,27	0,76
32,93	0,200	0,28	0,26	0,74
25,85	-0,008	0,28	0,20	0,68
25,47	-0,053	0,28	0,20	0,68
23,48	0,005	0,28	0,19	0,66
23,47	-0,005	0,28	0,19	0,66
20,01	0,102	0,28	0,16	0,62
19,63	-0,278	0,28	0,16	0,62
16,02	-0,129	0,27	0,13	0,59
15,81	0,048	0,28	0,12	0,59
12,95	0,350	0,28	0,10	0,59
10,53	-0,031	0,30	0,08	0,61
9,68	-0,052	0,31	0,08	0,62

Table 1. Winter-Kennedy uncertainty analysis results

Q_{thermo}	Residual	Model	Thermo	Total
y	$y-\hat{y}$	u_m	u_c	U
36,15	-0,030	0,060	0,29	0,57
36,00	0,100	0,060	0,28	0,57
34,73	-0,053	0,060	0,27	0,55
34,53	-0,036	0,060	0,27	0,55
34,52	0,048	0,060	0,27	0,55
32,93	-0,105	0,059	0,26	0,52
25,85	0,018	0,058	0,20	0,42
25,47	0,026	0,058	0,20	0,41
23,49	0,007	0,058	0,19	0,38
23,47	-0,023	0,058	0,19	0,38
20,01	-0,024	0,058	0,16	0,33
19,63	0,065	0,058	0,16	0,32
16,02	0,060	0,059	0,13	0,27
15,81	0,008	0,059	0,12	0,27
12,95	0,065	0,060	0,10	0,23
10,53	-0,064	0,061	0,08	0,20
9,68	-0,004	0,061	0,08	0,19

Table 2. Acoustic transit time uncertainty analysis results

4.3 Uncertainty - Acoustic Transit Time

Figure 2, the residual plot of the ATT, is the equivalent of figure 1 with $R_{ATT} = Q_r - Q_{c,ATT}$. The values are displayed in table 2.

We see from figure 2 that there is a good correlation between the reference values and the calibrated ATT measurement results. No obvious trends are visible in the variation of the residuals.

4.4 Uncertainty - Headloss based flow measurement

The uncertainty of the head-loss based flow measurement are displayed in figure 3 and table 3. The uncertainty is over 1.83 for all measurement.

Because of signal saturation only results for lower flows where obtained. The few measurement points compared with the WKM and ATT methods may partially be to blame for the large uncertainty. The test will have to be repeated to verify this hypothesis, visual inspection of the variation com-

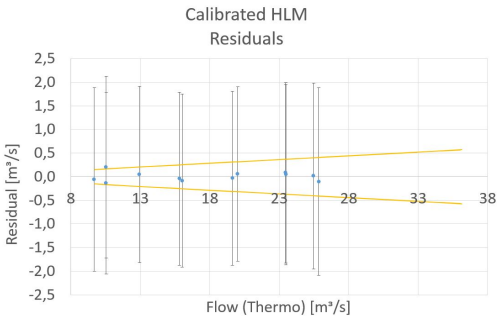

Fig. 3. Head-Loss based flow measurement Calibration - Residual plot with uncertainty bars. The yellow lines represent the uncertainty in the reference values.

Q_{thermo}	Residual	Model	Reference	Total
y	$y-\hat{y}$	u_m	u_c	U
25,85	-0,102	0,969	0,20	1,98
25,47	0,017	0,962	0,20	1,97
23,49	0,045	0,936	0,19	1,91
23,47	0,084	0,935	0,19	1,91
20,01	0,058	0,908	0,16	1,84
19,63	-0,033	0,907	0,16	1,84
16,02	-0,084	0,906	0,13	1,83
15,81	-0,044	0,907	0,12	1,83
12,95	0,049	0,927	0,10	1,87
9,68	-0,057	0,969	0,08	1,94
10,53	0,203	0,960	0,08	1,93
10,53	-0,137	0,955	0,08	1,92

Table 3. Headloss based flow measurement uncertainty analysis results

pared to the two other methods indicates that the model uncertainty may be improved.

4.5 Comparison

Figure 4 presents the residual values of the ATT, WKM and HLM. The uncertainty bands of the reference, ATT and WKM are added and provide a clear picture of the superiority of the ATT measurement method.

The uncertainty band of the HLM was omitted for visual purposes. The band is off-chart and clearly indicates that the two other methods are superior, based on the results of this measurements.

The uncertainty of the ATT model can be deemed insignificant compared to the reference uncertainty for flows above 18 m^3/s while the WKM measurements maintain a significantly larger uncertainty band over the whole range of tested flows. This is confirmed by the visual impression of a larger variance of the WKM measurements (green quares) compared to the ATT measurements (red dots).

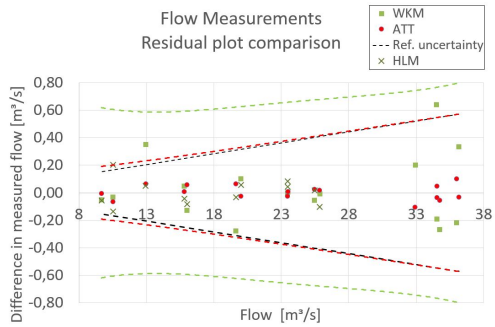

Fig. 4. HydroCord Flow measurements - Residual plot and measurement uncertainty. The Black, red and green lines represent in order the uncertainty of the reference, the Acoustic transit time measurement (ATT) and the Winter-Kennedy measurement (WKM). The red dots, green squares and black crosses represent in order the difference in m^3/s between the reference and the the ATT, WKM and headloss based flow measurements measured at site.

5 Conclusions

Based on the data presented here, it is apparent that the ATT measurement has a lower uncertainty than the Winter-Kennedy method. Depending on the power plant and the existence of a suited measurement section, the ATT measurement system is recommended, even with a mere two path-clamp on system.

This being said, the Winter-Kennedy method results are acceptable, and represents a good alternative if no such measurement section exist. It is also likely to be less costly both in terms of initial investment and in terms of maintenance.

6 Discussion and future works

After performing the uncertainty analysis on the measurements it became apparent that the contribution of the measurement random uncertainty was insignificant, as its order of magnitude was two decimals lower than that of the reference uncertainty. This was mainly due to the steady conditions during the calibration measurements and the high sample count for each measurement ($39776 < n_i$). These results indicate that the sampling time used during the calibration measurements are ample enough to be used during continuous monitoring of the efficiency (where the efficiency will be computed based on values averaged over a period of time).

A second test, similar to this one at Trollheim power plant should be undertaken. By using another method as a reference, possibly the current-meter method, the uncertainty

of the ATT measurement set-up may be improved as it is the thermodynamic reference uncertainty that is the largest contributor.

A second test would also permit a new test of the head-loss based measurement, who has shown interesting results. From visual inspection of figure 4 the spread of the residuals is lower that of the Winter-Kennedy index test.

Acknowledgements

We would like to thank Jarle Ekanger and the regional staff of Statkraft (Trollheim power plant group) for the support and aid during the thermodynamic efficiency test.

We also would like to thank Statkraft and the Norwegian Reseach Council for their financial support.

References

[1] Wiborg, E. J. "Continuous Efficiency Measurements on Hydro Power Plants". PhD Thesis, Norwegian University of Science and Technology, NTNU, NO-7491 Trondheim, Norway, [To be published in 2016/2017].

[2] TC4, 1991. Iec-60041, field acceptance tests to determine the hydraulic performance of hydraulic turbines, storage pumps and pump-turbines. International standard, International Electrotechnical Commission.

[3] US Army Corps of Engineers, 2006. Hydro plant risk assessment guide - appendix e6: Turbine condition assessment. Guide, US Army Corps of Engineers.

[4] Erik J. Wiborg, Håkon H. Francke, T. N. "Hydrocord condition monitoring system". Linz, International Group for Hydrodynamic Efficiency Measurements. [To be published in 2016].

[5] Kubiak, J., Urquiza, G., Adamkowski, A., Sierra, F., Janicki, W., and Rangel, R., 2005. "Special instrumentation and hydraulic turbine flow measurements using a pressure-time method". In ASME 2005 Fluids Engineering Division Summer Meeting, American Society of Mechanical Engineers, pp. 433–439.

[6] Honeywell. Pressure transmitter st 700 - technical sheet. https://www.honeywellprocess.com/library/support/Public/Documents/34-ST-25-44.pdf.

[7] Tobias Rau, M. E., 2012. "Comparison of discharge measurements - comparison of discharge measurements -thermodynamic to us clamp thermodynamic to us clamp thermodynamic to us clampon, stationary us and needle opening on, stationary us and needle openingcurve". 9th conference on hydraulic efficiency measurements, Trondheim, International Group for Hydrodynamic Efficiency Measurements.

[8] Ultraflux. Uf 811 - technical sheet. http://www.ultraflux.net/en/products/flowmeters-for-liquids-full-pipes/uf-811/.

[9] Brown, G. O., 2002. "The history of the darcy-weisbach equation for pipe flow resistance". *Environmental and Water Resources History,* **38**(7), pp. 34–43.

[10] Tobias Rau, M. E., 2012. Comparison of discharge measurements -thermodynamic to us clamp, stationary us and needle opening curve. Tech. rep., IGHEM.

[11] TUNGHAI UNIVERSITY. *Financial and Econometrics Lecture Notes - Chapter 4 Properties of the Least Squares Estimators*, 2 ed.

[12] JCGM - BIPM, 1995. Evaluation of measurement data guide to the expression of uncertainty in measurement.

E Calibration Reports

HydroCord
Winter-Kennedy Calibration

Erik J. Wiborg (erik.jacques.wiborg@statkraft.com)

August 12, 2016

Contents

1 General description

This document serves as the calibration certificate of the flow estimation through Winter-Kennedy measurements (WKM) at Trollheim power plant for measurement of the total flow through the runner. The measurement equipment in question is a Honeywell ST 700 pressure transmitter, see [1].

The accuracy of the device is stated to be up to 0.05% of the calibrated span by the supplier (see [1]).

The WKM is mounted on a section of the turbine spiral casing, see site 4 in figure 1.

The results from a standard thermodynamic field efficiency measurement (HFEM), according to IEC 60041 (IEC41, [2]), will be used to calibrate the HLM results. The HFEM measurement set-up can be found described in details in the IEC41. It is also described in the HFEM measurement report.

The WKM system output A can be represented as in equation 1.

$$Q = \alpha A^2 + \beta A + A_0 + \epsilon \tag{1}$$

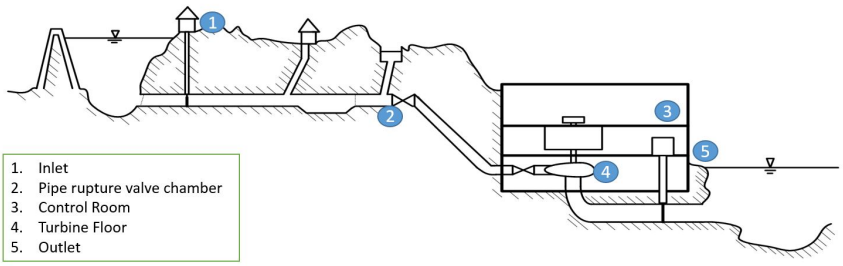

Figure 1: HydroCord measurement sites overview

With Q the true flow, α, β and A_0 the calibration constants, and ϵ the random error.

2 Uncertainty computation - theoretical background

The uncertainty computation of the calibration coefficients, as presented here, is done according to the *Guide to the Expression of Uncertainty in Measurement* (GUM) [3].

Measurement model
The mathematical representation of the measurement is given in equation 2.

$$Q = \alpha A^2 + \beta A + A_0 + \epsilon_Q + \epsilon \tag{2}$$

The equation can be recognized as equation 1, added the uncertainty of the flow measurement through the HFEM, ϵ_Q.

The uncertainty of A has proven to be in the magnitude of a hundredth of the uncertainty of the model and ϵ_Q. This is mainly because of steady state measurements and the high amount of repeated measurements ($39776 < n_i < 120199$). The impact on the total uncertainty is deemed insignificant, and the random uncertainty of A is ignored from this point on. Note that the systematic uncertainty of the measurements is the goal of this analysis.

Inputs and their evaluation type A/B
HFEM uncertainty, ϵ_Q will have a type B evaluation of the uncertainty. This because the reported flow is a derived value, based on the averaged value of several measurements.
The model uncertainty is found through a statistical analysis of the model regression and will also have a B type of uncertainty.
The random uncertainty of the measured values A would have been analysed as a type A evaluation, but as mentioned earlier, is not included in the report as the contribution is insignificant.

Input standard uncertainties $u(X)$
The computation of the thermodynamic flow uncertainty $u(\epsilon_{Q,i})$, can be found in the FEM report.
The model is found through a regression analysis and the uncertainty is calculated using MATLAB's "polyconf" function. The function generates 95% prediction intervals Y DELTA for new observations at the values in X. This uncertainty will be used as an estimation of the model uncertainty as a whole, i.e. including the uncertain of all three regression coefficients.

Combined and expanded uncertainty $u_c(Q)$,U
The combined uncertainty of the measurand Q will be computed according to equation 3.

$$u_c(Q) = \sqrt{\sum u_X^2} = \sqrt{\sum (c(X)u(X))^2} \tag{3}$$

With $c(X)$ the sensitivity coefficient and u_X the contribution of input X to the combined uncertainty defined as $u_X = c(X)u(X)$

The expanded uncertainty U is defined by equation

$$U = \kappa u_c \tag{4}$$

The uncertainty of the flow is assumed to be normally distributed, thus leading to the expansion factor $\kappa = 1.96$, with a 95 % confidence interval.

3 Results

Calibration coefficients

Figure 2 displays the calibration results. The curve polynomial fit through the least square method, equation 5, is displayed as the red curve in figure 2.

$$Q = -948.48 * A^2 + 1771.49 * A - 772.23 \tag{5}$$

The resulting calibration constants are therefore as bellow.

α	-948.48
β	1771.49
A_0	-772.23

WKM Flow uncertainty
For a better visual aid, the uncertainty can be viewed on the residual plot, figure 5. The figure displays the difference between the measured flow through the HFEM and the calibrated Winter-Kennedy measurements, $r = Q_t - \hat{Q}_{WK}$. The uncertainty bars indicate the uncertainty of measurement for each point.

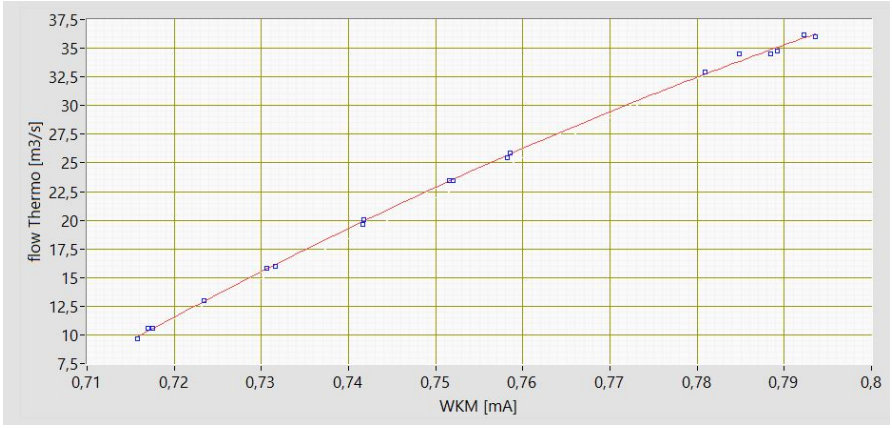

Figure 2: WKM calibration plot

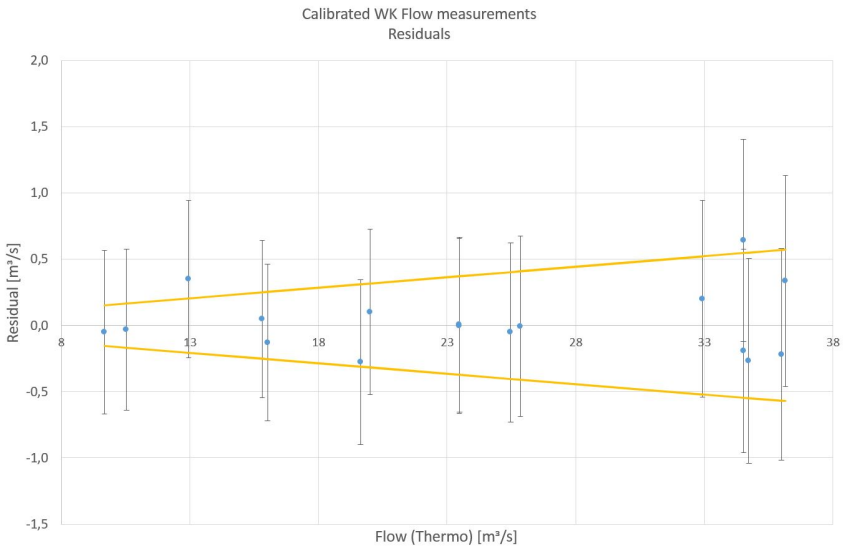

Figure 3: **Winter-Kennedy flow measurement - residual plot and uncertainty**
Blue points indicate the difference between the measured flow values through the Winter-kennedy method and the thermodynamic method. The orange lines indicate the uncertainty band of the thermodynamic method.

The values of the uncertainty analysis are displayed in the table bellow.

	Q_{WK-raw}	$Q_{WK-calib}$	Q_{thermo}	Residual	Model	Thermo	Total
	x	$\hat{y}$	y	$y - \hat{y}$	u_m	u_c	U
1	0,792	35,82	36,15	0,334	0,2886	0,29	0,80
2	0,7935	36,22	36	-0,218	0,2927	0,28	0,80
3	0,789	35,00	34,73	-0,267	0,2825	0,27	0,77
4	0,788	34,72	34,53	-0,190	0,2809	0,27	0,77
5	0,785	33,88	34,52	0,641	0,2775	0,27	0,76
6	0,781	32,73	32,93	0,200	0,2754	0,26	0,74
7	0,759	25,86	25,85	-0,008	0,2809	0,20	0,68
8	0,758	25,52	25,47	-0,053	0,2810	0,20	0,68
9	0,752	23,48	23,48	0,005	0,2804	0,19	0,66
10	0,752	23,48	23,47	-0,005	0,2804	0,19	0,66
11	0,742	19,91	20,01	0,102	0,2767	0,16	0,62
12	0,742	19,91	19,63	-0,278	0,2767	0,16	0,62
13	0,732	16,15	16,02	-0,129	0,2749	0,13	0,59
14	0,731	15,76	15,81	0,048	0,2752	0,12	0,59
15	0,723	12,60	12,95	0,350	0,2843	0,10	0,59
16	0,718	10,56	10,53	-0,031	0,2979	0,08	0,61
17	0,716	9,73	9,68	-0,052	0,3056	0,08	0,62

4 Conclusion and discussion

The following calibration has been done in accord to the *Evaluation of measurement data Guide to the expression of uncertainty in measurement* (GUM, [3]). The uncertainty analysis of the Winter-Kennedy flow measurement system at Trollheim power plant resulted in a calibration coefficients as listed bellow.

α	-948.48
β	1771.49
A_0	-772.23

The uncertainty is highly driven by the uncertainty of the flow measurement of the thermodynamic measurement. A better flow measurement would provide the means to improve on the uncertainty of the Winter-Kennedy flow measurement.

To assess the uncertainty of the measured value the table provided in this report should

be used for interpolation of a uncertainty estimate. As a simple first estimate, the function shown in figure 4 can be used.

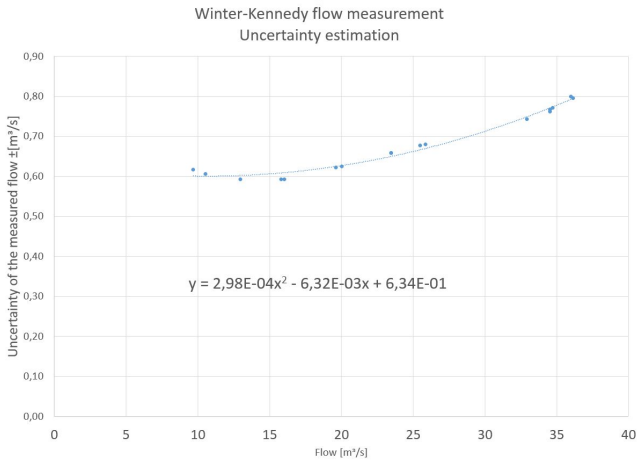

Figure 4: **Winter-Kennedy flow measurement - Uncertainty of measurement**

References

[1] Honeywell, "Pressure transmitter st 700 - technical sheet." [Online]. Available: https://www.honeywellprocess.com/library/support/Public/Documents/34-ST-25-44.pdf

[2] IEC, "Iec-60041, field acceptance tests to determine the hydraulic performance of hydraulic turbines, storage pumps and pump-turbines," 1991.

[3] JCGM, "Evaluation of measurement data - guide to the expression of uncertainty in measurement," 1995. [Online]. Available: http://www.bipm.org/en/publications/guides/gum.html

HydroCord
Acoustic Transit Time Calibration

Erik J. Wiborg (erik.jacques.wiborg@statkraft.com)

August 12, 2016

Contents

1 General description

This document serves as the calibration certificate of the Acoustic Transit Time measurement (hereby referred to as ATT) at Trollheim power plant for measurement of the total flow through the runner. The measurement equipment in question is an Ultraflux Uf811 flowmeter with four clamp-on audio-sensors (Two paths) technical sheet can be found at Ultraflux home page [1].

The accuracy of the device is stated to be up tp 0.5 % by the supplier (see [1]). A thermodynamic efficiency measurement was performed on cite to determine the uncertainty.

The ATT measurement is mounted upstream the power plant emergency closing valve, see site 2 in figure 1.

The results from a standard thermodynamic field efficiency measurement (HFEM), according to IEC 60041 (IEC41, [2]), will be used to calibrate the ATT results.

The HFEM measurement set-up can be found described in details in the IEC41. It is also decribed in the HFEM measurement report.

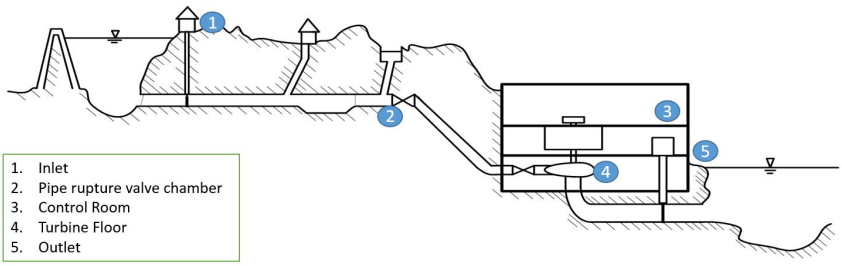

Figure 1: HydroCord measurement sites overview

The ATT system output flow Q_{ATT} can be represented as in equation 1.

$$Q = kQ_{ATT} + q_0 + \epsilon \tag{1}$$

With Q the true flow, k the systematic error, q_0 a zero-point calibration error (bias), and ϵ the random error.

The goal of the calibration is to estimate the systematic uncertainty k, the bias Q_0 and estimate the uncertainty of the flow given by the ATT.

2 Uncertainty computation - theoretical background

The uncertainty computation of the calibration coefficient k, as presented here, is done according to the *Guide to the Expression of Uncertainty in Measurement* (GUM) [3].

Measurement model
The mathematical representation of the measurement is given in equation 2.

$$Q = kQ_{ATT} + q_0 + \epsilon_Q + \epsilon \tag{2}$$

The equation can be recognized as equation 1, added the uncertainty of the flow measurement through the HFEM, ϵ_Q.

The random uncertainty of A has proven to be in the magnitude of a hundredth of the uncertainty of the model and ϵ_Q. This is mainly because of steady state measurements and the high amount of repeated measurements ($39776 < n_i < 120199$). The impact on the total uncertainty is deemed insignificant, and the random uncertainty of A is ignored from this point on. Note that the systematic uncertainty of the measurements is the goal of this analysis.

Inputs and their evaluation type A/B
HFEM uncertainty, ϵ_Q will have a type B evaluation of the uncertainty. This because the reported flow is a derived value, based on the averaged value of several measurements. The model uncertainty is found through a statistical analysis of the model regression and will also have a B type of uncertainty.
The random uncertainty of the measured values A would have been analysed as a type A evaluation, but as mentioned earlier, is not included in the report as the contribution is insignificant.

Input standard uncertainties $u(X)$
The computation of the thermodynamic flow uncertainty $u(\epsilon_{Q,i})$, can be found in the FEM report.
The model is found through a regression analysis and the uncertainty is calculated using MATLAB's "polyconf" function. The function generates 95% prediction intervals Y DELTA for new observations at the values in X. This uncertainty will be used as an estimation of the model uncertainty as a whole, i.e. including the uncertain of both regression coefficients.

Combined and expanded uncertainty $u_c(Q)$**,** U
The combined uncertainty of the measurand Q will be computed according to equation 3.

$$u_c(Q) = \sqrt{\sum u_X^2} = \sqrt{\sum (c(X)u(X))^2} \tag{3}$$

With $c(X)$ the sensitivity coefficient and u_X the contribution of input X to the combined uncertainty defined as $u_X = c(X)u(X)$

The expanded uncertainty U is defined by equation

$$U = \kappa u_c \tag{4}$$

The uncertainty of the flow is assumed to be normally distributed, thus leading to the expansion factor $\kappa = 1.96$, with a 95 % confidence interval.

3 Results

Calibration coefficients

Figure 2 displays the calibration results.The calibration coefficient is $k = 1.099$, the bias $q_0 = 0.1$.

ATT Flow uncertainty
For a better visual aid, the uncertainty can be viewed on the residual plot, figure 3. The figure displays the difference between the measured flow through the HFEM and the calibrated Acoustic Transit Time method, $r = Q_t - \hat{Q}_{WK}$. The uncertainty bars

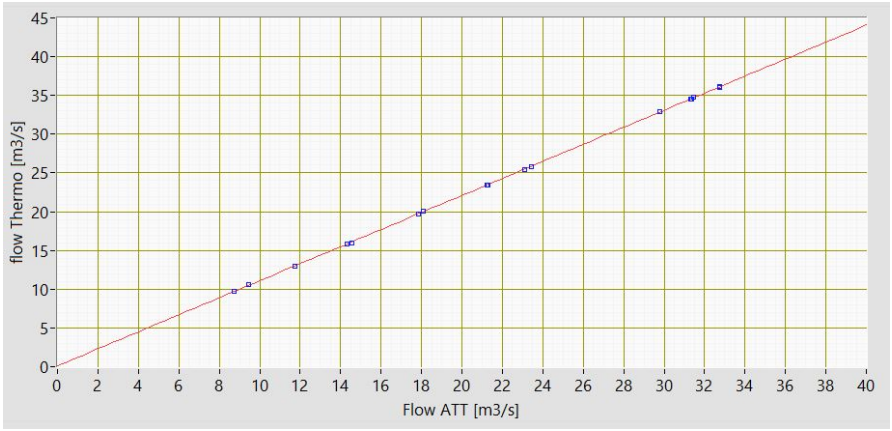

Figure 2: ATT calibration plot

indicate the uncertainty of measurement for each point. The values of the uncertainty analysis are displayed in the table bellow.

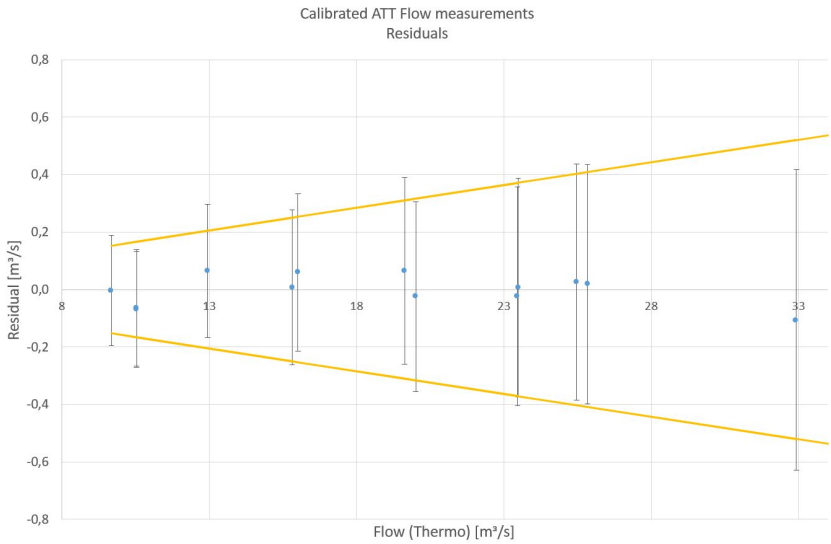

Figure 3: **Acoustic Transit Time Flow measurement - residual plot and uncertainty**
Blue points indicate the difference between the measured flow values through the ATT method and the thermodynamic method. The orange lines indicate the uncertainty band of the thermodynamic method.

	$Q_{ATT-raw}$	$Q_{ATT-calib}$	Q_{thermo}	Residual	Model	Thermo	Total
	x	$\hat{y}$	y	$y - \hat{y}$	u_m	u_c	U
1	31,29	34,49	34,53	-0,036	0,0598	0,27	0,55
2	31,46	34,68	34,73	-0,053	0,0599	0,27	0,55
3	32,75	36,10	36,00	0,100	0,0604	0,28	0,57
4	32,77	36,12	36,15	-0,030	0,0605	0,29	0,57
5	31,36	34,57	34,52	0,048	0,0598	0,27	0,55
6	23,44	25,86	25,85	0,018	0,0578	0,20	0,42
7	23,11	25,50	25,47	0,026	0,0578	0,20	0,41
8	21,28	23,49	23,49	0,007	0,0577	0,19	0,38
9	21,24	23,45	23,47	-0,023	0,0577	0,19	0,38
10	18,10	19,99	20,01	-0,024	0,0579	0,16	0,33
11	17,83	19,70	19,63	0,065	0,0580	0,16	0,32
12	14,54	16,08	16,02	0,060	0,0587	0,13	0,27
13	14,31	15,82	15,81	0,008	0,0587	0,12	0,27
14	11,75	13,01	12,95	0,065	0,0596	0,10	0,23
15	8,72	9,68	9,68	-0,004	0,0609	0,08	0,19
16	9,44	10,47	10,53	-0,064	0,0606	0,08	0,20
17	9,43	10,47	10,53	-0,068	0,0606	0,08	0,20
18	29,77	32,82	32,93	-0,105	0,0592	0,26	0,52

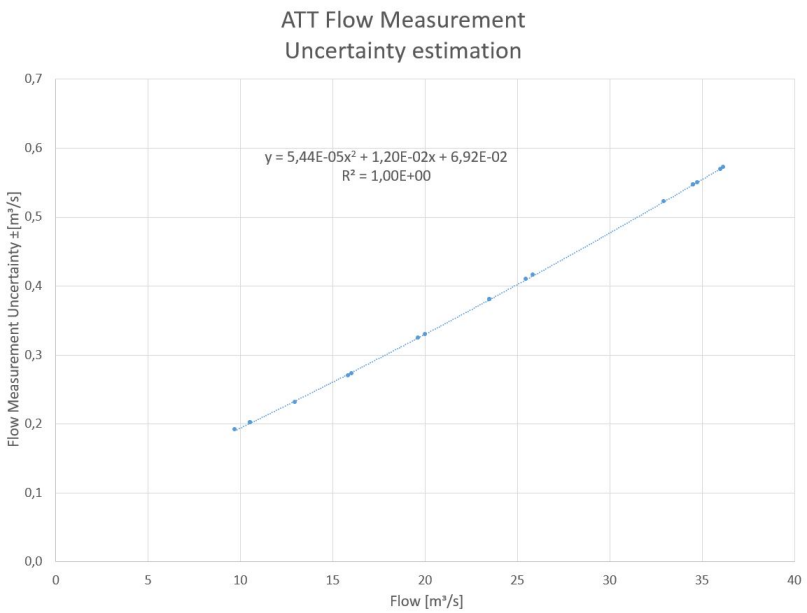

Figure 4: **ATT flow measurement - Uncertainty of measurement**

4 Conclusion

The following calibration has been done in accord to the *Evaluation of measurement data Guide to the expression of uncertainty in measurement* (GUM, [3]). The uncertainty analysis of the acoustic transit time flow measurement system at Trollheim power plant resulted in a calibration coefficient $k = 1.099$ and bias $q_0 = 0,1$.

The uncertainty of the measurement is greatly dependent on the uncertainty of the HFEM measurement of the flow, especially for higher flows the model uncertainty is insignificant. An estimation of the uncertainty at any flow can be found by using the function displayed in the figure bellow.

References

[1] Ultraflux, "Uf 811 - technical sheet." [Online]. Available: http://www.ultraflux.net/en/products/flowmeters-for-liquids-full-pipes/uf-811/

[2] IEC, "Iec-60041, field acceptance tests to determine the hydraulic performance of hydraulic turbines, storage pumps and pump-turbines," 1991.

[3] JCGM, "Evaluation of measurement data - guide to the expression of uncertainty

in measurement," 1995. [Online]. Available: http://www.bipm.org/en/publications/guides/gum.html

HydroCord
Head Loss Based Flow Calibration

Erik J. Wiborg (erik.jacques.wiborg@statkraft.com)

August 12, 2016

Contents

1. General description

This document serves as the calibration certificate of the flow estimation through head loss measurements (HLM) at Trollheim power plant for measurement of the total flow through the runner. The measurement equipment in question is a Honeywell ST 700 pressure transmitter, see [1].

The accuracy of the device is stated to be up to 0.05% of the calibrated span by the supplier (see [1]).

The HLM is mounted upstream the power plant emergency closing valve, see site 2 in figure 1.

The results from a standard thermodynamic field efficiency measurement (HFEM), according to IEC 60041 (IEC41, [2]), will be used to calibrate the HLM results. The HFEM measurement set-up can be found described in details in the IEC41. It is also described in the HFEM measurement report.

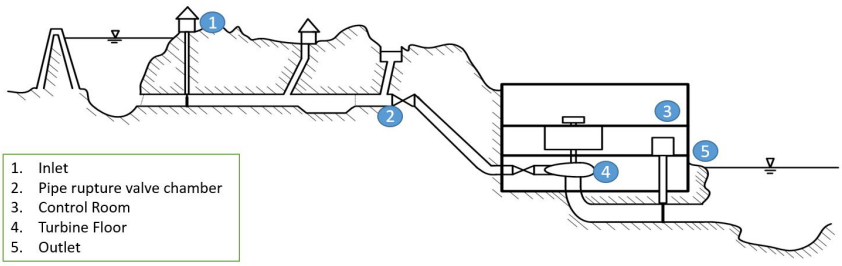

Figure 1: HydroCord measurement sites overview

The HLM system output A can be represented as in equation 1.

$$Q = \alpha A^2 + \beta A + A_0 + \epsilon \tag{1}$$

With Q the true flow, α, β and A_0 the calibration constants, and ϵ the random error.

2. Uncertainty computation - theoretical background

The uncertainty computation of the calibration coefficients, as presented here, is done according to the *Guide to the Expression of Uncertainty in Measurement* (GUM) [3].

Measurement model
The mathematical representation of the measurement is given in equation 2.

$$Q = \alpha A^2 + \beta A + A_0 + \epsilon_Q + \epsilon \tag{2}$$

The equation can be recognized as equation 1, added the uncertainty of the flow measurement through the HFEM, ϵ_Q.

$$q(i) = \alpha \bar{a}_i^2 + \beta \bar{a}_i + A_0 + \epsilon_{Q,i} + \epsilon \tag{3}$$

Equation 3 represents equation 2 in its in finite form with $q(i)$ the true flow at index i, $\bar{a}_i$ the mean of the recorded HLM index i series and $\epsilon_{Q,i}$ the uncertainty of the flow (estimated through the HFEM).

Inputs and their evaluation type A/B
HFEM uncertainty, ϵ_Q will have a type B evaluation of the uncertainty. This because the reported flow is a derived value, based on the averaged value of several measurements. The calibration coefficient α, β and A_0 will have their uncertainty evaluated by statistical analysing of the spread between the measured values and the modelled ideal values (least squared polynomial fit). This will be considered as repeated measurements, and

is deemed acceptable for an A type evaluation.
A are repeated measurement over time and will have an A-type evaluation.

Input standard uncertainties $u(X)$
The computation of the thermodynamic flow uncertainty $u(\epsilon_{Q,i})$, can be found in the FEM report.
The computation of the uncertainty in the mean recorded HLM values are $u(\bar{a}_i) = s(A_i)/\sqrt{n_i}$, with $s(A_i)$ the standard deviation of the measured HLM values A_i, and n_i the series size.
The uncertainty of the three calibration coefficients must be combined to describe the variation between the modelled values and the actual. This leads to the uncertainty definitions of α, β and A_0, in order $u(\alpha)$, $u(\beta)$ and $u(A_0)$ as in equation 4.

$$u(\alpha) = u(\beta) = u(A_0) = \sqrt{\frac{1}{m}\sum_{i=1}^{m}\frac{(\bar{a}_i - a_{M,i})^2}{3}} \tag{4}$$

With m the number of measurement series, and $a_{M,i}$ the computed value using a least square polynomial fit.

Sensitivity coefficients $c(X)$
The sensitivity coefficients of the inputs $c(\alpha)$, $c(\beta)$, $c(A_0)$, $c(\bar{a}_i)$ and $c(\epsilon_{Q,i})$ are given by the results of the partial derivative of the measurement model.

$$c(\alpha) = \bar{a}_i^2$$

$$c(\beta) = \bar{a}_i$$

$$c(A_0) = 1$$

$$c(\bar{a}_i) = 2\alpha\bar{a}_i + \beta$$

$$c(\epsilon_{Q,i}) = 1$$

Combined uncertainty $u_c(Q)$
The combined uncertainty of the measurand Q will be computed according to equation 5.

$$u_c(Q) = \sqrt{\sum u_X^2} = \sqrt{\sum (c(X)u(X))^2} \tag{5}$$

With u_X the contribution of input X to the combined uncertainty defined as $u_X = c(X)u(X)$

Expanded uncertainty
The expanded uncertainty U is defined by equation

$$U = \kappa u_c \tag{6}$$

The uncertainty of the flow is assumed to be normally distributed, thus leading to the expansion factor $\kappa = 1.96$, with a 95 % confidence interval.

3. Results

Saturated signal
It is obvious that the head loss signal reaches saturation at 10,5 mA, see figure 2. This is a configuration error and can be rectified by adjusting the signal amplification. Only measurements with mean values bellow 10mA will be analysed further.

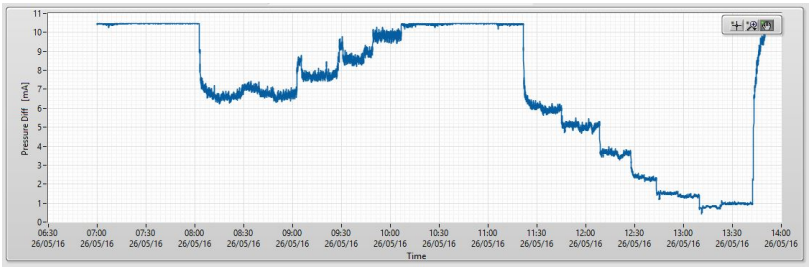

Figure 2: Trollheim HLM - Saturated signal at 10,5 mA

As will be shown through this analysis, the flow measurement has such high uncertainties even for lower flows than these, that the value of these measurements is marginal.

Calibration coefficients

Figure 3 displays the calibration results. The curve polynomial fit through the least square method, equation 7, is displayed as the red curve in figure 3.

$$Q = -0.274 * A^2 + 4.82 * A + 6,23 \tag{7}$$

The resulting calibration constants are therefore as bellow.

α	-0.274
β	4.82
A_0	6,23

HLM Flow uncertainty
Referring to equation 2, the uncertainty budget is described in the table bellow for the first measurement. The rest of the uncertainty values can be found in appendix A.

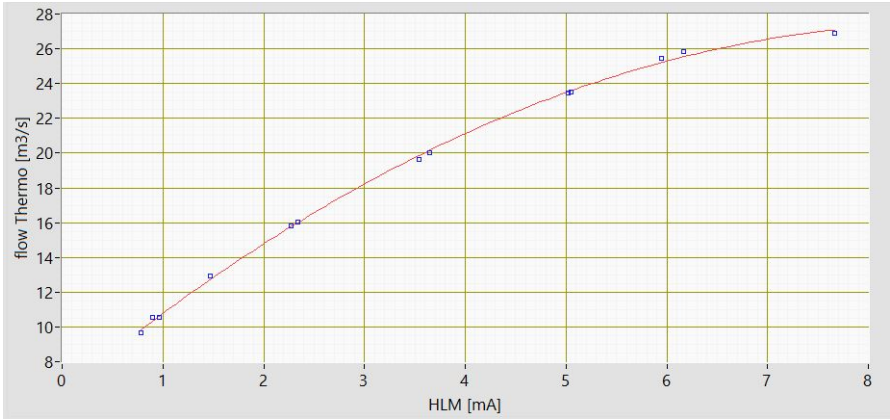

Figure 3: HLM calibration plot

Input X	**Size**	**Type**	**Samples**	**std**	$u(X)$	$c(X)$	$u_X(Q)$	$u_c(Q)$	U
α	-0,27	A	13	0,106	0,01498	58,8289	0,881	0,91	1,79
β	4,82	A	13	0,106	0,01498	7,67	0,115		
A_0	6,234	A	13	0,106	0,01498	1	0,015		
$\bar{a}$	7,67	A	119788	0,19	0,00055	0,68	0,000		
ϵ_Q	26,87	B	-		0,21227	1	0,212		

This leads to a combined standard uncertainty $u_c(Q) = 0.91$, and an expanded uncertainty of $U = 1.79$.

The combined standard uncertainty values can be seen in figure 4. Where the HLM values - in blue - have their uncertainty outlined by the dotted lines, and the flow measurements reported from the thermodynamic measurements are marked by red crosses and their uncertainty according black uncertainty bars.

The uncertainties of each measurement are listed in the following table, and the relative uncertainty in figure 5. All values are in $[m^3/s]$

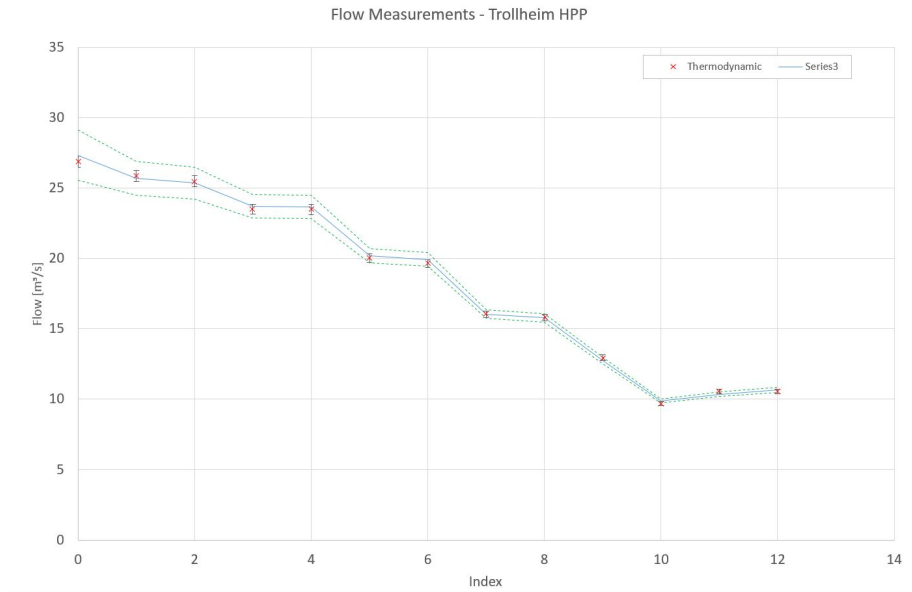

Figure 4: Trollheim Flow Measurements

index	Q (Thermo)	U (Thermo)	HLM	u_c	$U[m^3/s]$	$U[\%]$
0	26,87	0,42	27,32	0,91	1,79	6,6
1	25,85	0,20	25,69	0,61	1,20	4,7
2	25,47	0,20	25,35	0,57	1,13	4,4
3	23,49	0,19	23,69	0,43	0,85	3,6
4	23,47	0,19	23,65	0,43	0,84	3,6
5	20,01	0,16	20,20	0,26	0,51	2,5
6	19,63	0,16	19,91	0,25	0,49	2,5
7	16,02	0,13	16,03	0,16	0,30	1,9
8	15,81	0,12	15,78	0,15	0,30	1,9
9	12,95	0,10	12,74	0,11	0,22	1,7
10	9,68	0,08	9,87	0,08	0,16	1,6
11	10,53	0,08	10,35	0,09	0,17	1,6
12	10,53	0,08	10,66	0,09	0,17	1,6

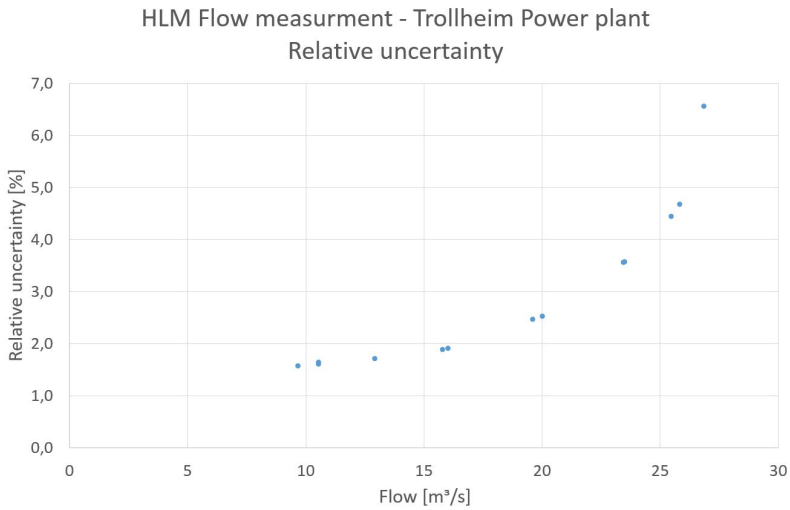

Figure 5: Trollheim Flow Measurements - relative uncertainty

4. Conclusion and discussion

The following calibration has been done in accord to the *Evaluation of measurement data Guide to the expression of uncertainty in measurement* (GUM, [3]). The uncertainty analysis of the headloss based flow measurement system at Trollheim power plant resulted in a calibration coefficients as listed bellow.

α	-0.274
β	4.82
A_0	6,23

The uncertainty increases exponentially and even for the 7,6 mA values the uncertainty in the flow is above 6 %, see figure 5. Although the signal amplification needs to be adjusted to provide head loss measurements, the use for flow estimation is discouraged for flows above 15 m^3/s (Where the uncertainty is bellow 2%).

It can still be, to a certain extent, used as a control measurement for the ATT and winter Kennedy measurements at cite in particular for low flows.

References

[1] Honeywell, "Pressure transmitter st 700 - technical sheet." [Online]. Available: https://www.honeywellprocess.com/library/support/Public/Documents/34-ST-25-44.pdf

[2] IEC, "Iec-60041, field acceptance tests to determine the hydraulic performance of hydraulic turbines, storage pumps and pump-turbines," 1991.

[3] JCGM, "Evaluation of measurement data - guide to the expression of uncertainty in measurement," 1995. [Online]. Available: http://www.bipm.org/en/publications/guides/gum.html

A. Uncertainty budget table - ATT Flow Measurement

Index	**X**	**Size**	**Type**	**n**	**std**	$u(X)$	$c(X)$	$u_X(Q)$	$u_c(Q)$	U
0	α	-0,27	A	13	0,106	0,015	58,83	0,881	0,91	1,79
	β	4,82	A	13	0,106	0,015	7,67	0,115		
	A_0	6,234	A	13	0,106	0,015	1	0,015		
	$\bar{a}$	7,67	A	119788	0,19	0,00055	0,68	0,000		
	ϵ_Q	26,87	B	-		0,212	1	0,212		
1	α	-0,27	A	13	0,106	0,015	38,07	0,570	0,61	1,20
	β	4,82	A	13	0,106	0,015	6,17	0,092		
	A_0	6,234	A	13	0,106	0,015	1	0,015		
	$\bar{a}$	6,17	A	68661	0,2	0,00076	1,49	0,001		
	ϵ_Q	25,85	B	-		0,204	1	0,204		
2	α	-0,27	A	13	0,106	0,015	35,40	0,530	0,57	1,13
	β	4,82	A	13	0,106	0,015	5,95	0,089		
	A_0	6,234	A	13	0,106	0,015	1	0,015		
	$\bar{a}$	5,95	A	118943	0,19	0,00055	1,61	0,001		
	ϵ_Q	25,47	B	-		0,201	1	0,201		
3	α	-0,27	A	13	0,106	0,015	25,50	0,382	0,43	0,85
	β	4,82	A	13	0,106	0,015	5,05	0,076		
	A_0	6,234	A	13	0,106	0,015	1	0,015		
	$\bar{a}$	5,05	A	119776	0,17	0,00049	2,09	0,001		
	ϵ_Q	23,49	B	-		0,186	1	0,186		
4	α	-0,27	A	13	0,106	0,015	25,30	0,379	0,43	0,84
	β	4,82	A	13	0,106	0,015	5,03	0,075		
	A_0	6,234	A	13	0,106	0,015	1	0,015		
	$\bar{a}$	5,03	A	95966	0,17	0,00055	2,10	0,001		
	ϵ_Q	23,47	B	-		0,185	1	0,185		
5	α	-0,27	A	13	0,106	0,015	13,25	0,198	0,26	0,51
	β	4,82	A	13	0,106	0,015	3,64	0,055		
	A_0	6,234	A	13	0,106	0,015	1	0,015		
	$\bar{a}$	3,64	A	118943	0,14	0,00041	2,85	0,001		
	ϵ_Q	20,01	B	-		0,158	1	0,158		
6	α	-0,27	A	13	0,106	0,015	12,53	0,188	0,25	0,49
	β	4,82	A	13	0,106	0,015	3,54	0,053		
	A_0	6,234	A	13	0,106	0,015	1	0,015		
	$\bar{a}$	3,54	A	89366	0,15	0,00050	2,91	0,001		
	ϵ_Q	19,63	B	-		0,155	1	0,155		

Index	X	Size	Type	n	std	$u(X)$	$c(X)$	$u_X(Q)$	$u_c(Q)$	U
7	α	-0,27	A	13	0,106	0,015	5,47	0,082	0,16	0,30
	β	4,82	A	13	0,106	0,015	2,33879	0,035		
	A_0	6,234	A	13	0,106	0,015	1	0,015		
	$\bar{a}$	2,33879	A	119999	0,13	0,00038	3,56	0,001		
	ϵ_Q	16,02	B	-		0,127	1	0,127		
8	α	-0,27	A	13	0,106	0,015	5,15	0,077	0,15	0,30
	β	4,82	A	13	0,106	0,015	2,27	0,034		
	A_0	6,234	A	13	0,106	0,015	1	0,015		
	$\bar{a}$	2,27	A	38240	0,13	0,00066	3,59	0,002		
	ϵ_Q	15,81	B	-		0,125	1	0,125		
9	α	-0,27	A	13	0,106	0,015	2,16	0,032	0,11	0,22
	β	4,82	A	13	0,106	0,015	1,47	0,022		
	A_0	6,234	A	13	0,106	0,015	1	0,015		
	$\bar{a}$	1,47	A	120199	0,11	0,00032	4,03	0,001		
	ϵ_Q	12,95	B	-		0,102	1	0,102		
10	α	-0,27	A	13	0,106	0,015	0,62	0,009	0,08	0,16
	β	4,82	A	13	0,106	0,015	0,79	0,012		
	A_0	6,234	A	13	0,106	0,015	1	0,015		
	$\bar{a}$	0,79	A	120199	0,11	0,00032	4,39	0,001		
	ϵ_Q	9,68	B	-		0,076	1	0,076		
11	α	-0,27	A	13	0,106	0,015	0,81	0,012	0,09	0,17
	β	4,82	A	13	0,106	0,015	0,9	0,013		
	A_0	6,234	A	13	0,106	0,015	1	0,015		
	$\bar{a}$	0,9	A	119999	0,12	0,00035	4,33	0,002		
	ϵ_Q	10,53	B	-		0,083	1	0,083		
11	α	-0,27	A	13	0,106	0,015	0,94	0,014	0,09	0,17
	β	4,82	A	13	0,106	0,015	0,97	0,015		
	A_0	6,234	A	13	0,106	0,015	1	0,015		
	$\bar{a}$	0,97	A	119999	0,07	0,00020	4,30	0,001		
	ϵ_Q	10,53	B	-		0,083	1	0,083		

F Permission To Release Efficiency Measurements

Publisering av Trollheim data

Lysaker, Henning

on 31.08.2016 11:36

Til:Wiborg Erik Jacques <Erik.Jacques.Wiborg@statkraft.com>;

Hei Erik

Ref. Telefonsamtale

Vi gir tillatelse til pubilisering av data på Trollheim, inkludert virkningsgrad.
Forutsetter at Geometrien ikke publiseres.

Lykke til innspurten

Mvh
Henning

RAINPOWER

Henning Lysaker
CTO & Department manager
Turbinlaboratoriet

Rainpower Norge AS

Postal address:
PB 6088
7434 Trondheim

Visit adress:
S.P.Andersensvei 7
7031 Trondheim
Norway

M:+ 47 90 66 69 70
T:+47 73 83 80 42
henning.lysaker@rainpower.no
rainpower.no

G Thermodynamic Efficiency Measurement Report

Flow Design Bureau AS
C/O IPark, Stavanger
PO Box 8034, N 4068 Stavanger, Norway
Tel: +47 51 87 44 94, www.fdb.no

Rapport

Tittel: **Trollheim Kraftverk: Virkningsgradsmåling**			
Forfatter(e): Dr. Håkon Francke			Rapport nr.: **284**
Kunde: **Statkraft Energi AS**			Statkraft
Prosjekt nr: **913102**	Kundes ref: **Wiborg/701547**	Dato: **25.08.2016**	Antall sider / Appendiks: **31/18**

Oppsummering:

Rapporten presenterer resultater fra Termodynamisk virkningsgradsmåling på Trollheim Kraftverk 25.05.2016. Målingene ble utført av Håkon Hjort Francke, PhD, og Jarle Vikør Ekanger, PhD, begge representanter for Flow Design Bureau AS.

En virkningsgrad på 94,66% ble målt i turbinens bestpunkt, med en usikkerhet på ±0,71%. Falltapet ble målt til å være 6,6 meter ved full-last.

Revisjoner/Distribusjon:

Nr:	Dato:	Distribusjonsliste:
1	25/8-2016	Elektronisk kopi E.Wiborg@Statkraft

1 Prosjektbeskrivelse og sammendrag

26. mai 2016 ble det gjennomført hydrauliske virkningsgradsmålinger og falltapsmålinger på Trollheim kraftverk. Virkningsgradsmålingen ble gjort ved hjelp av den termodynamiske målemetode. Målingene ble utført av Flow Design Bureau AS, ved Dr. Håkon H. Francke og Dr. Jarle V. Ekanger.

Målingene var vellykkede, og måleforholdene var gode under hele testperioden. Resultatene i BEP (Best Efficiency Point) var som følger:

H_n = 371.0m		Turbin 1
Hydraulisk virkningsgrad (BEP)	[%]	94,66
Måleusikkerhet (BEP)	[±%]	0,71
Total volumstrøm (BEP)	[m^3/s]	34,49
Totalt falltap (BEP)	[mVs]	6,60

Falltapsmålingene ble gjort parallelt med virkningsgradsmålingene. Det ble kun målt totalt falltap i hele vannveien fra innløp i Follsjø til innløp på turbin. Største falltap ble målt til 6,60 mVs ved fullast med en volumstrøm på 36 m^3/s og virkningsgrad på 94,62%.

Tilstede under målingene:

Flow Design Bureau AS

Prosjektstatus	Arbeidstittel	Navn
Teknisk ansvarlig	Strømningsspesialist	Dr. Håkon H. Francke
	Instrumentansvarlig	Dr. Jarle V. Ekanger

Statkraft

Prosjektstatus	Arbeidstittel	Navn
Kjøring av turbin	Fagarbeider mekanisk	Arild Taknes Henden

Dr. Håkon H. Francke (sign)

Dr. Jarle V. Ekanger (sign)

25.08.2016, Stabekk/Trondheim

2 Innholdsfortegnelse

3 Symbolliste

Term	Symbol	Benevning
Areal	A	[m²]
Diameter	D	[m]
Effekt	P	[W] = [J/s]
Gravitasjonsakselerasjon	g	[m/s²]
Hastighet	c	[m/s]
Nominell fallhøyde	H_n	[mVs]
Motstand	R	[Ω]
Spenning	U	[V]
Strøm	I	[A]
Tetthet	ρ	[Kg/m³]
Tid	t	[s]
Trykk	p	[Pa]
Virkningsgrad	η	[%]
Volumstrøm	Q	[m³/s]
Absolutt måleusikkerhet	e	[]
Relativ måleusikkerhet	f	[%]

En del av symbolene er også forklart i teksten.

Forkortelser:

DAQ	-	Data Acquisition
IEC	-	International Electromechanical Commission
RSS	-	Root of the Sum of the Squares
BEP	-	Best Efficiency Point

4 Introduksjon

Trollheim kraftverk, i Surnadal kommune i Møre og Romsdal, produserer på vannet fra magasinet Follsjø/Foldsjø (LRV=375m, og HRV=420m), og leverer til elva Surna (ca 20m). Alle data fra NVE Atlas. I følge tegningsunderlag fra turbinleverandør, Kværner, er nominell fallhøyde for turbindesignet H=371m, og tilhørende hoved-data: n= 375 o/min og P= 126.5MW. Data i henhold til løpehjuls-tegning 126105-0 datert 1/7-1967.

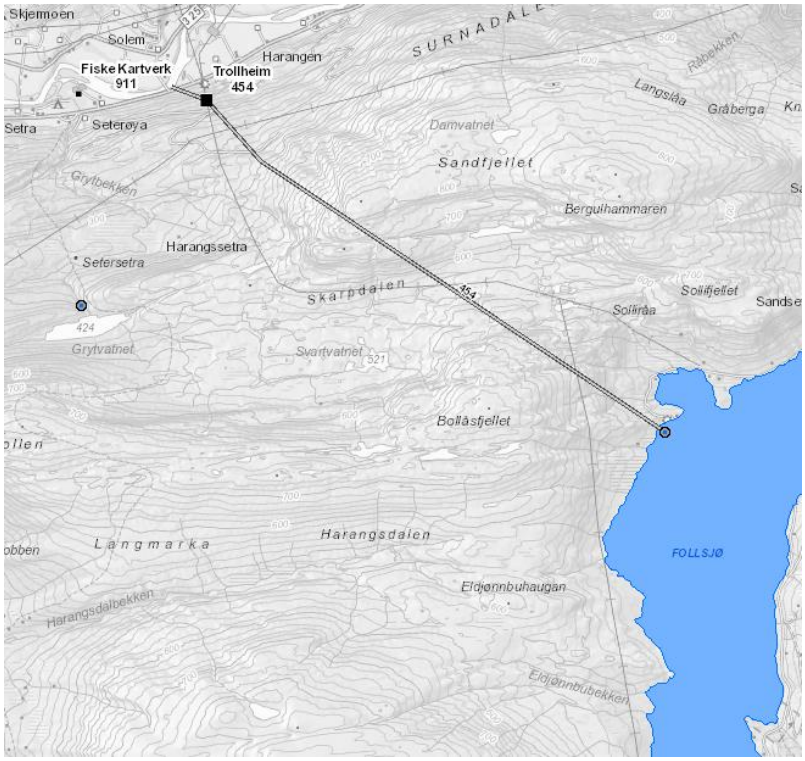

Figur 1 Situasjonskart Trollheim kraftverk. Fra NVE Atlas.

Statkraft Energi AS har planlegger, prosjekterer, oppfører og driver energianlegg. Statkraft har registrert forretningsadresse i Oslo. Flow Design Bureau AS (FDB) utvikler blant annet måle- og instrumentløsninger og leverer måletjenester relatert til vannkraft. FDB har registrert forretningsadresse i Stavanger, Norge.

FDB har bistått Statkraft Energi i utvikling av HydroCord ved Trollheim Kraftverk. Parallelt arbeider Erik Wiborg i Statkraft med utvikling av målemetoder for kontinuerlig overvåking av virkningsgrad på vannkraftverk. Metodene Wiborg benytter baserer seg på direkte og indirekte måling av volumstrøm. Virkningsgradsmålingen som presenteres her anses i Wiborg sitt arbeid som kalibrering og oppstart av den kontinuerlige virkningsgradsmålingen.

5 Resultat

5.1 Virkningsgradsmåling

Beregningene er utført i henhold til teori og prosedyrer beskrevet i appendiks. Fallhøyden for prøvene ble i etterkant redusert til H = 371.0 m ved hjelp av affinitetsligningene. Resultatene er presentert i Tabell 5-1 nedenfor, og Figur 2 og Figur 3 på sidene 20 og 21.

Tabell 5-2 oppsummerer målte verdier som ligger til grunn for beregning av virkningsgrad, Tabell 5-3 viser mellomregningene som er benyttet, mens Tabell 5-4 tabulerer usikkerheter.

Tabell 5-1 Resultat hydraulisk virkningsgrad Trollheim kraftverk

Indeks	Fallhøyde - [mVs]	Volumstrøm - [m^3/s]	Lekkasjetap- [Prosentpoeng %]	**Hydraulisk virkningsgrad - [%]**
1	373.10	27.09	1.17	**93.64**
2	372.53	28.84	1.11	**94.15**
3	372.15	30.70	1.06	**94.40**
4	371.29	32.59	1.01	**94.60**
5	370.60	34.56	0.96	**94.59**
6	370.00	36.02	0.91	**94.62**
7	370.60	34.49	0.89	**94.66**
8	373.68	25.51	1.20	**93.10**
9	374.22	23.55	1.27	**92.38**
10	375.16	19.95	1.46	**89.54**
11	375.93	15.87	1.81	**88.09**
12	376.39	12.09	2.35	**84.34**
13	376.81	9.36	2.92	**78.22**
14	376.84	10.16	2.72	**80.20**
15	371.31	32.54	1.00	**94.56**

Tabell 5-2 Målte verdier for utregning av virkningsgrad

	1	2	3	4	5	6	7	8	9	10	11	12	13	14	15
Generator Power - [MW]	91,25	97,6	104,13	110,6	117,1	121,93	116,93	85,47	78,3	64,22	50,13	36,4	26	29	110,36
Generator Efficiency - [%]	98,16	98,24	98,31	98,37	98,41	98,44	98,41	98,07	97,93	97,59	97,13	96,53	95,96	96,14	98,36
Temperature Inlet - [Deg C]	2,5446	2,5481	2,5567	2,5732	2,6049	2,6192	2,6324	2,6407	2,6468	2,6454	2,6467	2,6522	2,6548	2,6554	2,6611
Temperature Outlet - [Deg C]	2,5922	2,5916	2,5984	2,6135	2,6452	2,66	2,6731	2,6923	2,7041	2,7261	2,7375	2,7717	2,8232	2,8079	2,7014
Temperature Leak - [Deg C]	4,5742	4,5647	4,5658	4,5673	4,5945	4,6004	4,6171	4,6743	4,698	4,7265	4,7655	4,778	4,8073	4,8028	4,6627
Pressure Inlet - [kPa]	3768,029	3757,831	3748,649	3735,129	3723,104	3712,369	3723	3776,83	3786,521	3801,736	3815,317	3823,873	3830,834	3830,106	3735,53
Pressure Probe - [kPa]	3796,923	3791,183	3787,611	3780,326	3773,93	3770,356	3775,723	3800,367	3805,089	3812,796	3819,947	3824,736	3828,001	3827,54	3779,967
Water Level Outlet - [mas]	25,48	25,50	25,5	25,58	25,7	25,72	25,67	25,39	25,37	25,2	25,09	24,98	24,97	24,95	25,6
Pressure Barometric - [kPa]	101,98	101,965	101,941	101,937	101,91	101,891	101,882	101,864	101,841	101,823	101,8	101,764	101,76	101,765	101,752
Flow Through Probe - [l/s]	0,32	0,32	0,32	0,32	0,32	0,29	0,31	0,36	0,35	0,35	0,35	0,35	0,35	0,35	0,35
Flow Leakage - [m^3/sec]	0,14118	0,14274	0,14519	0,14709	0,14854	0,14698	0,13807	0,13617	0,13250	0,12904	0,1257	0,12570	0,12225	0,12325	0,14519

Tabell 5-3 Mellomregning virkningsgrad

	1	2	3	4	5	6	7	8	9	10	11	12	13	14	15
Water Density - Inlet - [Kg/m3]	1001,7854	1001,7803	1001,7759	1001,7694	1001,7637	1001,7586	1001,7640	1001,7907	1001,7955	1001,8030	1001,8098	1001,8140	1001,8175	1001,8172	1001,7704
Water Density - Outlet - [Kg/m3]	999,9855	999,9856	999,9857	999,9865	999,9877	999,9882	999,9882	999,9872	999,9874	999,9870	999,9867	999,9868	999,9878	999,9874	999,9884
Water Density - Average - [Kg/m3]	1000,8854	1000,8830	1000,8808	1000,8779	1000,8757	1000,8734	1000,8761	1000,8889	1000,8914	1000,8950	1000,8982	1000,9004	1000,9026	1000,9023	1000,8794
Isothermal Factor - Inlet - [m^3/Kg]	1,0012	1,0011	1,0011	1,0011	1,0009	1,0009	1,0008	1,0007	1,0007	1,0007	1,0007	1,0006	1,0006	1,0006	1,0007
Isothermal Factor - Outlet - [m^3/Kg]	1,0064	1,0064	1,0063	1,0063	1,0061	1,0060	1,0060	1,0059	1,0058	1,0058	1,0057	1,0056	1,0053	1,0054	1,0059
Isothermal Factor - Average - [m^3/Kg]	1,0038	1,0038	1,0037	1,0037	1,0035	1,0035	1,0034	1,0033	1,0033	1,0032	1,0032	1,0031	1,0030	1,0030	1,0033
Specific Heat Hapacity - Inlet - [J/KgK]	4188,2270	4188,2495	4188,2593	4188,2800	4188,2867	4188,2927	4188,2608	4188,1488	4188,1244	4188,0921	4188,0603	4188,0360	4188,0202	4188,0218	4188,2234
Specific Heat Hapacity - Outlet - [J/KgK]	4204,2903	4204,2900	4204,2837	4204,2658	4204,2306	4204,2157	4204,2055	4204,1997	4204,1894	4204,1761	4204,1701	4204,1425	4204,0936	4204,1092	4204,1823
Specific Heat Hapacity - Average - [J/KgK]	4196,2586	4196,2698	4196,2715	4196,2729	4196,2586	4196,2542	4196,2331	4196,1743	4196,1569	4196,1341	4196,1152	4196,0893	4196,0569	4196,0655	4196,2028

Pressure Inlet - [kPa abs]	3782,7611	3772,5631	3763,3811	3749,8611	3737,8361	3727,1011	3737,7321	3791,5621	3801,2531	3816,4681	3830,0491	3838,6051	3845,5661	3844,8381	3750,2621
Pressure Inlet - [kPa abs]	3798,6909	3792,9509	3789,3789	3782,0939	3775,6979	3772,1239	3777,4909	3802,1349	3806,8569	3814,5639	3821,7149	3826,5039	3829,7689	3829,3079	3781,7349
Pressure Outlet - [kPa abs]	158,2566	158,4381	158,4141	159,1958	160,3473	160,5248	160,0247	157,2567	157,0373	155,3496	154,2463	153,1299	153,0277	152,8363	159,2072
Pressure Outlet - [kPa abs]	152,8549	153,0363	153,0123	153,7940	154,9456	155,1230	154,6229	151,8549	151,6355	149,9479	148,8445	147,7282	147,6259	147,4345	153,8054
Temperature Average - [Deg C]	2,5684	2,5698	2,5776	2,5934	2,6250	2,6396	2,6528	2,6665	2,6754	2,6858	2,6921	2,7119	2,7390	2,7317	2,6812
Velocity Inlet - [m/s]	8,6238	9,1806	9,7723	10,3751	11,0011	11,4665	10,9773	8,1193	7,4963	6,3489	5,0513	3,8498	2,9794	3,2347	10,3576
Velocity Inlet - [m/s]	1,4098	1,4098	1,4098	1,4098	1,4098	1,2776	1,3658	1,5860	1,5420	1,5420	1,5420	1,5420	1,5420	1,5420	1,5420
Velocity Outlet - [m/s]	1,7202	1,8312	1,9492	2,0695	2,1943	2,2872	2,1896	1,6195	1,4953	1,2664	1,0076	0,7679	0,5943	0,6452	2,0660
Velocity Outlet - [m/s]	1,7202	1,8312	1,9492	2,0695	2,1943	2,2872	2,1896	1,6195	1,4953	1,2664	1,0076	0,7679	0,5943	0,6452	2,0660
Leakage Average Pressure - [kPa]	127,4174	127,5006	127,4766	127,8655	128,4278	128,5070	128,2525	126,8595	126,7382	125,8854	125,3223	124,7461	124,6930	124,5998	127,7787
Leakage Average Temperature - [DegC]	3,5832	3,5781	3,5821	3,5904	3,6199	3,6302	3,6451	3,6833	3,7011	3,7263	3,7515	3,7748	3,8152	3,8054	3,6821
Leakage Isothermal Factor - [m^3/kg]	1,0020	1,0020	1,0020	1,0019	1,0018	1,0018	1,0017	1,0015	1,0014	1,0013	1,0012	1,0011	1,0009	1,0010	1,0015

Leakage Spesific Heat Capasity - [J/KgK]	4203,4403	4203,4450	4203,4412	4203,4312	4203,3993	4203,3886	4203,3748	4203,3427	4203,3254	4203,3039	4203,2810	4203,2601	4203,2196	4203,2300	4203,3399
Pressure Saturated Steam 1 - [kPa]	735,1531	735,1220	735,4750	736,2594	737,9086	738,6797	739,3628	740,3651	740,9817	742,1325	742,7294	744,5229	747,2311	746,4256	740,8405
Pressure Saturated Steam 2 - [kPa]	735,1531	735,1220	735,4750	736,2594	737,9086	738,6797	739,3628	740,3651	740,9817	742,1325	742,7294	744,5229	747,2311	746,4256	740,8405
Mechanical Energy Leakage Pressure - [J/Kg]	-50,9746	-51,1726	-51,1717	-51,9570	-53,1309	-53,3252	-52,8298	-50,0669	-49,8662	-48,1889	-47,1019	-46,0155	-45,9090	-45,7144	-52,1327
Mechanical Energy Leakage Thermal - [J/Kg]	8331,2187	8293,8173	8269,8501	8212,6638	8193,6862	8156,2552	8171,3606	8331,0252	8381,0106	8408,2890	8524,2539	8433,0007	8339,6080	8385,0235	8244,0105
Mechanical Energy Leakage Potential - [J/Kg]	-27,4999	-27,4999	-27,4999	-27,4999	-27,4999	-27,4999	-27,4999	-27,4999	-27,4999	-27,4999	-27,4999	-27,4999	-27,4999	-27,4999	-27,4999
Mechanical Energy Leakage Total - [J/Kg]	8252,7442	8215,1448	8191,1785	8133,2069	8113,0554	8075,4300	8091,0308	8253,4584	8303,6444	8332,6002	8449,6521	8359,4852	8266,1990	8311,8091	8164,3779
Mechanical Energy Pressure - [J/Kg]	3659,5171	3653,5657	3649,8906	3641,5581	3633,4901	3629,5021	3635,1665	3662,3902	3667,1909	3676,4300	3684,5904	3690,1783	3693,1009	3692,9540	3639,7802
Mechanical Energy Thermal - [J/Kg]	-199,7419	-182,5377	-174,9845	-169,1098	-169,1092	-171,2072	-170,7867	-216,5226	-240,4398	-338,6280	-381,0073	-501,4327	-706,6160	-639,9000	-169,1070

Mechanical Energy Potential - [J/Kg]	14,9285	14,9285	14,9285	14,9285	14,9285	14,9285	14,9285	14,9285	14,9285	14,9285	14,9285	14,9285	14,9285	14,9285	14,9285
Mechanical Energy Kinetic - [J/Kg]	-0,4857	-0,6829	-0,9060	-1,1476	-1,4138	-1,7994	-1,4645	-0,0537	0,0710	0,3870	0,6813	0,8940	1,0123	0,9807	-0,9453
Mechanical Energy Leakage Relative - [J/Kg]	-43,0054	-40,6576	-38,7379	-36,7030	-34,8692	-32,9491	-32,3934	-44,0603	-46,7183	-53,9084	-66,9307	-86,8811	-107,9617	-100,8092	-36,4295
Mechanical Energy Air Injection - [J/Kg]	-14,3833	-14,3848	-14,3951	-14,4110	-14,4471	-14,4649	-14,4796	-14,5018	-14,5171	-14,5422	-14,5572	-14,5975	-14,6512	-14,6347	-14,5270
Mechanical Energy Air Injection Relative - [J/Kg]	0,0000	0,0000	0,0000	0,0000	0,0000	0,0000	0,0000	0,0000	0,0000	0,0000	0,0000	0,0000	0,0000	0,0000	0,0000
Mechanical Energy Heat Exchange - [J/Kg]	0,0658	0,0618	0,0580	0,0545	0,0512	0,0490	0,0511	0,0689	0,0746	0,0879	0,1104	0,1445	0,1860	0,1715	0,0539
Mechanical Energy Heat Exchange Water Air - [J/Kg]	0,0000	0,0000	0,0000	0,0000	0,0000	0,0000	0,0000	0,0000	0,0000	0,0000	0,0000	0,0000	0,0000	0,0000	0,0000
Mechanical Energy Temperature Variation - [J/Kg]	0,0000	0,0000	0,0000	0,0000	0,0000	0,0000	0,0000	0,0000	0,0000	0,0000	0,0000	0,0000	0,0000	0,0000	0,0000
Mechanical Energy Total - [J/Kg]	3431,2784	3444,6777	3450,2487	3449,5807	3443,0776	3438,5239	3445,5015	3416,7511	3395,1068	3299,2971	3252,3726	3117,8316	2894,6501	2968,3256	3448,2809

Hydraulic Energy Pressure - [J/Kg]	3621,2981	3610,9367	3601,7946	3587,5158	3574,3586	3563,4641	3574,5758	3631,0776	3640,9701	3657,8447	3672,5041	3682,1596	3689,2083	3688,6736	3587,8997
Hydraulic Energy Potential - [J/Kg]	7,3661	7,3661	7,3661	7,3661	7,3661	7,3661	7,3661	7,3661	7,3661	7,3661	7,3661	7,3661	7,3661	7,3661	7,3661
Hydraulic Energy Kinetic - [J/Kg]	35,7055	40,4647	45,8494	51,6804	58,1046	63,1246	57,8539	31,6503	26,9795	19,3525	12,2500	7,1157	4,2620	5,0235	51,5053
Hydraulic Energy Total - [J/Kg]	3664,3697	3658,7675	3655,0100	3646,5622	3639,8292	3633,9548	3639,7958	3670,0939	3675,3157	3684,5632	3692,1202	3696,6414	3700,8364	3701,0632	3646,7711
Head - [m]	373,1005	372,5301	372,1476	371,2874	370,6019	370,0037	370,5985	373,6834	374,2150	375,1566	375,9261	376,3864	376,8135	376,8366	371,3087
Turbine Flow - [m^3/sec]	27,0925	28,8416	30,6997	32,5936	34,5602	36,0224	34,4857	25,5076	23,5504	19,9457	15,8690	12,0946	9,3604	10,1622	32,5384
Turbine Power - [MW]	92,9605	99,3485	105,9200	112,4327	118,9920	123,8623	118,8192	87,1520	79,9551	65,8059	51,6112	37,7085	27,0946	30,1643	112,2001
Hydraulic Efficiency - [%]	93,6390	94,1486	94,3978	94,5982	94,5945	94,6221	94,6619	93,0971	92,3759	89,5438	88,0896	84,3423	78,2161	80,2020	94,5571
Leakage Water Loss - [%]	1,1736	1,1112	1,0599	1,0065	0,9580	0,9067	0,8900	1,2005	1,2711	1,4631	1,8128	2,3503	2,9172	2,7238	0,9990
Nom Power Generator - [MW]	90,4805	96,9993	103,6487	110,4716	117,2887	122,4228	117,1201	84,5510	77,2931	63,1557	49,1479	35,6214	25,4006	28,3289	110,2224
Nom Power Turbine - [MW]	92,1765	98,7371	105,4305	112,3021	119,1838	124,3628	119,0124	86,2150	78,9269	64,7153	50,6001	36,9019	26,4700	29,4663	112,0602
Nom Flow Main - [m^3/sec]	27,0161	28,7823	30,6523	32,5810	34,5788	36,0708	34,5044	25,4159	23,4490	19,8349	15,7647	12,0078	9,2879	10,0832	32,5248
Total Uncertainty - [%]	0,7106	0,7104	0,7107	0,7114	0,7124	0,7134	0,7123	0,7109	0,7116	0,7160	0,7185	0,7270	0,7451	0,7385	0,7113

5.1.1 Måleusikkerhet

Usikkerheten i de termodynamiske målingene ble beregnet for hver utførte måleserie.

Tabell 5-4 Usikkerhetsanalyse av virkningsgradsmålingene

	1	2	3	4	5	6	7	8	9	10	11	12	13	14	15
Tabulated value rho - [±%]	0,1000	0,1000	0,1000	0,1000	0,1000	0,1000	0,1000	0,1000	0,1000	0,1000	0,1000	0,1000	0,1000	0,1000	0,1000
Tabulated value g - [±%]	0,1000	0,1000	0,1000	0,1000	0,1000	0,1000	0,1000	0,1000	0,1000	0,1000	0,1000	0,1000	0,1000	0,1000	0,1000
Tabulated value a - [±%]	0,2000	0,2000	0,2000	0,2000	0,2000	0,2000	0,2000	0,2000	0,2000	0,2000	0,2000	0,2000	0,2000	0,2000	0,2000
Tabulated value Cp - [±%]	0,5000	0,5000	0,5000	0,5000	0,5000	0,5000	0,5000	0,5000	0,5000	0,5000	0,5000	0,5000	0,5000	0,5000	0,5000
Atm random - [±kPa]	0,0000	0,0000	0,0000	0,0000	0,0000	0,0000	0,0000	0,0000	0,0000	0,0000	0,0000	0,0000	0,0000	0,0000	0,0000
Atm systematic - [±kPa]	0,5099	0,5098	0,5097	0,5097	0,5095	0,5095	0,5094	0,5093	0,5092	0,5091	0,5090	0,5088	0,5088	0,5088	0,5088
Atm total - [±kPa]	0,5099	0,5098	0,5097	0,5097	0,5095	0,5095	0,5094	0,5093	0,5092	0,5091	0,5090	0,5088	0,5088	0,5088	0,5088
Pressure Inlet 1_1 Measured - [±kPa]	3,0375	3,0329	3,0301	3,0243	3,0191	3,0163	3,0206	3,0403	3,0441	3,0502	3,0560	3,0598	3,0624	3,0620	3,0240
Pressure Inlet 1_1 - [±kPa]	3,0503	3,0457	3,0428	3,0370	3,0319	3,0291	3,0334	3,0530	3,0568	3,0629	3,0686	3,0724	3,0750	3,0747	3,0368
Pressure Outlet 2_1 Measured - [±kPa]	0,0000	0,0000	0,0000	0,0000	0,0000	0,0000	0,0000	0,0000	0,0000	0,0000	0,0000	0,0000	0,0000	0,0000	0,0000
Pressure Outlet 2_1 - [±kPa]	0,7382	0,7381	0,7381	0,7382	0,7382	0,7382	0,7381	0,7377	0,7375	0,7373	0,7370	0,7368	0,7368	0,7368	0,7376
Temperature Inlet Random - [±K]	0,0000	0,0000	0,0000	0,0000	0,0000	0,0000	0,0000	0,0000	0,0000	0,0000	0,0000	0,0000	0,0000	0,0000	0,0000
Temperature Inlet Systematic - [±K]	0,0000	0,0000	0,0000	0,0000	0,0000	0,0000	0,0000	0,0000	0,0000	0,0000	0,0000	0,0000	0,0000	0,0000	0,0000
Temperature Inlet Total - [±K]	0,0010	0,0010	0,0010	0,0010	0,0010	0,0010	0,0010	0,0010	0,0010	0,0010	0,0010	0,0010	0,0010	0,0010	0,0010
Temperature Outlet Random - [±K]	0,0000	0,0000	0,0000	0,0000	0,0000	0,0000	0,0000	0,0000	0,0000	0,0000	0,0000	0,0000	0,0000	0,0000	0,0000

Temperature Outlet Systematic - [±K]	0,0000	0,0000	0,0000	0,0000	0,0000	0,0000	0,0000	0,0000	0,0000	0,0000	0,0000	0,0000	0,0000	0,0000	0,0000
Temperature Outlet Total - [±K]	0,0010	0,0010	0,0010	0,0010	0,0010	0,0010	0,0010	0,0010	0,0010	0,0010	0,0010	0,0010	0,0010	0,0010	0,0010
Energy Distribution Inlet - [±J/Kg]	6,8626	6,8894	6,9005	6,8992	6,8862	6,8770	6,8910	6,8335	6,7902	6,5986	6,5047	6,2357	5,7893	5,9367	6,8966
Energy Distribution Outler - [±J/Kg]	20,5877	20,6681	20,7015	20,6975	20,6585	20,6311	20,6730	20,5005	20,3706	19,7958	19,5142	18,7070	17,3679	17,8100	20,6897
Potential Inlet - [±J/Kg]	0,0000	0,0000	0,0000	0,0000	0,0000	0,0000	0,0000	0,0000	0,0000	0,0000	0,0000	0,0000	0,0000	0,0000	0,0000
Potential Outlet - [±J/Kg]	0,0000	0,0000	0,0000	0,0000	0,0000	0,0000	0,0000	0,0000	0,0000	0,0000	0,0000	0,0000	0,0000	0,0000	0,0000
Kinetic Inlet - [±%]	2,5486	2,5484	2,5483	2,5482	2,5482	2,5483	2,5482	2,5488	2,5491	2,5504	2,5512	2,5537	2,5589	2,5570	2,5482
Kinetic Inlet Probe- [±%]	10,1980	10,1980	10,1980	10,1980	10,1980	10,1980	10,1980	10,1980	10,1980	10,1980	10,1980	10,1980	10,1980	10,1980	10,1980
Kinetic Outlet - [±%]	2,5486	2,5484	2,5483	2,5482	2,5482	2,5483	2,5482	2,5488	2,5491	2,5504	2,5512	2,5537	2,5589	2,5570	2,5482
Temperature Leakage Random - [±K]	0,0000	0,0000	0,0000	0,0000	0,0000	0,0000	0,0000	0,0000	0,0000	0,0000	0,0000	0,0000	0,0000	0,0000	0,0000
Temperature Leakage Systematic - [±K]	0,0000	0,0000	0,0000	0,0000	0,0000	0,0000	0,0000	0,0000	0,0000	0,0000	0,0000	0,0000	0,0000	0,0000	0,0000
Temperature Leakage - [±K]	0,0000	0,0000	0,0000	0,0000	0,0000	0,0000	0,0000	0,0000	0,0000	0,0000	0,0000	0,0000	0,0000	0,0000	0,0000
Mechanic Leakage Pressure - [±%]	1,7748	1,7679	1,7676	1,7413	1,7031	1,6968	1,7121	1,8043	1,8110	1,8725	1,9145	1,9583	1,9624	1,9707	1,7329
Mechanic Leakage Temperature - [±%]	0,5025	0,5026	0,5026	0,5026	0,5026	0,5026	0,5026	0,5025	0,5025	0,5025	0,5024	0,5025	0,5025	0,5025	0,5026

Mechanic Leakage Potential - [±%]	0,1000	0,1000	0,1000	0,1000	0,1000	0,1000	0,1000	0,1000	0,1000	0,1000	0,1000	0,1000	0,1000	0,1000	0,1000
Mechanic Leakage - [±%]	1,8473	1,8407	1,8404	1,8152	1,7786	1,7725	1,7872	1,8756	1,8821	1,9413	1,9818	2,0242	2,0282	2,0363	1,8071
Mechanic Leakage - [±/Kg]	152,4494	151,2139	150,7522	147,6323	144,2956	143,1356	144,6032	154,8017	156,2796	161,7602	167,4564	169,2124	167,6515	169,2493	147,5364
Mechanic Leakage Q Relative - [±%]	1,5828	1,5825	1,5823	1,5822	1,5823	1,5823	1,5822	1,5831	1,5836	1,5858	1,5871	1,5910	1,5993	1,5963	1,5822
Mechanic Leakage Q Relative - [±%]	0,0001	0,0001	0,0001	0,0001	0,0001	0,0001	0,0001	0,0001	0,0001	0,0001	0,0001	0,0002	0,0002	0,0002	0,0001
Mechanic Pressure - [±/Kg]	7,9681	7,9554	7,9475	7,9299	7,9130	7,9045	7,9164	7,9739	7,9841	8,0033	8,0205	8,0321	8,0383	8,0379	7,9260
Mechanic Thermal - [±%]	22,5202	22,5983	22,6308	22,6256	22,5859	22,5585	22,6010	22,4356	22,3099	21,7600	21,4933	20,7445	19,5667	19,9472	22,6176
Mechanic Potential - [±%]	0,3428	0,3428	0,3428	0,3428	0,3428	0,3428	0,3428	0,3428	0,3428	0,3428	0,3428	0,3428	0,3428	0,3428	0,3428
Mechanic Kinetic - [±%]	0,2163	0,2200	0,2246	0,2302	0,2369	0,2133	0,2261	0,2651	0,2491	0,2459	0,2439	0,2429	0,2426	0,2427	0,2658
Mechanic Leakage Water - [±/Kg]	-0,6807	-0,6434	-0,6130	-0,5807	-0,5517	-0,5213	-0,5125	-0,6975	-0,7398	-0,8549	-1,0622	-1,3823	-1,7266	-1,6092	-0,5764
Mechanic Air Injection - [±/Kg]	0,0000	0,0000	0,0000	0,0000	0,0000	0,0000	0,0000	0,0000	0,0000	0,0000	0,0000	0,0000	0,0000	0,0000	0,0000
Mechanic Heat Exchange Walls - [±/Kg]	0,0000	0,0000	0,0000	0,0000	0,0000	0,0000	0,0000	0,0000	0,0000	0,0000	0,0000	0,0000	0,0000	0,0000	0,0000

Mechanic Heat Exchange Water Air - [±J/Kg]	0,0000	0,0000	0,0000	0,0000	0,0000	0,0000	0,0000	0,0000	0,0000	0,0000	0,0000	0,0000	0,0000	0,0000	0,0000
Mechanic Temperature Variation- [±J/Kg]	0,0000	0,0000	0,0000	0,0000	0,0000	0,0000	0,0000	0,0000	0,0000	0,0000	0,0000	0,0000	0,0000	0,0000	0,0000
Mechanic Total - [±J/Kg]	23,9015	23,9698	23,9971	23,9856	23,9419	23,9124	23,9563	23,8246	23,7108	23,2047	22,9694	22,2921	21,2280	21,5700	23,9771
Mechanic Pressure - [±%]	0,2177	0,2177	0,2177	0,2178	0,2178	0,2178	0,2178	0,2177	0,2177	0,2177	0,2177	0,2177	0,2177	0,2177	0,2178
Mechanic Thermal - [±%]	-11,2747	-12,3801	-12,9330	-13,3792	-13,3558	-13,1762	-13,2335	-10,3618	-9,2788	-6,4259	-5,6412	-4,1371	-2,7691	-3,1172	-13,3747
Mechanic Potential - [±%]	2,2963	2,2963	2,2963	2,2963	2,2963	2,2963	2,2963	2,2963	2,2963	2,2963	2,2963	2,2963	2,2963	2,2963	2,2963
Mechanic Kinetic - [±%]	-44,5290	-32,2125	-24,7941	-20,0599	-16,7592	-11,8521	-15,4367	-493,9260	351,0424	63,5440	35,7945	27,1748	23,9709	24,7488	-28,1142
Mechanic Leakage - [±%]	1,5828	1,5825	1,5823	1,5822	1,5823	1,5823	1,5822	1,5831	1,5836	1,5858	1,5871	1,5910	1,5993	1,5963	1,5822
Mechanic Air Injection - [±%]	0,0000	0,0000	0,0000	0,0000	0,0000	0,0000	0,0000	0,0000	0,0000	0,0000	0,0000	0,0000	0,0000	0,0000	0,0000
Mechanic Heat Exchange Through Walls - [±%]	0,0000	0,0000	0,0000	0,0000	0,0000	0,0000	0,0000	0,0000	0,0000	0,0000	0,0000	0,0000	0,0000	0,0000	0,0000
Mechanic Heat Exchange Water Surface to Air - [±%]	0,0000	0,0000	0,0000	0,0000	0,0000	0,0000	0,0000	0,0000	0,0000	0,0000	0,0000	0,0000	0,0000	0,0000	0,0000

Mechanic Temperature Variation - [±%]	0,0000	0,0000	0,0000	0,0000	0,0000	0,0000	0,0000	0,0000	0,0000	0,0000	0,0000	0,0000	0,0000	0,0000	0,0000
Mechanic Total - [±%]	0,6966	0,6959	0,6955	0,6953	0,6954	0,6954	0,6953	0,6973	0,6984	0,7033	0,7062	0,7150	0,7334	0,7267	0,6953
Pressure Inlet 1 Measured	3,0144	3,0063	2,9989	2,9881	2,9785	2,9699	2,9784	3,0215	3,0292	3,0414	3,0523	3,0591	3,0647	3,0641	2,9884
Pressure Inlet 1 - [±kPa]	3,0273	3,0192	3,0119	3,0011	2,9915	2,9830	2,9914	3,0343	3,0420	3,0542	3,0650	3,0718	3,0773	3,0768	3,0014
Pressure Outlet 2 Measured	0,0000	0,0000	0,0000	0,0000	0,0000	0,0000	0,0000	0,0000	0,0000	0,0000	0,0000	0,0000	0,0000	0,0000	0,0000
Pressure Outlet 2 - [±kPa]	0,7390	0,7389	0,7389	0,7390	0,7391	0,7390	0,7389	0,7384	0,7383	0,7380	0,7378	0,7375	0,7375	0,7375	0,7384
Potential Inlet - [±J/Kg]	0,0000	0,0000	0,0000	0,0000	0,0000	0,0000	0,0000	0,0000	0,0000	0,0000	0,0000	0,0000	0,0000	0,0000	0,0000
Potential Outlet - [±J/Kg]	0,0000	0,0000	0,0000	0,0000	0,0000	0,0000	0,0000	0,0000	0,0000	0,0000	0,0000	0,0000	0,0000	0,0000	0,0000
Kinetic Inlet - [±%]	2,5486	2,5484	2,5483	2,5482	2,5482	2,5483	2,5482	2,5488	2,5491	2,5504	2,5512	2,5537	2,5589	2,5570	2,5482
Kinetic Outlet - [±%]	0,0000	0,0000	0,0000	0,0000	0,0000	0,0000	0,0000	0,0000	0,0000	0,0000	0,0000	0,0000	0,0000	0,0000	0,0000
Hydraulic Pressure - [±J/Kg]	4,7757	4,7627	4,7511	4,7335	4,7175	4,7038	4,7176	4,7875	4,7998	4,8202	4,8382	4,8498	4,8586	4,8578	4,7339
Hydraulic Kinetic - [±J/Kg]	1,8969	2,1495	2,4355	2,7452	3,0864	3,3531	3,0731	1,6816	1,4336	1,0289	0,6515	0,3788	0,2273	0,2678	2,7359
Hydraulic Potential - [±J/Kg]	0,2407	0,2407	0,2407	0,2407	0,2407	0,2407	0,2407	0,2407	0,2407	0,2407	0,2407	0,2407	0,2407	0,2407	0,2407
Hydraulic Total - [±J/Kg]	5,1443	5,2309	5,3444	5,4772	5,6426	5,7816	5,6354	5,0799	5,0151	4,9347	4,8878	4,8705	4,8699	4,8712	5,4729

Hydraulic Pressure - [±%]	0,1319	0,1319	0,1319	0,1319	0,1320	0,1320	0,1320	0,1318	0,1318	0,1318	0,1317	0,1317	0,1317	0,1317	0,1319
Hydraulic Kinetic - [±%]	5,3125	5,3121	5,3119	5,3118	5,3119	5,3119	5,3118	5,3130	5,3136	5,3164	5,3181	5,3232	5,3340	5,3300	5,3118
Hydraulic Potential - [±%]	3,2675	3,2675	3,2675	3,2675	3,2675	3,2675	3,2675	3,2675	3,2675	3,2675	3,2675	3,2675	3,2675	3,2675	3,2675
Hydraulic Total - [±%]	0,1404	0,1430	0,1462	0,1502	0,1550	0,1591	0,1548	0,1384	0,1365	0,1339	0,1324	0,1318	0,1316	0,1316	0,1501
Hydraulic Efficiency - [±%]	**0,7106**	**0,7104**	**0,7107**	**0,7114**	**0,7124**	**0,7134**	**0,7123**	**0,7109**	**0,7116**	**0,7160**	**0,7185**	**0,7270**	**0,7451**	**0,7385**	**0,7113**
Flow - [±%] - {f_Q_1}	**1,5796**	**1,5793**	**1,5792**	**1,5791**	**1,5791**	**1,5791**	**1,5791**	**1,5799**	**1,5804**	**1,5826**	**1,5839**	**1,5878**	**1,5962**	**1,5931**	**1,5791**

5.2 Falltap

Falltapet er beregnet med utgangspunkt i teorien presentert i appendiks. Det ble kun beregnet falltap for vannveien oppstrøms Trollheim kraftverk. Resultatene fra falltapsmålingene er presentert i Tabell 5-5, se også Figur 2 på side 20.

Tabell 5-5 Resultat av falltapsmålinger sortert etter beregnet volumstrøm (hele vannvei oppstrøms)

Index	Turbineffekt - [MW]	Volumstrøm - [m^3/s]	**Falltap [mVs]**	Spesifikk, Energi [mVs]
13	26.00	9.36	**0.81**	376.81
14	29.00	10.16	**0.82**	376.84
12	36.40	12.09	**1.21**	376.39
11	50.13	15.87	**1.54**	375.93
10	64.22	19.95	**2.16**	375.16
9	78.30	23.55	**2.88**	374.22
8	85.47	25.51	**3.37**	373.68
1	91.25	27.09	**3.82**	373.10
2	97.60	28.84	**4.35**	372.53
3	104.13	30.70	**4.72**	372.15
15	110.36	32.54	**5.52**	371.31
4	110.60	32.59	**5.48**	371.29
7	116.93	34.49	**6.06**	370.60
5	117.10	34.56	**6.03**	370.60
6	121.93	36.02	**6.59**	370.00

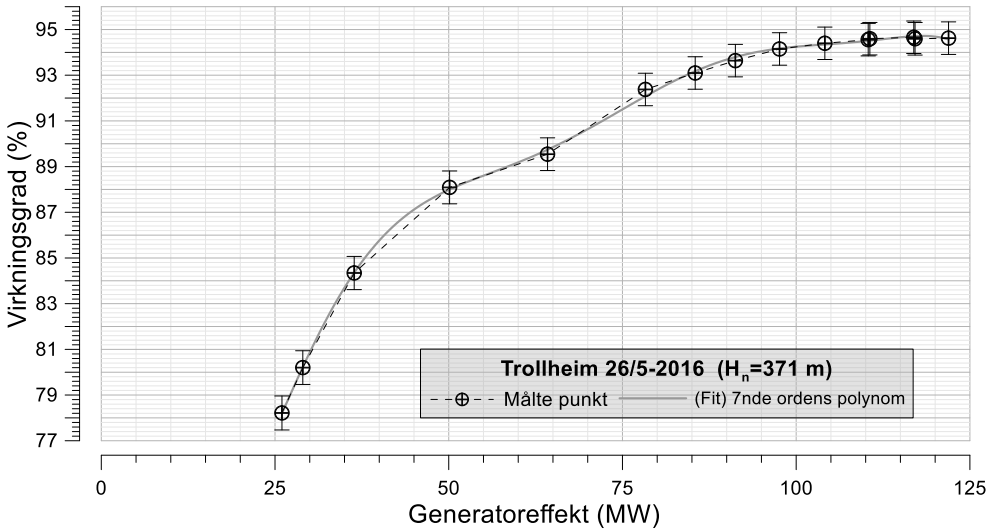

Figur 2 Hydraulisk virkningsgrad mot generatoreffekt Trollheim 26/5-2016. Fit: $\eta = 119.106 - 8.01347 * P + 0.507634 * P^2 - 0.0149195 * P^3 + 0.000238058 * P^4 - 2.11989\ 10^{-6} * P^5 + 9.908125\ 10^{-9} * P^6 - 1.89531\ 10^{-11} * P^7$. P=Generatoreffekt. R-squared = 0.999541.

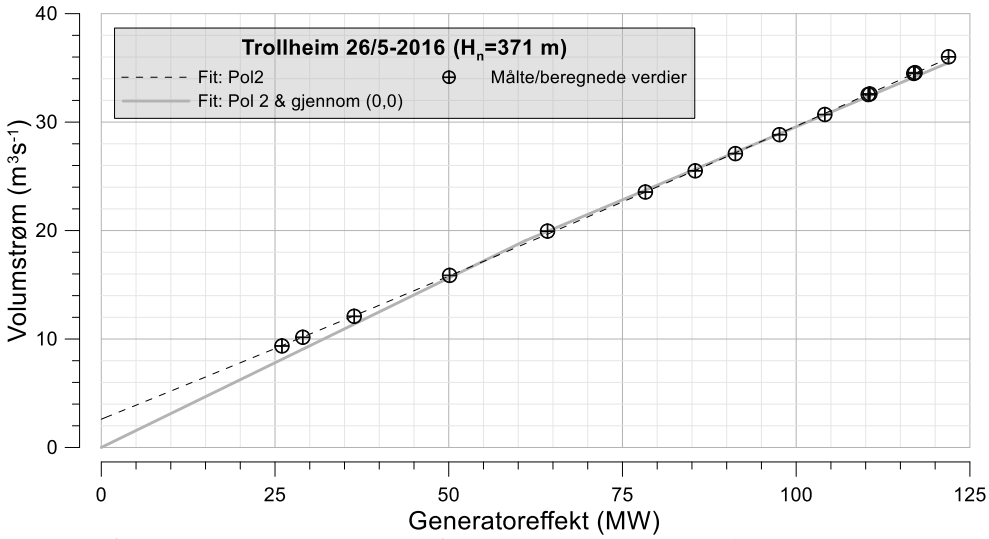

*Figur 3 Vannføring/volumstrøm mot generatoreffekt Trollheim kraftverk 26/5-2016. Q = 2.6094 + 0.25747 * P + 1.2738 10^{-4} * P^2 · R-squared = 0.999889. Q= -3.5463 10^{-4}*P^2+0.33420*P. R-squared = 0.99763.*

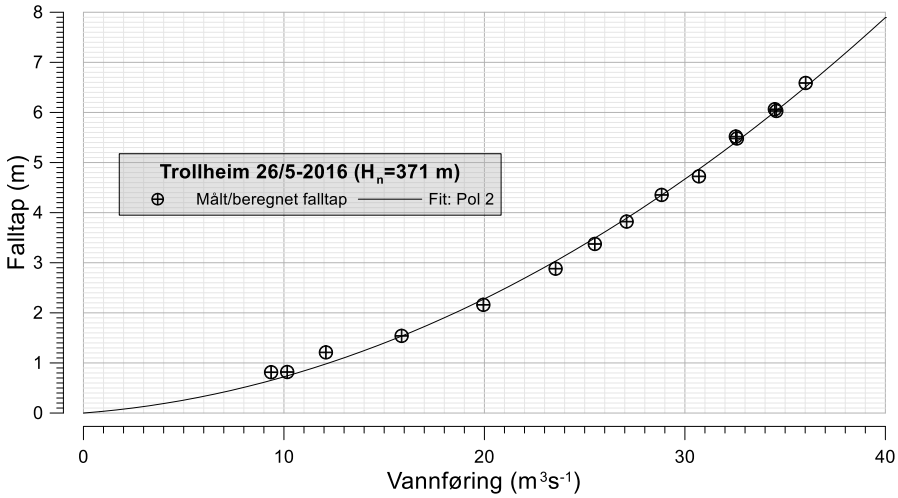

Figur 4 Falltap Trollheim kraftvert 26/5-2016. $h_f = 4.1674*Q^2+0.030621*Q$. R-squared = 0.996845

6 Måleoppsett og forberedelser

6.1 Gjennomførte målinger

Følgende målinger ble gjennomført:

- **Temperatur**
  - Temperatur innløp turbin(1-1), like nedstrøms kuleventil
  - Temperatur sugerørsutløp ved senterlinje til sugerør (2-1)
  - Temperatur spaltevann
- **Trykk**
  - Statisk trykk ved innløp turbin (1)
  - Trykk i termodynamisk målesonde (1-1)
  - Atmosfærisk trykk
- **Nivå**
  - Referansehøyder for plassering av måleutstyr, med utgangspunkt i tegninger
  - Vannivå fjernavlesning Follsjø
  - Vannivå ved utløp av sugerør
- **Andre**
  - Generatoreffekt fra kwh-teller på kontrollrom
  - Servoslag ledeapparat
  - Vannføring i termodynamisk målesonde
  - Volumstrøm spaltevann

I tillegg ble samtlige måledata fra HydroCord systemet på Trollheim både notert i logg og lagret på disk.

6.1.1 Temperatur

6.1.1.1 Temperaturmålinger innløp

Termometer av typen Seabird Electronics 38 ble plassert i den termodynamiske målesonden (FIGUR 6-2). Sonden ble så påmontert innløpsrøret til turbin. Her ble turbinens uttak for luftestuss benyttet, plassert like oppstrøms spiraltromme og nedstrøms kuleventil.

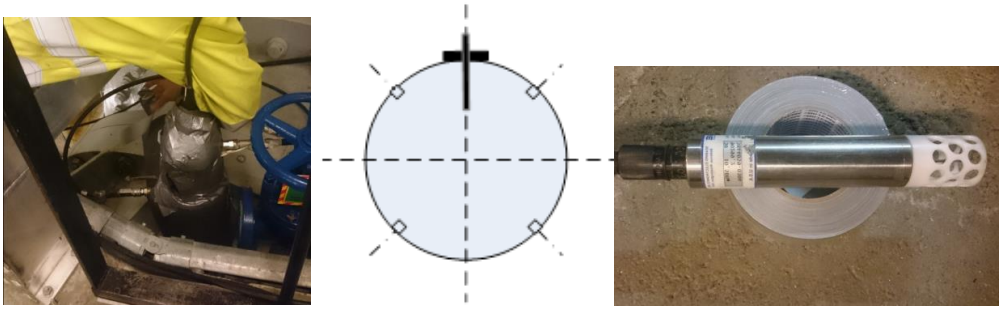

FIGUR 6-1: Plassering av termodynamisk målesonde (t.v), prinsipiell skisse av plasseringen (midt), Seabird 38 temperatursensor (t.h.)

Innløpshullet på målesonden ble rettet parallelt mot strømningen. Til slutt ble sonden godt termisk isolert med flere lag isolerende skumplast.

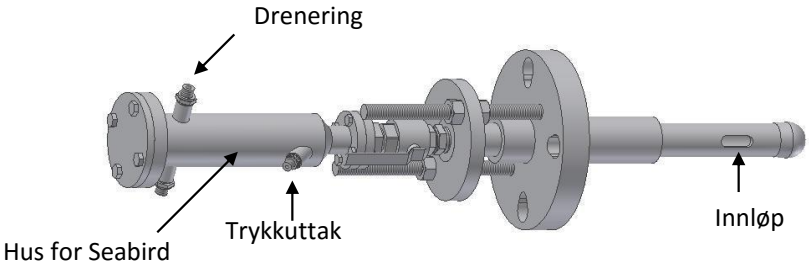

FIGUR 6-2: Prinsipiell skisse av termodynamisk målesonde for trykk- og temperaturmålinger før turbin

Vannet tappet via sonden strømmet kontinuerlig forbi termometeret, og ble deretter drenert vekk.

6.1.1.2 *Temperaturmålinger sugerørsavløp*

Temperaturen i avløpet ble målt ved hjelp av Seabird Electronics 38 termometer montert i en termodynamisk måleramme. Rammen ble festet mot braketter boltet fast i sugerørsvegg og tak. Rammens oppgave var å samle vann fra forskjellige snitt i avløpet, slik at en gjennomsnittlig måling av Temperaturen i avløpsvannet kunne måles. De tre horisontale stålrørene hadde derfor jevnt fordelte små hull rettet mot strømretningen, slik at vannet ble ledet inn i disse og ført forbi temperaturføleren lokalisert nederst i enden av det vertikale røret.

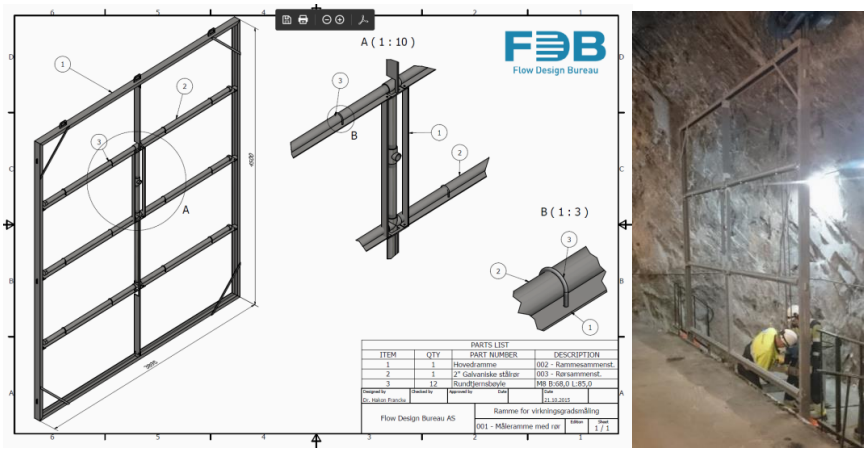

FIGUR 6-3: Konstruksjonstegning måleramme i avløpet (t.v), måleramme før nedsenking av avløpet(t.h)

6.1.1.3 *Temperaturmåling spaltevann*

Spaltevannstemperaturen ble målt med et Seabird Electronics 38 termometer. Det ble drenert vann fra spaltevannsrøret over i en isolert tank med lokk. Termometeret ble plassert nede i tanken.

FIGUR 6-4 – Isolert tank for måling av spaltevannstemperatur.

6.1.2 Trykk

6.1.2.1 Statisk trykk innløp turbin

Absolutte presisjonstrykkmålere av typen Digiquartz 9002K-105, ble koblet mot trykkuttak lokalisert på innløpsrøret like nedstrøms kuleventil. Det ble laget en midlertidig ringledning koblet mot alle 4 trykkuttakene. Trykkmåleren ble plassert liggende på gulv med kjent referansehøyde. Det ble i ettertid korrigert for høydeforskjellen mellom trykkmåler og senterlinjen på innløpet.

FIGUR 6-5 – Diqiquarts trykksensorer plassert på gulv med kjent kote (t.v). Trykkslange koblet mot en av de fire trykkuttakene(t.h.). Alle trykkuttakene ble fysisk koblet sammen til en samlestokk.

6.1.2.2 Sondetrykk

Trykket i sonden ble tatt ut i trykkuttak lokalisert på sonden (se figur forrige side), og logget med trykkmåler av typen Digiquartz 9002K-105. Trykkmåleren ble plassert liggende på gulv med kjent referansehøyde. Det ble i ettertid korrigert for høydeforskjellen mellom trykkmåler og senterlinjen på innløpet.

6.1.2.3 Atmosfærisk trykk

Det atmosfæriske trykket ble avlest for hvert testpunkt. Instrumentet ble lagt på kontorpulten i kontrollrommet , med kjent referansehøyde.

6.1.3 Nivåmålinger

6.1.3.1 Vannivå avløp

Vannivå i avløp ble målt ved å måle avstanden fra kjent kote og ned til vannflaten. Det ble benyttet målebånd ved vannsensor som avga et akustisk signal ved vannkontakt.

6.1.3.2 Referansehøyder (koter) og turbingeometri

Alle referansehøyder og turbindimensjoner benyttet under målingene er med utgangspunkt i verdier funnet i tegninger over kraftverket.

6.1.4 Andre målinger

6.1.4.1 Effektmåling – Avgitt generatoreffekt

Kraftverkets eksisterende kWh-teller ble benyttet. Det ble avlest verdi direkte fra displayet. Denne verdien ble igjen kontrollert mot avlesning fra driftssentralen ved testenes start og slutt. Effekten ble også avlest fra regulatorens skjerm ved turbindørken.

FIGUR 6-6: Effektmåler benyttet for avlesning av effekt.

6.1.4.2 Vannføring termodynamisk målesonde

Vannføringen igjennom den termodynamiske målesonden ble målt med et rotameter. Rotameteret ble kalibrert.

FIGUR 6-7: Rotameter benyttet for volumstrømsmåling av vannet som strømmer forbi termometeret i den termodynamiske proben i innløpet

6.1.4.3 Generatorvirkningsgrad

Generatorvirkningsgraden som ble benyttet er hentet fra Ramdal [6]. I tabellen under er konstantene til polynomet som er benyttet for å beregne virkningsgraden.

TABELL 6-1: Generatorvirkningsgrad polynom hentet fra Ramdal [6]. η_{Gen}=A+Bx+Cx^2+Dx^3, her x= generatoreffekt.

	A	B (x)	C (x^2)	D (x^3)
Koeffisient-verdier	9.4078E-01	8.6927E-04	-5.9264E-06	1.4211E-08

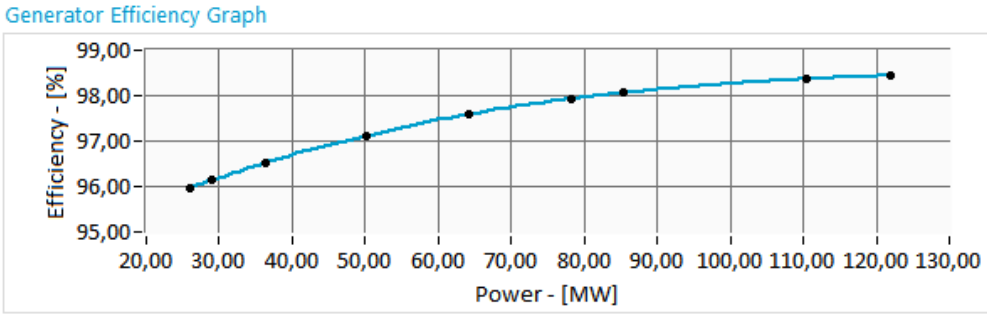

FIGUR 6-8: Generatorvirkningsgrad aggregat 1 . Tallverdiene er basert på polynom hentet fra Ramdal [6]

6.1.5 Benyttede koter

Alle koter benyttet under målingene hentet fra tegninger over kraftverket. Disse er listet i tabellen under:

TABELL 6-2: Koter benyttet – Virkningsgradsmålinger og falltapsmålinger

Turbin nr		**[]**	**1**
Senter innløp	z_{1}	[moh]	20,5
Senter utløp	z_{2}	[moh]	19,75
Temp innløp	$z\_T\_{1\text{-}1}$	[moh]	21,82
Temp utløp	$z\_T\_{2\text{-}1}$	[moh]	20,3
Temp spaltevann	z_T_{Leak}	[moh]	17,5
P innløp	z_p_{1}	[moh]	22
P probe	$z\_p\_{1\text{-}1}$	[moh]	22
P atm	z_p_{atm}	[moh]	33,6
Utløpsplatåreferanse	z_utløpsplatå	[moh]	34,2

6.1.6 Gravitasjonskonstanten

For å beregne gravitasjonskonstanten, ble formelverket I IEC41 benyttet.
Gravitasjonskonstanten ble da funnet til å være 9,8214 m/s^2 ved turbinsenter.

6.1.7 Turbingeometri

Følgende verdier for turbingeometri ble benyttet ved beregningene.

Sted	Short Name	Enhet	
Turbin innløpsareal	A_1	m^2	3,14159
Turbin utløpsareal	A_2	m^2	15,75

Turbine inlet area – [m2] – 3,14159
Turbine outlet area

6.1.8 Kalibrering og nullpunkttest

Digiquartz trykkgiverene ble kontrollert mot trykkalibrator før og etter avreise.

Det ble gjennomført nullpunktstest av benyttede SeaBird-termometere før og etter at alle målingene var avsluttet.

6.2 Gjennomføring av målingene

Det ble gjennomført 15 måleserier på ulike driftspunkt. Det ble tatt prøver fra og med 26 MW til 122 MW. Det ble tatt repetisjonspunkt rundt 110 MW som var antatt å være BEP (Best Efficiency Point).

Måleseriene ble innledet ved at det aktuelle aggregat ble stilt inn på ønsket driftspunkt. For at aggregatet skulle gå så stabilt som mulig over hele måleperioden, ble slagbegrenser benyttet for å holde ledeapparatet stivt. Det ble tilstrebet at aggregatet kjørte med Mvar ≈ 0, slik at cosΦ ≈ 1.

Videre ble innløpstrykk og temperatur overvåket. Ved stabile trykk og temperaturforhold ble måleperioden startet. Temperatur og trykk ble logget kontinuerlig gjennom måleperiodene. Hver måleserie varte i ca 10 min, noe som tilsvarte ca 200 temperaturmålinger.

Vannivået i avløpet ble avlest flere ganger over en periode på noen minutter for hver test. Gjennomsnittet av disse målingene ble benyttet.

Etter endt måleserie, ble maskinen stilt inn på nytt driftspunkt, og ny måleserie ble innledet.

7 Korreksjoner

7.1 Korreksjonsledd i utregninger

7.1.1 Varmeovergang mellom vegg og vann

Det ble korrigert for varmeovergang mellom infrastruktur (vegger, rørvegger osv) og vannet mellom temperaturmålepunktene, etter metode spesifisert i IEC-standardens kap. 14.6.2.1. Det ble antatt at aktuelt veggareal var 24m^2, varmeoverføringen foregikk ved en rate på 10W/m^{2}K. Temperaturdifferansen ble satt til 10K.

7.2 Korrigerte målefeil

7.2.1 Volumstrøm Spaltevann

Verdiene for volumstrøm av spaltevann baserte seg på avlesing av målingen fra HydroCord-systemet, som har en ultralydbasert probe montert på spaltevannsavløpet. De to ultralydprobene som utgjør det nødvendige probepar for målingene var plassert på hver side av eneste mulige tappepunkt for måling av spaltevannets temperatur. Kontroll av verdiene i etterkant har vist at det var feil i disse målingen, muligens forårsaket av tappingen for temperaturmåling.

En korrigert verdi for denne volumstrømmen ble derfor utarbeidet, og det er disse korrigerte verdiene som utgjør grunnlaget for virkningsgradsutregningene. De korrigerte verdiene baserer seg på loggførte målinger fra det samme systemet ca tre måneder tidligere. En regresjon ble gjennomført for å finne spaltevannsstrøm som funksjon av ledeapparatåpning. Forskjell i fallhøyde mellom de to tidspunktene ble funnet å være ikke signifikant.

8 Kommentarer

Forholdene under virkningsgradsmålingene var generelt meget stabile og gode. Repeterbarheten i målingene er gode, hvilket indikerer at påliteligheten i målingene er gode.

Referansemålingene som ble tatt rundt BEP er gode og godt innenfor måleusikkerheten. Dette er med på å styrke troverdigheten i målingene.

Usikkerheten i målingene ligger som forventet rundt ± 0,7 %. Dette er det normale ved termodynamiske målinger på maskiner av denne typen med lignende fallhøyde.

9 Referanser

[1] Arne Kjølle, *Hydraulisk måleteknikk*, Vannkraftlaboratoriet Trondheim 2003

[2] Frank M. White, *Fluid Mechanics*, fifth edition 2003

[3] IEC publication 41 (IEC 41, 1991-11)

[4] Anthony J. Wheeler & Ahmad R. Ganji, *Introduction to Engineering Experimentation*, 2 Utgivelse 2004

[5] Møller, *Norske Vannkraftverk,* Bind 1 og 2

[6] Harald Hulaas , *Termodynamisk virkningsgradsmåling Svorka kraftverk*, 1999

10 Appendix – Teori

10.1 Virkningsgradsmåling av vannturbiner

Teorien benyttet i dette kapittelet er hentet fra [1] Kjølle, 2003.

10.1.1 Virkningsgraden

Virkningsgraden for en hydraulisk turbin beskriver hvor mange prosent av den tilgjengelige hydrauliske effekten turbin omdanner til roterende effekt ut på turbinakslingen (akseleffekt). Turbinvirkningsgraden kan derfor beskrives som produsert effekt dividert med tilgjengelig effekt.

$$\eta = \frac{\text{Produsert effekt}}{\text{Tilgjengelig effekt}} = \frac{P_{\text{Produsert}}}{P_{\text{Tilgjengelig}}}$$ *Ligning 10-1*

Turbinvirkningsgraden kan videre deles inn i to hovedkategorier, hydraulisk og mekanisk virkningsgrad. Den hydrauliske virkningsgraden beskriver hvor stor del av den tilgjengelige hydrauliske energien løpehjulet omformer til mekanisk effekt, mens den mekaniske virkningsgraden forteller oss hvor stor del av effekten avgitt fra løpehjulet som fortsatt er tilgjengelig på turbinakslingen. Med andre ord forteller den mekaniske virkningsgraden oss hvor mye av effekten som går bort i mekaniske tap mellom turbin og generatoren, som for eksempel friksjonstap i lager. Mekanisk og hydraulisk virkningsgrad kan uttrykkes ved følgende ligninger:

Mekanisk virkningsgrad:

$$\eta_{\text{Mekanisk}} = \frac{P_{\text{Aksel}}}{P_{\text{Løpehjul}}}$$ *Ligning 10-2*

Hydraulisk virkningsgrad:

$$\eta_{\text{Hydraulisk}} = \frac{P_{\text{Løpehjul}}}{P_{\text{Hydraulisk}}}$$ *Ligning 10-3*

Her er leddene i ligningene representert ved:

$P_{\text{Hydraulisk}}$	–	Tilgjengelig hydraulisk effekt på løpehjul
$P_{\text{Løpehjul}}$	–	Avgitt effekt fra løpehjul
P_{Aksel}	–	Avgitt effekt fra turbinaksling (akseleffekt)

En turbins totalvirkningsgrad blir dermed et produkt av den mekaniske og den hydrauliske virkningsgraden og kan skrives følgende:

$$\eta_{\text{Turbin}} = \eta_{\text{Hydraulisk}} \cdot \eta_{\text{Mekanisk}} = \frac{P_{\text{Løpehjul}}}{P_{\text{Hydraulisk}}} \cdot \frac{P_{\text{Aksel}}}{P_{\text{Løpehjul}}} = \frac{P_{\text{Aksel}}}{P_{\text{Hydraulisk}}}$$ *Ligning 10-4*

Den teoretiske tilgjengelige effekten tilført løpehjulet er et produkt av volumstrømmen, trykkhøyden, vannets massetetthet og gravitasjonskonstanten. $P_{\text{Hydraulisk}}$ kan dermed utrykkes ved følgende formel:

$$P_{\text{Hydraulisk}} = \rho \cdot g \cdot Q \cdot H_e$$ *Ligning 10-5*

Her er variablene gitt som:

$P_{\text{Hydraulisk}}$	–	Hydraulisk effekt	[W]
ρ	–	Vannets massetetthet	[kg/m³]
g	–	Gravitasjonskonstant	[m/s²]
H_e	–	Tilgjengelig fallhøyde	[mVs]

Akseleffekten kan beregnes ved å måle avgitt effekt fra generatoren, gitt at generatorvirkningsgraden er kjent.

Vi har følgende uttrykk for generatorvirkningsgraden:

$$\eta_{\text{Generator}} = \frac{\text{Produsert effekt}}{\text{Tilgjengelig effekt}} = \frac{P_{\text{Generator}}}{P_{\text{Aksel}}}$$ *Ligning 10-6*

Dette gir akseleffekten utrykket ved generatorvirkningsgraden og generatoreffekten.

$$P_{\text{Aksel}} = \frac{P_{\text{Generator}}}{\eta_{\text{Generator}}}$$ *Ligning 10-7*

Turbinvirkningsgraden kan dermed skrives som

$$\eta_{\text{Turbin}} = \frac{P_{\text{Aksel}}}{P_{\text{Hydraulisk}}} = \frac{P_{\text{Generator}}}{P_{\text{Hydraulisk}} \cdot \eta_{\text{Generator}}}$$ *Ligning 10-8*

$$\eta_{\text{Turbin}} = \frac{P_{\text{Generator}}}{(\rho \cdot g \cdot Q \cdot H_e) \cdot \eta_{\text{Generator}}}$$ *Ligning 10-9*

Generatoreffekten måles ofte ved hjelp av en effektmåler koblet mot kraftstasjonens måletransformator, eller ved avlesning av kraftverkets egen kWh-teller.

Generatorvirkningsgraden endrer seg lite over tid. Det er derfor ikke uvanlig å benytte seg av virkningsgradsdata på generatoren som da den var ny. Dersom det er ønskelig å utføre nye virkningsgradsmålinger på generatoren, må disse utføres av elektromaskinkyndig personell.

Vannets massetetthet kan i de fleste tilfeller settes lik 1000 kg/m³, men er en termodynamisk parameter som varierer i verdi avhengig av trykk og temperatur. Målinger med krav til stor nøyaktighet krever at tetthet beregnes for hver måleserie.

Gravitasjonskonstanten varierer med geografisk breddegrad, samt avstanden fra jordens sentrum i radiell retning. For nøyaktige målinger av virkningsgraden bør dermed også denne bestemmes. Dette kan enten gjøres ved målinger på stedet, eller ved å benytte uttrykk i [3] IEC 41.

Den effektive fallhøyden H_e finnes ved å beregne den totale tilgjengelige trykkenergien. Ved å benytte Bernoullis ligning kan følgende uttrykk settes opp for fallhøyden:

$$H_e = \frac{1}{\rho \cdot g}(p_1 - p_2) + \frac{1}{2g}\left(c_1^2 - c_2^2\right) + (z_1 - z_2) \qquad \textit{Ligning 10-10}$$

Her er punkt 1 like oppstrøms Turbin der statisk trykkmåling foretas. Punkt 2 er for en fullturbin senterlinjen for utløpet til sugerøret, mens det for en fristråleturbin er målt over midlere stråleinnløp på skovlene.

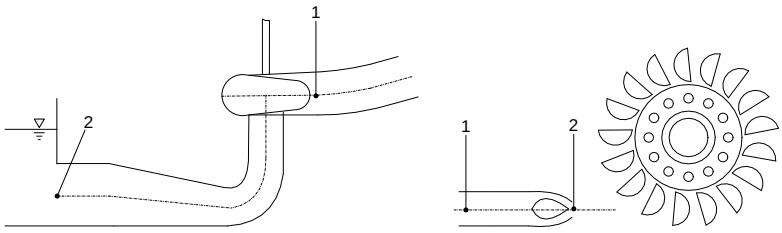

FIGUR 10-1: Bernoullis referansepunkter for beregning av fallhøyden H_{head} for en fullturbin til venstre, og en fristråleturbin til høyre

For å beregne hastighetshøyden i de to punktene, benyttes middelhastigheten med mindre andre forhold tilsier at det må korrigeres for hastighetsprofilet.

Bestemmelse av volumstrømmen på vannkraftverk byr som regel på størst problemer i forbindelse med virkningsgradsmålingene. Det er utviklet flere metoder som alle har sine fordeler og ulemper.

10.1.2 Affinitetsligningene

Når det gjennomføres virkningsgradsmålinger på et kraftverk, blir det tatt prøver med turbinen på ulike driftspunkt. Disse målepunktene og deres tilhørende virkningsgrad kan normalt ikke plottes mot en todimensjonal graf, da ikke bare volumstrømmen, men også fallhøyden H_e varerier fra et driftspunkt til et annet. Det er derfor nødvendig å i etterkant justere volumstrøm og effekt til en spesifikk fallhøyde H_e. Her blir som regel designhøyden valgt, med mindre andre forhold tilsier at en annen fallhøyde bør brukes. Til denne justeringen benyttes affinitetsligningene som definert nedenfor.

$$P_2 = P_1\left(\frac{H_2}{H_1}\right)^{3/2} \qquad \textit{Ligning 10-11}$$

$$Q_2 = Q_1\left(\frac{H_2}{H_1}\right)^{1/2} \qquad \textit{Ligning 10-12}$$

10.1.3 Termodynamisk virkningsgradsmåling

Teori er hentet fra Kjølle, 2003 [1].

Den termodynamiske metoden for virkningsgradsmåling skiller seg noe fra de andre metodene, hovedsakelig ved at det her ikke er volumstrømmen som måles for å finne virkningsgraden. I stedet blir den hydrauliske virkningsgraden beregnet ved å måle volumstrømavhengige tap i systemet.

Den fysiske bakgrunnen for metoden bygger på at strømningstapene i systemet går over til varme i vannstrømmen. Vannet får dermed en høyere temperatur under gjennomløpet. Ved å måle temperaturdifferansen over turbinens innløp og avløp kan de spesifikke strømningstapene beregnes. Dette gir grunnlag for å beregne den hydrauliske virkningsgraden.

Dersom problemet forenkles ved at vannets kompressibilitet og temperaturutvidelse neglisjeres, fås følgende uttrykk for virkningsgraden:

$$\eta_h = \frac{P_m}{P_h} = 1 - \frac{\Delta H_{tap}}{H}, \quad \Delta H_{tap} = \frac{E_{tap}}{g} = \frac{c_p}{g}\Delta T \qquad \textit{Ligning 10-13}$$

Temperaturdifferansen blir svært liten ved lav fallhøyde og høy virkningsgrad. Et overslag for en turbin med 95 % virkningsgrad og fallhøyde på 50m, gir en temperaturdifferanse på 0,0059 °C. Det kreves derfor svært temperaturømfintlig måleapparatur for nøyaktige målinger. Ved så små temperaturdifferanser viser det seg også at vannets kompressibilitet og temperaturutvidelse påvirker resultatet. Nevnte egenskaper må derfor inkluderes i beregning av hydraulisk energi.

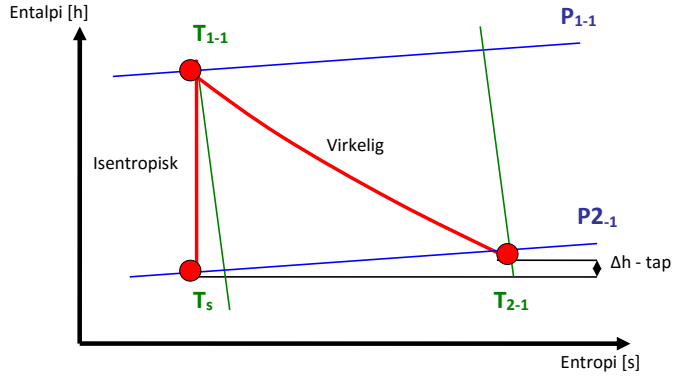

FIGUR 10-2: Isentropisk (teoretisk) og virkelig prosessen tegnet i entalpi- entropidiagram

En isentropiske prosessen er en ideell tapsfri prosess med fullkommen energiavgivelse til Turbin. Det innbærer at den hydrauliske energien tapsfritt blir overført til mekanisk energi. Ingen varme genereres i vannstrømmen, prosessen er adiabatisk.

I den virkelige prosessen oppstår det alltid strømningstap. Tapene bidrar til en økning av vannets entropi som fører til redusert entalpidifferanse. Ved å måle vannets entalpi før og etter at det har passert Turbin kan derfor strømningstapene i maskinen beregnes, og dermed også den hydrauliske virkningsgrad.

Fra tidligere har vi at:

$$\eta = \frac{\text{Produsert effekt}}{\text{Tilgjengelig effekt}}$$ *Ligning 10-14*

Effekten kan skrives som:

$$P = \rho Q E$$ *Ligning 10-15*

Vi setter sammen likningene og får følgende uttrykk for virkningsgraden:

$$\eta = \frac{E_{mekanisk} \cdot Q \cdot \rho}{E_{hydraulisk} \cdot Q \cdot \rho} = \frac{E_{mekanisk}}{E_{hydraulisk}}$$ *Ligning 10-16*

Energien kan som tidligere nevnt uttrykkes som funksjon av entalpidifferansene.

$$E_m = h_{1-1} - h_{2-1}$$
$$E_h = h_{1-1} - h_s$$ *Ligning 10-17*

Tar først for oss det hydrauliske (adiabatiske) leddet. Den hydrauliske energien er summen av potensiell, trykk- og hastighetsenergi, og kan skrives som:

$$E_h = E_{h\ \text{pressure}} + E_{h\ \text{potential}} + E_{h\ \text{kinetic}}$$ *Ligning 10-18*

Setter inn for hvert av leddene, og den hydrauliske energien kan beskrives med følgende uttrykk:

$$E_h = \frac{1}{\overline{\rho}}\left(p_1 - p_2\right) + g\left(z_1 - z_2\right) + \frac{1}{2}\left(c_1^2 - c_2^2\right)$$ *Ligning 10-19*

$\overline{\rho}$ er vannets tetthet [Kg/m³], midlet over målepunktene

Tilsvarende består det mekaniske leddet av potensiell, trykk-, hastighets-, og termisk energi.

$$E_m = E_{m\ \text{pressure}} + E_{m\ \text{thermal}} + E_{m\ \text{potential}} + E_{m\ \text{kinetic}}$$ *Ligning 10-20*

Setter inn for hvert ledd og ender opp med:

$$E_m = \overline{a}\left(p_1 - p_2\right) + \overline{C_p}\left(T_1 - T_2\right) + g\left(z_1 - z_2\right) + \frac{1}{2}\left(c_1^2 - c_2^2\right)$$ *Ligning 10-21*

$\overline{a}$ er den isotermale faktoren for vann [m³/Kg], midlet over målepunktene

$\overline{C}_p$ er spesifikk varmekoeffisient for vann [J/Kg], midlet over målepunktene

Vi ender da opp med dette uttrykket for virkningsgraden:

$$\eta = \frac{E_m}{E_h} = \frac{\bar{a}\left(p_{1\text{–}1} - p_{2\text{–}1}\right) + \overline{C_p}\left(T_{1\text{–}1} - T_{2\text{–}1}\right) + g\left(z_{1\text{–}1} - z_{2\text{–}1}\right) + \frac{1}{2}\left(c_{1\text{–}1}^2 - c_{2\text{–}1}^2\right)}{\frac{1}{\rho}\left(p_1 - p_2\right) + g\left(z_1 - z_2\right) + \frac{1}{2}\left(c_1^2 - c_2^2\right)}$$

Ligning 10-22

I dette uttrykket er det ikke tatt hensyn til tapet som går igjennom øvre spalt. Dette må derfor legges til i tapet i den mekaniske energien, og vi får følgende likning:

$$E_m = \bar{a}\left(p_{1\text{–}1} - p_{2\text{–}1}\right) + \overline{C_p}\left(T_{1\text{–}1} - T_{2\text{–}1}\right) + g\left(z_{1\text{–}1} - z_{2\text{–}1}\right) + \frac{1}{2}\left(c_{1\text{–}1}^2 - c_{2\text{–}1}^2\right) + \delta E_m$$

Ligning 10-23

Her representerer δE_m spaltevannstapet, og kan skrives som:

$$\delta E_m = -\frac{Q_{clearence}}{Q_{turbine}} E_{Clearence}$$

Ligning 10-24

Antar hastighetsenergien ≈0, og vi kan skrive den mekaniske energien som følger:

$$E_{m_{clearence}} = \bar{a}\left(p_{atm} - p_{2\text{–}1}\right) + \overline{C_p}\left(T_{clearence} - T_{2\text{–}1}\right) + g\left(z_{clearence} - z_{2\text{–}1}\right)$$

Ligning 10-25

Det endelige uttrykket for den hydrauliske virkningsgraden er da:

$$\eta = \frac{E_m}{E_h} = \frac{\bar{a}\left(p_{1\text{–}1} - p_{2\text{–}1}\right) + \overline{C_p}\left(T_{1\text{–}1} - T_{2\text{–}1}\right) + g\left(z_{1\text{–}1} - z_{2\text{–}1}\right) + \frac{1}{2}\left(c_{1\text{–}1}^2 - c_{2\text{–}1}^2\right) + \delta E_m}{\frac{1}{\rho}\left(p_1 - p_2\right) + g\left(z_1 - z_2\right) + \frac{1}{2}\left(c_1^2 - c_2^2\right)}$$

Ligning 10-26

10.2 Falltapsmåling

Virkningsgraden for en vannturbin er bestemt av volumstrømmen Q og fallhøyden H. Økes pådraget resulterer dette i at volumstrømmen øker, dermed får vannet en høyere hastighet fra inntaket til Turbin. Høyere vannhastighet gir høyere friksjon som resulterer i større falltap i tilløpssystemet. Det er av stor interesse å kartlegge falltapet, da dette er en direkte årsak til redusert avgitt effekt på vannkraftmaskinene.

Målingen skjer ved å logge vannivået på innløpssjøen, og trykket foran Turbin ved forskjellige driftspunkt. Ved å benytte Bernoullis ligning mellom inntak og turbin, beregnes så falltapet.

$$H_{tap} = \frac{1}{\rho g}(p_1 - p_2) + \frac{1}{2g}\left(c_1^2 - c_2^2\right) + (z_1 - z_2) \qquad \textit{Ligning 10-27}$$

Ved å plotte falltapet mot volumstrømmen oppnås en funksjon av andre grad.

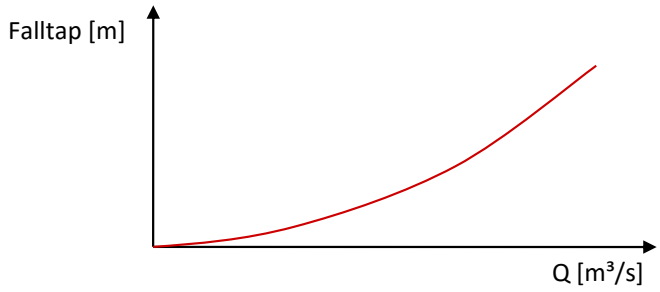

FIGUR 10-3: Falltapet som funksjon av volumstrømmen

Ved hjelp av denne grafen vil det være mulig å drøfte om falltapene er akseptable i driftsområdene, eller om det bør iverksettes tiltak for å minske falltapet. Slike tiltak kan eksempelvis være å øke tunneltverrsnittet så hastigheten reduseres, redusere friksjonen på tunnelveggene, eller så enkelt som å rense varegrinder for hindringer.

10.3 Usikkerhetsanalyse

Teorien bak usikkerhetsanalysen er med bakgrunn i IEC 41, kapittel 6.2, 14.7, appendiks A og appendiks C.

Alle målinger av fysiske størrelser innebærer at det blir et avvik mellom den målte størrelsen og den faktiske størrelsen. Dette skyldes tilfeldige og systematiske usikkerheter i målingene. Når det gjennomføres virkningsgradsmålinger på vannkraftmaskiner er det av stor interesse å vite usikkerheten i disse målingene. I den forbindelse blir det utført usikkerhetsanalyse.

Tilfeldige og ukontrollerbare påvirkninger vil gi avvik i måleinstruments avlesninger av de fysiske størrelsene man ønsker måle. Disse verdiene er det vanskelig å si noe om bare ved å se på måleresultatet. Det man kan si noe om er usikkerheten til instrumentet og dens virkemåte og kalibrering. I tillegg vil tilfeldige og ukontrollerbare påvirkninger være normalfordelte, og man kan således redusere innvirkningen av usikkerheten ved å finne aritmetisk middelverdi av mange målinger ved stasjonære forhold.

Usikkerheter følger målekjeder, slik at den absolutte usikkerheten øker utover i målekjeden. I kombinasjonen av forskjellige målinger for å beregne utledede størrelser, kan derimot den relative usikkerheten gå ned igjen, avhengig av størrelsesorden på de forskjellige målingene. Den absolutte usikkerheten vil derimot også i dette tilfellet øke.

Usikkerhetsanalyse benytter seg av den såkalte RSS- metoden, (Root-Sum-Square, på Norsk: Rot-Sum-Kvadrat), hvor enkeltusikkerheter kombineres ved å finne kvadratroten av summen til kvadratene av de enkelte usikkerhetene. Om usikkerhetene som skal benyttes er relative eller absolutte størrelser avhenger av hvordan de enkelte målestørrelser matematisk er knyttet sammen.

Usikkerhet for en målt størrelse kan skrives som følger

$$f_x = \frac{e_x}{x} \qquad \textit{Ligning 10-28}$$

Her er f_x måleusikkerheten. e_x er den absolutte usikkerheten i målingen av X med samme benevning som den målte størrelsen, og X er den målte størrelsen selv. Virkningsgraden er definert som spesifikk mekanisk energi dividert på spesifikk hydraulisk energi:

$$\eta_h = \frac{E_{mtotal}}{E_{htotal}} \qquad \textit{Ligning 10-29}$$

Dette gir relativ usikkerhet definert som:

$$f_{\eta_h} = \sqrt{f_{E_m}^2 + f_{E_h}^2} \qquad \textit{Ligning 10-30}$$

10.3.1 Spesifikk mekanisk energi

Spesifikk mekanisk energi er definert som:

$$E_{mtotal} = E_{mp} + E_{mc} + E_{mz} + E_{mT} + E_{\delta E_m}$$ *Ligning 10-31*

Som gir uttrykket for usikkerheten lik:

$$e_{E_{mtotal}} = \sqrt{e_{E_{mp}}^2 + e_{E_{mc}}^2 + e_{E_{mz}}^2 + e_{E_{mT}}^2 + e_{E_{\delta E_m}}^2}$$ *Ligning 10-32*

De forskjellige leddene i den spesifikke mekaniske energien og de korresponderende usikkerhetene er:

10.3.1.1 Spesifikk mekanisk trykkenergi:

$$E_{mp} = \bar{a} \cdot \left(p_{1\text{–}1} - p_{2\text{–}1} \right)$$ *Ligning 10-33*

$$f_{E_{mp}} = \sqrt{f_{\bar{a}}^2 + \frac{\left(e_{p_{1\text{–}1}}^2 + e_{p_{2\text{–}1}}^2 \right)}{\left(p_{1\text{–}1} - p_{2\text{–}1} \right)^2}}$$ *Ligning 10-34*

10.3.1.2 Spesifikk mekanisk hastighetsenergi:

$$E_{mc} = \frac{1}{2} \cdot \left(c_{1\text{–}1}^2 - c_{2\text{–}1}^2 \right)$$ *Ligning 10-35*

$$e_{E_{mc}} = \sqrt{c_{1\text{–}1}^4 \cdot f_{c_{1\text{–}1}}^2 + c_{2\text{–}1}^4 \cdot f_{c_{2\text{–}1}}^2}$$ *Ligning 10-36*

10.3.1.3 Spesifikk mekanisk termisk energi:

$$E_{mT} = Cp \cdot \left(T_{2\text{–}1} - T_{1\text{–}1} \right)$$ *Ligning 10-37*

$$e_{E_{mT}} = \sqrt{\left(E_{mT} \cdot \sqrt{f_{Cp}^2 + \frac{\left(e_{T_{1\text{–}1}}^2 + e_{T_{2\text{–}1}}^2 \right)}{\left(T_{1\text{–}1} - T_{2\text{–}1} \right)^2}} \right)^2 + e_{E_1}^2 + e_{E_2}^2}$$ *Ligning 10-38*

10.3.1.4 Spesifikk mekanisk potensiell energi:

$$E_{mz} = g \cdot \left(z_{1\text{–}1} - z_{2\text{–}1} \right)$$ *Ligning 10-39*

$$f_{E_{mz}} = \sqrt{f_g^2 + \frac{\left(e_{z_{1-1}}^2 + e_{z_{2-1}}^2\right)}{\left(z_{1-1} - z_{2-1}\right)^2}}$$ *Ligning 10-40*

10.3.1.5 Spesifikk mekanisk energi i lekkasjevannet:

$$E_{\delta E_h} = E_p + E_T + E_z$$ *Ligning 10-41*

$$e_{E_{\delta E_h}} = \sqrt{e_{E_p}^2 + e_{E_T}^2 + e_{E_z}^2}$$ *Ligning 10-42*

De enkelte delene er spesifikke størrelser for henholdsvis trykkenergi, termisk energi og potensiell energi i lekkasjevannet. Disse, og deres usikkerheter, er definert som:

10.3.1.5.1 *Trykk*:

$$E_p = a_{leakage} \cdot \left(p_{atm} - p_{2-1}\right)$$ *Ligning 10-43*

$$f_{E_p} = \sqrt{f_{a_{leakage}}^2 + \frac{\left(e_{p_{atm}}^2 + e_{p_{2-1}}^2\right)}{\left(p_{atm} - p_{2-1}\right)^2}}$$ *Ligning 10-44*

10.3.1.5.2 Termisk:

$$E_T = Cp_{leakage} \cdot \left(T_{leakage} - T_{2-1}\right)$$ *Ligning 10-45*

$$f_{E_T} = \sqrt{f_{Cp_{leakage}}^2 + \frac{\left(e_{T_{leakage}}^2 + e_{T_{2-1}}^2\right)}{\left(T_{leakage} - T_{2-1}\right)^2}}$$ *Ligning 10-46*

10.3.1.5.3 Potensiell:

$$E_z = g \cdot \left(z_{leakage} - z_{2-1}\right)$$ *Ligning 10-47*

$$f_{E_z} = \sqrt{f_g^2 + \frac{\left(e_{z_{leakage}}^2 + e_{z_{2-1}}^2\right)}{\left(z_{leakage} - z_{2-1}\right)^2}}$$ *Ligning 10-48*

10.3.2 Spesifikk hydraulisk energi:

Spesifikk hydraulisk energi er definert som:

$$E_{htotal} = E_{hp} + E_{hc} + E_{hz}$$ *Ligning 10-49*

De forskjellige leddene i den spesifikke hydrauliske energien og de korresponderende usikkerhetene er:

10.3.2.1 Spesifikk hydraulisk trykkenergi:

$$E_{hp} = \overline{\rho} \cdot (p_1 - p_2)$$ *Ligning 10-50*

$$f_{E_{hp}} = \sqrt{f_{\rho_{average}}^2 + \frac{\left(e_{p_1}^2 + e_{p_2}^2\right)}{(p_1 - p_2)^2}}$$ *Ligning 10-51*

10.3.2.2 Spesifikk hydraulisk hastighetsenergi:

$$E_{hc} = \frac{1}{2} \cdot \left(c_1^2 - c_2^2\right)$$ *Ligning 10-52*

$$e_{E_{hc}} = \sqrt{c_1^4 \cdot f_{c_1}^2 + c_2^4 \cdot f_{c_2}^2}$$ *Ligning 10-53*

10.3.2.3 Spesifikk hydraulisk potensiell energi:

$$E_{hz} = g \cdot (z_1 - z_2)$$ *Ligning 10-54*

$$f_{E_{hz}} = \sqrt{f_g^2 + \frac{\left(e_{z_1}^2 + e_{z_2}^2\right)}{(z_1 - z_2)^2}}$$ *Ligning 10-55*

10.3.3 Størrelser og usikkerheter som anvendes i den spesifikke mekaniske energiens usikkerhet

10.3.3.1 Isotropisk konstant ved midlere trykk og temperatur:

$$e_{\bar{a}} = \sqrt{\left(\left.\frac{\partial a}{\partial T}\right|_{T=\frac{T_{1-1}+T_{2-1}}{2}}\right)^2 \cdot \left(e_{T_{1-1}}^2 + e_{T_{2-1}}^2\right) + \left(\left.\frac{\partial a}{\partial p}\right|_{p=\frac{p_{1-1}+p_{2-1}}{2}}\right)^2 \cdot \left(e_{p_{1-1}}^2 + e_{p_{2-1}}^2\right) + e_{a_{table}}^2}$$ *Ligning 10-56*

I henhold til IEC41

$$f_{a_{table}} = 0,2\%$$

10.3.3.2 Trykk ved temperaturmålepunkt i probe:

$$p_{1-1} = p'_{1-1} + \rho_1 \cdot g \cdot \left(z_{inlet\&probe} - z_{1-1} \right)$$ *Ligning 10-57*

$$e_{p_{1-1}} = \sqrt{e^2_{p'_{1-1}} + \left(\rho_1 \cdot g \cdot \left(z_{inlet\&probe} - z_{1-1} \right) \right)^2 \cdot \left(f^2_{\rho_1} + f^2_g + \frac{\left(e^2_{z_{inlet\&probe}} + e^2_{z_{1-1}} \right)}{\left(z_{inlet\&probe} - z_{1-1} \right)^2} \right)}$$ *Ligning 10-58*

$$f_{p'_{1-1}} = \sqrt{\left(f_{p'_{1-1}random} \right)^2 + \left(f_{p'_{1-1}systematic} \right)^2}$$ *Ligning 10-59*

$$e_{p'_{1-1}random} = \pm \frac{t_{95,\upsilon} \cdot s_{p'_{1-1}}}{\sqrt{n}}$$ *Ligning 10-60*

$$e_{p'_{1-1}systematic} \approx \max_{calibration} \left(p_{1-1i} - p_{1-1i} \right)_{p_{1-1i} \approx p_{1-1}}$$ *Ligning 10-61*

$$e_{\rho_1} = \sqrt{\left(\left. \frac{\partial \rho}{\partial T} \right|_{T=T_{1-1}} \right)^2 \cdot e^2_{T_{1-1}} + \left(\left. \frac{\partial \rho}{\partial p} \right|_{p=p_1} \right)^2 \cdot e^2_{p_1} + e^2_{\rho_{table}}}$$ *Ligning 10-62*

I henhold til IEC41

$$f_{\rho_{table}} = 0,1\%$$

10.3.3.3 Trykk ved temperaturmålepunkt i måleramme på avløp:

$$p_{2-1} = p'_{2-1} + \rho_2 \cdot g \cdot \left(z_{drafttube} - z_{2-1} \right)$$ *Ligning 10-63*

$$e_{p_{2-1}} = \sqrt{e^2_{p'_{2-1}} + \left(\rho_2 \cdot g \cdot \left(z_{drafttube} - z_{2-1} \right) \right)^2 \cdot \left(f^2_{\rho_2} + f^2_g + \frac{\left(e^2_{z_{drafttube}} + e^2_{z_{2-1}} \right)}{\left(z_{drafttube} - z_{2-1} \right)^2} \right)}$$ *Ligning 10-64*

$$f_{p'_{2-1}} = \sqrt{\left(f_{p'_{2-1}random}\right)^2 + \left(f_{p'_{2-1}systematic}\right)^2}$$ *Ligning 10-65*

$$e_{p'_{2-1}random} = \pm \frac{t_{95,\upsilon} \cdot s_{p'_{2-1}}}{\sqrt{n}}$$ *Ligning 10-66*

$$e_{p'_{2-1}systematic} = \pm t_{95,\upsilon} s_{calibration} \cdot \sqrt{\frac{1}{n} + \frac{\left(x_{p=p} - \bar{x}\right)}{S_{XX}}}$$ *Ligning 10-67*

$$e_{\rho_2} = \sqrt{\left(\left.\frac{\partial \rho}{\partial T}\right|_{T=T_{2-1}}\right)^2 \cdot e_{T_{2-1}}^2 + \left(\left.\frac{\partial \rho}{\partial p}\right|_{p=p_2}\right)^2 \cdot e_{p_2}^2 + e_{\rho_{table}}^2}$$ *Ligning 10-68*

10.3.3.4 Hastighet ved temperaturmålepunkt i probe:

$$c_{1-1} = \frac{Q_{bucket}}{A_{probe}} = \frac{V_{bucket} / t_{bucket}}{A_{probe}}$$ *Ligning 10-69*

$$f_{c_{1-1}} = \sqrt{f_{V_{bucket}}^2 + f_{t_{bucket}}^2 + f_{A_{probe}}^2}$$ *Ligning 10-70*

10.3.3.5 Hastighet ved temperaturmålepunkt i måleramme på avløp:

$$c_{2-1} = c_2 = \frac{Q_{turbin}}{A_2}$$ *Ligning 10-71*

$$f_{c_{2-1}} = \sqrt{f_{Q_{turbine}}^2 + f_{A_2}^2}$$ *Ligning 10-72*

10.3.3.6 Spesifikk koeffisient for varmekapasitet:

$$Cp = Cp\left(T = \frac{T_{1-1} + T_{2-1}}{2}, p = \frac{p_{1-1} + p_{2-1}}{2}\right)$$ *Ligning 10-73*

$$e_{Cp} = \sqrt{\left(\left.\frac{\partial Cp}{\partial T}\right|_{T=\frac{T_{1-1}+T_{2-1}}{2}}\right)^2 \cdot \left(e_{T_{1-1}}^2 + e_{T_{2-1}}^2\right) + \left(\left.\frac{\partial Cp}{\partial p}\right|_{p=\frac{p_{1-1}+p_{2-1}}{2}}\right)^2 \cdot \left(e_{p_{1-1}}^2 + e_{p_{2-1}}^2\right) + e_{Cp_{table}}^2}$$ *Ligning 10-74*

10.3.3.7 Temperatur ved målepunkt i probe:

$$e_{T_{1-1}} = \sqrt{\left(e_{T_{1-1random}}\right)^2 + \left(e_{T_{1-1systematic}}\right)^2}$$ *Ligning 10-75*

$$e_{T_{1-1random}} = \pm \frac{t_{95,\upsilon} \cdot s_{T_{1-1}}}{\sqrt{n}}$$ *Ligning 10-76*

$$e_{T_{1-1}systematic} \approx \max_{calibration} \left(T_{1-1i} - T_{1-1i}\right)_{T_{1-1i} \approx T_{1-1}}$$ *Ligning 10-77*

$$e_{T_{2-1}} = \sqrt{\left(e_{T_{2-1random}}\right)^2 + \left(e_{T_{2-1systematic}}\right)^2}$$ *Ligning 10-78*

10.3.3.8 Temperatur ved målepunkt i måleramme på avløp:

$$e_{T_{2-1random}} = \pm \frac{t_{95,\upsilon} \cdot s_{T_{2-1}}}{\sqrt{n}}$$ *Ligning 10-79*

$$e_{T_{2-1}systematic} \approx \max_{calibration} \left(T_{2-1i} - T_{2-1i}\right)_{T_{2-1i} \approx T_{2-1}}$$ *Ligning 10-80*

10.3.3.9 Energifordelingen på innløpet:

$e_{E_1} = 0,2\% \cdot E_m$

10.3.3.10 Energifordelingen på utløpet:

$e_{E_1} = 0,6\% \cdot E_m$

10.3.3.11 Gravitasjonskonstanten:

$f_g \approx 0$

10.3.3.12 For alle stedshøyder er det satt:

$e_z = 0,05$

10.3.3.13 Isotropisk konstant ved midlere trykk og temperatur for lekkasjestrømmen:

$$e_{a_{leakage}} = \sqrt{\left(\left.\frac{\partial a}{\partial T}\right|_{T=\frac{T_{leakage}+T_{2-1}}{2}}\right)^2 \cdot \left(e_{T_{leakage}}^2 + e_{T_{2-1}}^2\right) + \left(\left.\frac{\partial a}{\partial p}\right|_{p=\frac{p_{atm}+p_{2-1}}{2}}\right)^2 \cdot \left(e_{p_{atm}}^2 + e_{p_{2-1}}^2\right) + e_{a_{table}}^2} \qquad \textit{Ligning 10-81}$$

$$e_{T_{leakage}} = \pm \frac{t_{95,\upsilon} \cdot s_{T_{leakage}}}{\sqrt{n}} \qquad \textit{Ligning 10-82}$$

$$e_{T_{leakage}} = \sqrt{\left(e_{T_{leakage,random}}\right)^2 + \left(e_{T_{leakage,systematic}}\right)^2} \qquad \textit{Ligning 10-83}$$

$$e_{T_{leakage,systematic}} \approx \max_{calibration}\left(T_{leakage,i} - T_{leakage,i}\right)_{T_{leakage,i} \approx T_{leakage,i}} \qquad \textit{Ligning 10-84}$$

10.3.3.14 Atmosfærisk trykk:

$$f_{p_{atm}} = \sqrt{f_{Patm,random}^2 + f_{Patm,systematic}^2} \qquad \textit{Ligning 10-85}$$

$$e_{p_{atm,random}} = \pm \frac{t_{95,\upsilon} \cdot s_{p_{atm}}}{\sqrt{n}} \qquad \textit{Ligning 10-86}$$

$$e_{p_{atm,systematic}} \approx \max_{calibration}\left(p_{atm,i} - p_{atm,i}\right)_{p_{atm,i} \approx p_{atm,i}} \qquad \textit{Ligning 10-87}$$

10.3.3.15 Spesifikk koeffisient for varmekapasitet for lekkasjestrømmen:

$$Cp_{leakage} = Cp\left(T = \frac{T_{leakage} + T_{2-1}}{2}, p = \frac{p_{atm} + p_{2-1}}{2}\right) \qquad \textit{Ligning 10-88}$$

$$e_{Cp_{leakage}} = \sqrt{\left(\left.\frac{\partial Cp}{\partial T}\right|_{T=\frac{T_{leakage}+T_{2-1}}{2}}\right)^2 \cdot \left(e_{T_{leakage}}^2 + e_{T_{2-1}}^2\right) + \left(\left.\frac{\partial Cp}{\partial p}\right|_{p=\frac{p_{atm}+p_{2-1}}{2}}\right)^2 \cdot \left(e_{p_{atm}}^2 + e_{p_{2-1}}^2\right) + e_{Cp_{table}}^2} \qquad \textit{Ligning 10-89}$$

I henhold til IEC41:

$$f_{Cp_{table}} = 0,5\%$$

10.3.4 Andre usikkerheter brukt i spesifikk hydrauliske energien

10.3.4.1 Tetthet ved gjennomsnittlig trykk og temperatur

$$\overline{\rho} = \rho\left(T = \frac{T_{1-1} + T_{2-1}}{2}, p = \frac{p_{1-1} + p_{2-1}}{2}\right)$$ *Ligning 10-90*

$$e_{\overline{\rho}} = \sqrt{\left(\left.\frac{\partial\rho}{\partial T}\right|_{T=\frac{T_{1-1}+T_{2-1}}{2}}\right)^2 \cdot \left(e_{T_{1-1}}^2 + e_{T_{2-1}}^2\right) + \left(\left.\frac{\partial\rho}{\partial p}\right|_{p=\frac{p_{1-1}+p_{2-1}}{2}}\right)^2 \cdot \left(e_{p_{1-1}}^2 + e_{p_{2-1}}^2\right) + e_{\rho_{table}}^2}$$ *Ligning 10-91*

10.3.4.2 Trykk ved senterlinje turbininnløp

$$p_1 = p_1^{'} + \rho_1 \cdot g \cdot \left(z_{inlet\&probe} - z_1\right)$$ *Ligning 10-92*

$$e_{p_1} = \sqrt{e_{p_1^{'}}^2 + \left(\rho_1 \cdot g \cdot \left(z_{inlet\&probe} - z_1\right)\right)^2 \cdot \left(f_{\rho_1}^2 + f_g^2 + \frac{\left(e_{z_{inlet\&probe}}^2 + e_{z_1}^2\right)}{\left(z_{inlet\&probe} - z_1\right)^2}\right)}$$ *Ligning 10-93*

$$f_{p_1^{'}} = \sqrt{\left(f_{p_{1\cdot random}^{'}}\right)^2 + \left(f_{p_{1,systematic}^{'}}\right)^2}$$ *Ligning 10-94*

$$e_{p_{1random}^{'}} = \pm\frac{t_{95,\upsilon} \cdot s_{p_1^{'}}}{\sqrt{n}}$$ *Ligning 10-95*

$$f_{p_{1,systematic}^{'}} = f_{p_{1-1}^{'}systematic}$$ *Ligning 10-96*

10.3.4.3 Trykk ved senterlinje turbinutløp

$$p_2 = p_2^{'} + \rho_2 \cdot g \cdot \left(z_{drafttube} - z_2\right)$$ *Ligning 10-97*

$$e_{p_2} = \sqrt{e_{p_2}^{2} + \left(\rho_2 \cdot g \cdot \left(z_{drafttube} - z_2\right)\right)^2 \cdot \left(f_{\rho_2}^2 + f_g^2 + \frac{\left(e_{z_{drafttube}}^2 + e_{z_2}^2\right)}{\left(z_{drafttube} - z_2\right)^2} \right)}$$ *Ligning 10-98*

$$f_{p_2} = \sqrt{\left(f_{p_{2,random}}\right)^2 + \left(f_{p_{2,systematic}}\right)^2}$$ *Ligning 10-99*

$$e_{p_{2\,random}} = \pm \frac{t_{95,\upsilon} \cdot s_{p_2}}{\sqrt{n}}$$ *Ligning 10-100*

$$f_{p_{2,systematic}} = f_{p_{2-1,systematic}}$$ *Ligning 10-101*

10.3.4.4 Hastighet utløp

$$f_{c_2} = f_{c_{2-1}}$$ *Ligning 10-102*

$$f_{A_1} = \pm 0{,}1\%$$

10.3.4.5 Hastighet innløp

$$f_{c_1} = \sqrt{f_{Q_{turbine}}^2 + f_{A_1}^2}$$ *Ligning 10-103*

$$f_{p_{1,systematic}} = f_{p_{1-1}systematic}$$ *Ligning 10-104*

Dedicated to my little family.
Maxim, Celine and Lene Sophie, thank you for your patience.